QUANTUM CHEMICAL SIMULATION OF NITRIC OXIDE REDUCTION
BY AMMONIA (SCR REACTION) ON V2O5 / TiO2 CATALYST SURFACE

A THESIS SUBMITTED TO
THE GRADUATE SCHOOL OF NATURAL AND APPLIED SCIENCES
OF
MIDDLE EAST TECHNICAL UNIVERSITY

BY

SEZEN SOYER

IN PARTIAL FULFILLMENT OF THE REQUIREMENTS
FOR
THE DEGREE OF MASTER OF SCIENCE
IN
CHEMICAL ENGINEERING

SEPTEMBER 2005

Approval of the Graduate School of Natural and Applied Sciences

<div style="text-align: right">

Prof. Dr. Canan ÖZGEN

Director

</div>

I certify that this thesis satisfies all the requirements as a thesis for the degree of Master of Science.

<div style="text-align: right">

Prof. Dr. Nurcan BAÇ

Head of Department

</div>

This is to certify that we have read this thesis and that in our opinion it is fully adequate, in scope and quality, as a thesis for the degree of Master of Science

<div style="text-align: right">

Prof. Dr. Işık ÖNAL

Supervisor

</div>

Examining Committee Members

Prof. Dr. İnci EROĞLU	(METU, CHE)	
Prof. Dr. Işık ÖNAL	(METU, CHE)	
Prof. Dr. Suzan KINCAL	(METU, CHE)	
Prof. Dr. Saim ÖZKAR	(METU, CHEM)	
Prof. Dr. Şinasi ELLİALTIOĞLU	(METU, PHYS)	

I hereby declare that all information in this document has been obtained and presented in accordance with academic rules and ethical conduct. I also declare that, as required by these rules and conduct, I have fully cited and referenced all material and results that are not original to this work.

Name, Last Name : Sezen SOYER

Signature :

ABSTRACT

QUANTUM CHEMICAL SIMULATION OF NITRIC OXIDE REDUCTION BY AMMONIA (SCR REACTION) ON V_2O_5 / TiO_2 CATALYST SURFACE

Soyer, Sezen

M.S., Department of Chemical Engineering

Supervisor: Prof. Dr. Işık Önal

September 2005, 186 pages

The reaction mechanism for the selective catalytic reduction (SCR) of nitric oxide by ammonia on (010) V_2O_5 surface represented by a $V_2O_9H_8$ cluster was simulated by density functional theory (DFT) calculations. The computations indicated that SCR reaction consisted of three main parts. In the first part ammonia activation on Brønsted acidic V-OH site as NH_4^+ species by a non-activated process takes place. The second part includes the interaction of NO with pre-adsorbed NH_4^+ species to eventually form nitrosamide (NH_2NO). The rate limiting step for this part as well as for the total SCR reaction is identified as NH_3NHO formation reaction. The last part consists of the decomposition of NH_2NO on the cluster which takes advantage of a hydrogen transfer mechanism between the active V=O and V-OH groups.

Water and ammonia adsorption and dissociation are investigated on (101) and (001) anatase surfaces both represented by totally fixed and partially relaxed $Ti_2O_9H_{10}$ clusters. Adsorption of H_2O and NH_3 by H-bonding on previously H_2O and NH_3 dissociated systems are also considered.

By use of a (001) relaxed $Ti_2O_9H_{10}$ cluster, the role of anatase support on SCR reaction is investigated. Since NH_2NO formation on $Ti_2O_9H_{10}$ cluster requires lower activation barriers than on V_2O_5 surface, it is proposed that the role of titanium dioxide on SCR reaction could be forming NH_2NO. The role of vanadium oxide is crucial in terms of dissociating this product into H_2O and N_2.

Finally, NH_3 adsorption is studied on a $V_2TiO_{14}H_{14}$ cluster which represents a model for vanadia/titania surface.

Keywords: Selective Catalytic Reduction, SCR, NO Reduction, NH_3, Quantum Chemical Calculations, Density Functional Theory, DFT, V_2O_5, TiO_2.

ÖZ

NİTRİK OKSİTİN AMONYAK İLE V_2O_5 / TiO_2 KATALİZÖR YÜZEYİ ÜZERİNDE SEÇİCİ KATALİTİK İNDİRGENMESİ REAKSİYONUNUN KUANTUM KİMYASAL SİMÜLASYONU

Soyer, Sezen

Yüksek Lisans, Kimya Mühendisliği Bölümü

Tez Yöneticisi : Prof. Dr. Işık Önal

Eylül 2005,186 sayfa

Nitrik oksitin $V_2O_9H_8$ atom kümesi ile temsil edilen (010) V_2O_5 yüzeyi üzerinde amonyak ile katalitik indirgenme reaksiyonu (SCR) elektron yoğunluk teorisi hesaplamaları ile simüle edilmiştir. Hesaplamalara göre SCR reaksiyonu üç temel kısımdan oluşmaktadır. İlk kısımda amonyağın Brønsted asidik V-OH bölgesi üzerinde, aktivasyon bariyerine ihtiyaç duymayan bir prosesle, NH_4^+ iyonu olarak adsorbe olduğu bulunmuştur. İkinci kısım, nitric oksitin NH_2NO oluşturmak üzere NH_4^+ iyonu ile girdiği interaksiyondan ibarettir. Bu kısmın, aynı zamanda bütün SCR reaksiyonunun hız belirleyici adımı NH_3NHO molekülünün oluştuğu adımdır. Son kısım ise NH_2NO'nun atom kümesi üzerinde aktif V=O ve V-OH bölgeleri ve adsorbe olan molekül arasında gerçekleşen hidrojen transferi mekanizmasına göre H_2O ve N_2'ye parçalanma adımlarından oluşmaktadır.

Her ikisi de bazı yüzey atomları serbest bırakılmış ve bütün atomları sabit tutulmuş $Ti_2O_9H_{10}$ atom kümeleri ile temsil edilen (101) ve (001) anataz yüzeyleri üzerinde su ve amonyak adsorpsiyon ve parçalanma reaksiyonlari incelenmiştir. Parçalanma reaksiyonlarını takiben, su ve amonyağın daha önce üzerlerinde H_2O

ve NH_3 parçalanmış sistemler üzerine hidrojen bağları ile adsorpsiyonu da ele alınmıştır.

Bölgesel olarak atomlarının bir kısmı serbest bırakılmış olan (001) $Ti_2O_9H_{10}$ atom kümesi vasıtasıyla anataz destek malzemesinin SCR reaksiyonu üzerindeki etkisi araştırılmıştır. NH_2NO oluşumu $Ti_2O_9H_{10}$ atom kümesi üzerinde saf vanadia üzerindekine kıyasla çok daha düşük aktivasyon bariyerleri ile oluştuğundan, titanyum oksitin SCR reaksiyonundaki rolünün NH_2NO oluşumunu vanadia yüzeyine kıyasla daha düşük aktivasyon bariyerleriyle temin etmek olduğu ileri sürülmektedir. Vanadyum oksitin reaksiyon üzerindeki rolü ise oluşan NH_2NO'yu H_2O ve N_2'ye parçalamak açısından büyük önem taşımaktadır.

Son olarak, vanadia/titania yüzeyini temsil eden $V_2TiO_{14}H_{14}$ atom kümesi üzerinde amonyak adsorpsiyonu çalışılmıştır.

Anahtar Kelimeler: Seçici Katalitik İndirgenme (SCR), NO indirgenmesi, NH_3, Kuantum Kimyasal Hesaplamalar, Elektron Yoğunluk Teorisi (DFT), V_2O_5, TiO_2.

To My Father,

ACKNOWLEDGMENTS

TABLE OF CONTENTS

LIST OF TABLES

LIST OF FIGURES

FIGURE

CHAPTER 1

INTRODUCTION

1.1. SCR Reaction

NO_x, together with SO_x, is one of the most serious atmospheric pollutants which cause serious world ecological problems such as acid rains and town smog (Henry et al., 1989). Most of the NO_x are produced during the combustion process (*thermal NO_x*) by the oxidation of the atmospheric nitrogen at very high temperatures:

$$N_2 + O_2 \rightarrow 2NO \tag{1.1}$$
$$NO + \tfrac{1}{2}\,O_2 \rightarrow NO_2 \tag{1.2}$$
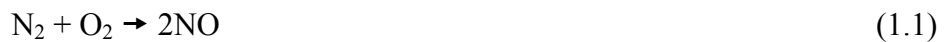
NO_x typically consists of a mixture of 95% NO and 5% NO_2. Other NO_x are formed by the oxidation of the organic nitrogen present in the fuel (*fuel NO_x*) and from HCN formed from fuel nitrogen (*prompt NO_x*) (Cheremisinoff, 1993).

Many efforts have been made to minimize NO_x emission (DeNOxing) either by combustion or post-combustion abatement technologies. Combustion control is achieved by the use of low NO_x burners, flue gas recirculation, fuel reburning, staged combustion and water or steam injection. Post-combustion DeNOxing includes wet methods, as sorption and dry methods, such as catalytic (heterogeneous) or homogeneous reduction (Busca et al., 1998). Although wet methods are insensitive to particulate levels, they are very expensive processes due to their complexity and NO insolubility; also, they require extensive

equipments and usually result in the formation of NO_3^- and other potential water pollutants with only moderate NO_x removal levels. Moreover, wet methods are very sensitive to the flue gas composition of SO_x, NO_x and O_2. On the other hand, the dry methods are simple and low capital processes with high NO_x removal efficiency (<90%). Therefore dry methods are more attractive than wet methods for the reduction of NO_x emission. Among the flue gas treatment methods the selective catalytic reduction (SCR) is best developed and used world-wide for the control of stationary sources due to its efficiency, selectivity and economics (Forzatti, 2001).

Selective Catalytic Reduction (SCR) refers to the process wherein NO_x is reduced by NH_3 over a heterogeneous catalyst in the presence of O_2. The process is termed selective because the NH_3 preferentially reacts with NO_x rather than with O_2. Oxygen, however, enhances the reaction and is a necessary component of the process. The reaction stoichiometry in typical SCR reaction condition is the following:

$$4NH_3 + 4NO + O_2 \rightarrow 4N_2 + 6\ H_2O \qquad\qquad (1.3)$$

Using isotopically labeled reactants, it has been demonstrated that for both vanadia and nobel metal-based catalysts, the two nitrogen atoms of N_2 arise, one from NO and the other from ammonia.

V_2O_5-based catalysts also catalyze the reduction of NO_2 in the presence of oxygen.

$$4NH_3 + 2NO_2 + O_2 \rightarrow 3N_2 + 6\ H_2O \qquad\qquad (1.4)$$

In general, authors agree that under typical SCR conditions, with NH_3/NO_x near 1, few percent oxygen and $T<400^oC$, reaction (1.3) stands for the overall

stoichiometry on vanadia based catalysts. Accordingly, the SCR process occurs when N_2 is produced with selectivity close to 100% and the ratio of converted moles of NO_x and NH_3 is 1 (Busca et al., 1998).

For the SCR process one undesirable reaction is the formation of N_2O which is considered to be a powerful greenhouse gas:

$$2NH_3 + 2O_2 \rightarrow N_2O + 3H_2O \qquad\qquad (1.5)$$

During the SCR process, the injected ammonia can be wasted by catalytic partial oxidation to elemental nitrogen. This is a nonselective reaction.

$$4NH_3 + 3O_2 \rightarrow N_2 + 6H_2O \qquad\qquad (1.6)$$

It can also be completely oxidized to NO. This is another nonselective reaction.

$$4NH_3 + 5O_2 \rightarrow 4NO + 6H_2O \qquad\qquad (1.7)$$

At temperatures below about 100-200°C, the ammonia can also react with the NO_2 present in the process gas producing explosive NH_4NO_3.

$$2NH_3 + 2NO_2 + H_2O \rightarrow NH_4NO_3 + NH_4NO_2 \qquad\qquad (1.8)$$

This reaction can be avoided by never allowing the temperature to fall below about 200°C. The tendency for the formation of NH_4NO_3 can also be minimized by metering into the gas stream less than the precise amount of NH_3 necessary to react stoichiometrically with the NO_x (Heck and Farrauto, 1995).

SCR is the most technically advanced post-combustion technology capable of reducing NO_x emissions to the extremely low levels mandated in many areas of

the world. Compared to other post-combustion NO_x reduction processes, SCR clearly is the most mature process. The technology has been employed throughout the world to reduce emissions generated by gas-, oil-, and low-sulfur-coal-fired utility power plants.

The advantages of the selective catalytic reduction technology can be listed as follows:

- It is one of the few NO_x technologies capable of removing high levels (80% or more) from high-sulfur coals.
- It is applicable to all types of boilers, including cyclone-fired boilers that cannot be retrofitted easily with other types of NO_x control technologies.
- It can be used by new and existing power plants.
- It potentially can create thousand of jobs in various industries (raw material supply, catalyst manufacturing, construction and operation of facilities) while helping save jobs associated with high-sulfur coal mining.
- No chemical by-products that require marketing or off-gases that require regeneration or disposal are produced. (Only nitrogen and water are formed)
- No significant re-engineering of the boiler heat exchange cycle is required.
- No solid adsorbents are required. This eliminates the need for energy-consuming handling and transfer processes.
- Relatively little capital and operating costs are incurred.
- The process relies on a simple chemical reaction. This simplicity improves the overall reliability of the technology.
- SCR is a dry process with few moving parts. The system requires only a few boiler alterations.
- All catalysts perform well at the targeted NO_x removal rates with slip less than 2 ppm under baseline conditions (i.e., 80% NO_x removal) and in many cases the measured slip was below the 1ppm detection limit.

The SCR processes are relatively simple, requiring only a reactor, a catalyst, and an ammonia storage and injection system. An illustration of a simple SCR reactor is given in Figure 1.1. The optimum temperature for the non-catalytic reaction is about $1000^{o}C$. The catalyst effectively reduces the reaction temperature to the range 300 to $500^{o}C$. In order to avoid the need to reheat the flue gas, the reactor is usually located just after the boiler, either before or after the particulate control device (Flagan and Seinfeld, 1988).

Performance criteria for SCR are analogous to those for other catalytic oxidation systems: NO_x conversion, pressure drop, catalyst/system life, cost, and minimum SO_2 oxidations to SO_3. An optimum SCR catalyst is one that meets both the pressure drop and NO_x conversion targets with the minimum catalyst volume. Because of the interrelationship between cell density, pressure drop, and catalyst volume, a wide range of optional catalyst cell densities are needed for optimizing SCR system performance.
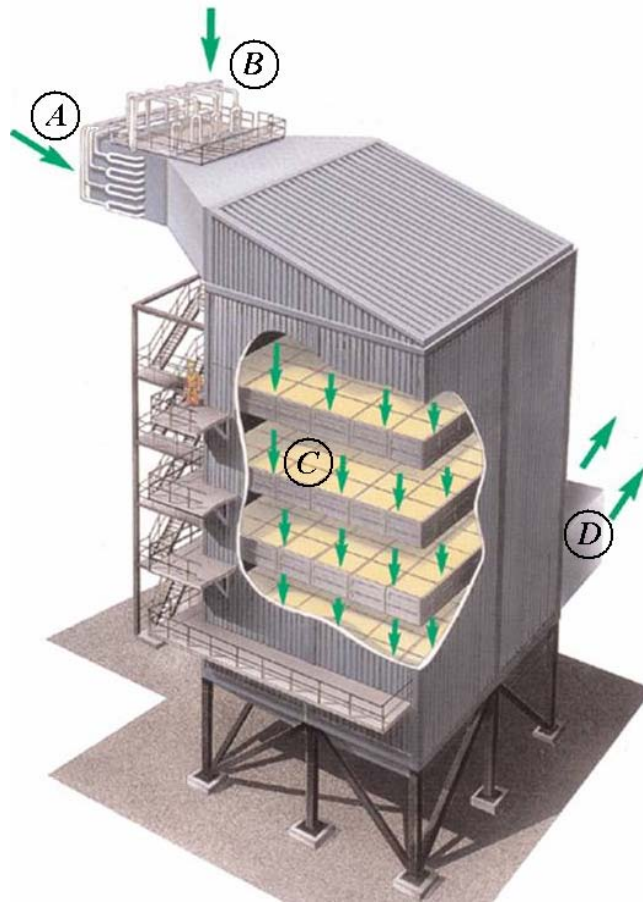
Figure 1.1. A simple SCR reactor, A) Flue gas containing NO_x is admitted from the boiler to the SCR reactor, **B)** Ammonia is added to the flue gas, **C)** The gas mixture flows over catalyst elements, which cause nitrogen oxides and ammonia to react, **D)** The reaction converts the nitrogen oxide to pure nitrogen and water (Figure is taken from the ABB Alstom Power Environmental Systems Brochure).

1.2. SCR Catalysts

Three types of commercial catalysts have been developed for SCR systems: Noble metals, zeolites and metal oxides.

Noble metals which have first been considered for the SCR of NO are very active in the selective reduction of NO_x, but they also oxidize NH_3. For these reasons, noble metal catalysts were soon replaced by metal oxide catalysts for conventional SCR, and are now considered primarily for low temperature and natural gas applications (Forzatti, 2001).

A family of zeolite catalysts has been developed, and is being increasingly used in SCR applications. Zeolites which can function at higher temperatures than the conventional catalysts are claimed to be effective over the range of 350 to 600°C, having an optimum temperature range from 360 to 580°C (Campbell et al., 1991 and Shareef et al., 1992). However, ammonia oxidation to NO_x begins around 450°C and is predominant at temperatures in excess of 500°C. Zeolites suffer the same performance and potential damage problems as conventional catalysts when used outside the optimum temperature range. In particular, at around 550°C the zeolite structure may be irreversibly degraded because of loss of pore density. Zeolite catalysts have not been continuously operated commercially at temperatures above 500°C (Campbell et al., 1991).

The most popular SCR catalyst formulations are those that were developed in Japan in the late 1970s, comprised of base metal oxides such as vanadium pentoxide, V_2O_5, supported on titanium dioxide TiO_2 (Farrauto et al., 1992). As for low temperature catalysts, NO_x conversion rises with increasing temperatures to a plateau and then falls as ammonia oxidation begins to dominate the SCR reaction. However, peak conversion occurs in the temperature range between 300 and 450°C, and the fall-off in NO_x conversion is more gradual than for low temperature catalysis (Speronello et al., 1992). Moreover vanadia/titania catalysts

7

have higher resistance to poisoning by SO_x than the other catalyst formulations. The industrial metal oxide catalysts for the SCR process are based on TiO_2-supported V_2O_5-WO_3 and/ or V_2O_5-MoO_3 oxides. Among metal oxides, pure vanadia and vanadia supported on oxide carriers such as alumina, silica, zirconia and titania (which is choice support nowadays) exist. Every metal oxide which is active in oxidation catalysis can act as an active component in the SCR reaction. Transition metal oxides which are poorly active in oxidation catalysis (such as TiO_2 and ZrO_2) are also poorly active in SCR catalysis (Busca et al., 1998).

It has been found that the best catalyst contains just a few less than a full monolayer of vanadium plus tungsten (or molybdenum) oxides over the TiO_2-anatase support. The amount of vanadium oxide is variable but generally very small (<1% (w/w)) (Alemany et al., 1996).

SCR catalysts are made of a ceramic material that is a mixture of carrier and active components. The two leading shapes of SCR catalyst used today are honeycomb and plate. The honeycomb form usually is an extruded ceramic with the catalyst either incorporated throughout the structure (homogeneous) or coated on the substrate. In the plate geometry, the support material is generally coated with catalyst. When processing flue gas containing dust, the reactors are typically vertical, with down flow of flue gas. The catalyst is typically arranged in a series of two to four beds, or layers. For better catalyst utilization, it is common to use three or four layers, with provisions for an additional layer which is not initially installed.

Although many different types of catalyst compositions and configurations have been developed for SCR process, there is no SCR catalyst that can operate economically over the whole temperature range possible for combustion systems. Therefore, catalyst selection depends largely on the temperature of the flue gas being treated. A given catalyst exhibits optimum performance within a

temperature range of about 300 to 500°C. Below this optimum temperature range, the catalyst activity is greatly reduced, allowing unreacted ammonia to slip through. Above this range, ammonia begins to be oxidized to form additional NO_x. Operations having adequate temperature controls are important, as are uniform flue gas temperatures (Campbell et al, 1991). The active catalytic component and temperature ranges may be classified as:

Low temperature (175-250°C) : Platinum

Medium temperature (260-450°C) : Vanadium

High temperature (350-600°C) : Zeolite

The precious-metal platinum catalysts were primarily developed in the 1960s for operation at temperatures between about 175 and 250°C. However, because of sensitivity to poisons, these catalysts are unsuitable for many combustion applications. Variations in sulfur levels of as little as 0.4 ppm can shift the required catalyst temperature window completely out of a system's operating temperature range. Additionally, operation with liquid fuels is further complicated by the potential for deposition of ammonium sulfate salts within the pores of the catalyst (Speronello et al., 1992). These low temperature catalysts exhibit NOx conversion that rise with increasing temperature, then rapidly drops off, as oxidation of ammonia to nitrogen oxides begins to dominate the reaction.

1.3. Objective of This Study

The objective of this study is to investigate the full reaction sequence for the selective catalytic reduction (SCR) reaction of NO by NH_3 on vanadia/titania catalytic surface by means of density functional theory (DFT) calculations. Firstly, the reaction pathways of the SCR reaction are investigated on pure vanadia surface which represents the active phase of the SCR catalysts. Most of

the experimentalists agree that the SCR reaction follows an Eley-Rideal mechanism, where NO attacks adsorbed NH_3; however there is a disagreement on the activation mode of the ammonia on the catalyst surface. Therefore before continuing with the reaction mechanism, it is desired to determine the activation mode of the ammonia over the catalytic surface. Then, it is aimed to complete the catalytic cycle by introducing NO to the system. After investigating the SCR reaction mechanism on pure V_2O_5, the role of titanium oxide which represents the support of the catalyst on the SCR reaction is investigated by use of an anatase cluster. A cluster model for a vanadia/titania surface is also proposed and studied for ammonia adsorption. Moreover, it is also aimed to develop a computational methodology in the field of catalysis in order to use this powerful and newly developing tool more efficiently.

CHAPTER 2

LITERATURE SURVEY

2.1. Studies on SCR Reaction

2.1.1. Experimental Studies

Although there are several studies carried out on the selective catalytic reduction (SCR) reaction of NO by NH_3 over the V_2O_5 catalytic surface, the complete elucidation of the reaction mechanism has not been achieved. Accordingly, there are two different possible mechanism suggested by different researchers for the SCR reaction of NO by NH_3 over vanadium oxide catalyst surface that are: **1.** Langmuir-Hinshelwood type mechanism.**2.** Eley-Rideal type mechanism.

The Langmuir-Hinshelwood type mechanism was first suggested by Takagi et al. (1976). In their work, they separately studied the elementary steps of the reaction for the elucidation of the reaction mechanism by using volumetric, infrared, x-ray photoelectron spectroscopy, and mass spectroscopy techniques. Accordingly, no adsorption of NO was observed on the V_2O_5 catalyst surface, even when the surface was oxidized by oxygen or reduced by hydrogen. However, when a gas mixture of NO and O_2 was introduced onto the V_2O_5 surface, the adsorption took place and NO_2 was adsorbed onto the surface. Also, NH_3 was adsorbed as NH_4^+ over the catalyst surface. Therefore, as the first step of the SCR reaction, NO oxidized by ambient O_2 was adsorbed as NO_2 on V_2O_5, and NH_3 as NH_4^+, respectively. Then these adsorbates react to form the product via a Langmuir-Hinshelwood type mechanism.

On the other hand, Eley-Rideal type mechanism for the SCR reaction of NO by NH_3 is the other possible mechanism type suggested by several researchers. Inomata et al. (1980) were the first group that suggested this kind of a mechanism. By means of the temperature programmed desorption (TPD) experiments they observed a single desorption peak of NH_3, but for NO they did not. Furthermore, from the pulse chromatographic measurements of the adsorptions of NO and NH_3 they found out that NH_3 is strongly adsorbed whereas NO is hardly adsorbed on V_2O_5 at 150^oC. When NH_3 gas was introduced onto the catalyst treated with NO gas in the absence or in the presence of O_2 at 250^oC, N_2 was not obtained at all as a reaction product, while in the reverse case a considerable amount of N_2 was produced. Also, in the IR spectra, they did not observe any adsorption bonds corresponding to NO, such as NO^+ (ad), NO^- (ad), and NO_2 (ad) species, when NO gas was introduced onto V_2O_5 at temperature higher than room temperature. Nevertheless, when NH_3 gas was introduced onto V_2O_5 surface, they observed peaks contributed to NH_4^+ species. From these results they concluded that the strongly adsorbed NH_3 species on V_2O_5, i.e. NH_4^+ (ad), can react readily with a gaseous NO to form N_2 and H_2O, suggesting an Eley-Rideal mechanism.

Another suggestion for the Eley-Rideal type mechanism was made by Janssen et al. (1987). By means of the isotopic transient studies with oxygen-18 and nitrogen-15, they found out that ammonia did not react with O_2 or O from any source during the reaction and NO did not oxidize to NO_2. For the reaction mechanism it was suggested that both chemisorbed ammonia species and the physisorbed ammonia species were able to react with nitric oxide via an Eley-Rideal mechanism. Chemisorbed ammonia species were defined as being nitrogen-hydrogen-containing species present on the surface during the reaction at 400^oC and physisorbed ammonia species were defined as the result of the reaction of OH groups present on the surface with NH_3. They also suggested that two types of water molecule were formed during the reaction: one was originated from the reaction of gaseous NO with the chemisorbed ammonia species and the other was

12

formed as a result of the dehydration of OH groups present on the surface of the catalyst. Thus, it was concluded that lattice oxygen shared with adjacent sites was involved in the reaction.

In order to probe the catalytic chemistry of nitric oxide reduction by ammonia on V_2O_5 surface, temperature programmed desorption (TPD) and temperature programmed reaction (TPR) studies were conducted by Srnak et al. in 1992. Accordingly, TPR studies of the reaction between nitric oxide and ammonia probed a Langmuir-Hinshelwood step between adsorbed nitric oxide and ammonia under vacuum conditions, whereas powder TPR studies involve an Eley-Rideal step between adsorbed ammonia and gaseous (or weakly adsorbed) nitric oxide. From their results they concluded that both the Langmuir-Hinshelwood and the Eley-Rideal mechanisms may be effective for selective catalytic reduction of nitric oxide, depending on the reaction conditions. Furthermore, the reactivities appear to be comparable for the strongly and weakly adsorbed nitric oxide species in these two mechanisms, respectively, since the reaction is controlled by the activation of ammonia. Under typical SCR reaction conditions the amount of strongly adsorbed nitric oxide is negligible, and the Eley-Rideal mechanism would seem to dominate.

Nan-Yu Topsøe et al. (2001) tried to get insight into the SCR of NO by NH_3 over vanadia/titania catalysts from a combination of Raman and FTIR spectroscopic investigations and density functional theory (DFT) calculations. Significant changes were observed in the surface V-OH and V=O functional groups with varying temperatures. These changes observed in the in situ IR and Raman spectra could be explained by the mobility of the hydrogen atoms at elevated temperatures in accordance with DFT calculations on vanadium oxide clusters. It was shown by the DFT computations that H atoms were bonded more strongly to oxygen atoms that are coordinated to a single vanadium atom (V=O species),

compared to bonding at oxygen atoms that are coordinated to multiple vanadium atoms (V-O-V species).

Schneider et al. (1994) investigated the selective catalytic reduction of NO by NH_3 on high surface area catalyst by diffuse reflectance FTIR spectroscopy coupled with mass spectroscopy under reaction conditions and by temperature-programmed desorption of preadsorbed NH_3 and NO. It was observed that the activity of the catalysts increased with the vanadia loading. It was found that a similarly prepared titania aerogel does not exhibit significant NO conversion in this temperature range (440-545 K).On pure titania aerogel, mainly Lewis-bound ammonia was observed while in the SCR reaction Brønsted-bound ammonia was observed subsequent to NH_3 adsorption at ambient temperature. Similar to Janssen et al. (1987), the results of this research suggests that the binding of NO to the adsorbed ammonium ions is the first step of an Eley-Rideal type of mechanism which takes place in the SCR process.

In 1992 Went et al. studied V_2O_5-TiO_2 (anatase) catalysts under oxidizing and reducing conditions using *in situ* laser Raman spectroscopy (LRS) and temperature-programmed reduction (TPR) and oxidation (TPO). In situ Raman spectroscopy indicated that V_2O_5-TiO_2 catalysts contain monomeric vanadyl and polymeric vanadate species, as well as crystallites of V_2O_5. It was shown by the quantitative analysis of Raman spectra that monomeric species dominated at low vanadia loadings and then react to form polymeric vanadates as vanadium loading increases. If the vanadia loading increases above the dispersive capacity of the TiO_2 support, crystallites of V_2O_5 form. Upon reduction in H_2, Raman spectroscopy indicated that oxygen atoms from terminal V=O groups associated with monomeric and polymeric species are removed preferentially to V-O-V bridging oxygens. It was also reported that only one oxygen atom per vanadium is involved in the reduction/reoxidation process.

Dumesic et al. (1996) investigated the kinetics of SCR of NO by ammonia over a 6 wt% vanadia/titania catalyst in the presence of oxygen. Their reaction scheme involves the adsorption of ammonia on Brønsted acid sites (V^{5+}-OH), followed by the activation of ammonia via reaction with redox sites (V=O). The activated ammonia then reacts with gaseous or weakly adsorbed NO, producing N_2 and H_2O, and leading to partial reduction of the catalyst. The V^{4+-}OH species formed by the SCR process combine to form water and the catalytic cycle is completed by the reaction of the reduced sites with O_2.

Lietti et al. (1998) studied the unsteady-state kinetics of the selective catalytic reduction (SCR) of NO with NH_3 over V_2O_5-WO_3/TiO_2 model catalysts by means of the transient response method. It was reported that the surface heterogeneity must be considered to describe the kinetics of NH_3 adsorption-desorption on TiO_2 supported V_2O_5-based catalysts: a model assuming a non-activated NH_3 adsorption process represented the dynamic data. On the other hand, NO did not adsorb appreciably on the catalyst surface in line with an Eley-Rideal mechanism for the SCR reaction. It was concluded that the rate of the $DeNO_x$ reaction is virtually independent on the NH_3 surface concentration for θ_{NH_3} above a characteristic 'critical' value that is of the same order of magnitude of the V surface coverage. It is explained by the assumption of a 'reservoir' of adsorbed NH_3 species (likely on W and Ti sites) is present on the catalyst surface and is available for the reaction via desorption and subsequent fast readsorption over reactive V-sites, in line with the results of the kinetic data analysis. Moreover, as a result of a comparison among the estimates of the adsorption, desorption and reaction rates calculated at different reactor axial position, temperatures and catalysts it is found that the assumption of equilibrated ammonia adsorption under steady-state $DeNO_x$ conditions is likely incorrect, specifically at high temperatures and over active catalysts.

Blushev et al. (2002) characterized surface vanadia species formed on vanadia/titania catalysts consisting of 0.2-2.6 monolayers of VO_x by FT-Raman spectroscopy under controlled atmosphere, temperature-programmed reduction in hydrogen (TPR), and solubility in diluted HNO_3. Three types of species were observed with the maximum peak temperatures: isolated monomeric species ($\leq$770-780 K), polymeric species (810 K), and bulk amorphous V_2O_5 (852 K). The monomeric species was the most stable in diluted HNO_3 suggesting strong attachment to the titania support. Previously, Went et al. (1990) also studied vanadia catalysts by Raman spectroscopy. Similar to Blushev et al. (2002) it was reported in their study that three types of vanadia species were found to be present on TiO_2 supports: monomeric vanadyls, one and two dimensional vanadate chains, and crystallites of V_2O_5. The morphologies and structures of nanostructurally assembled V_2O_5 doped with Ti as well as of the inverse system, V doped TiO_2 have been studied by Kryukova et al. (1997) using transmission electron microscopy and Raman spectroscopy.

Gasior et al. (1988) investigated the mechanism of the SCR reaction over unsupported vanadium pentoxide catalyst by pulse reaction technique and suggested that ammonia was strongly adsorbed onto the catalytic surface as NH_4^+ ion, whereas, NO was either weakly adsorbed or not adsorbed at all. Therefore, the reaction was believed to be proceeding by an Eley-Rideal type reaction mechanism.

In 1991, Nan-Yu Topsøe suggested the same type of mechanism by conducting FTIR studies on V_2O_5 surface structures and on the adsorption properties. In order to simulate the different states of the catalyst which may be present during a catalytic cycle, the catalyst had been investigated both in oxygen and after exposure to the reactants NO and NH_3 alone or together. The catalyst had also been studied after more extensive pre-reduction in hydrogen. Accordingly, no adsorption of NO was evidenced on the oxidized or the NH_3-reduced surface of

V_2O_5 and adsorption occurred only on the H_2-reduced samples. On a partially reduced catalyst with pre-adsorbed NH_3, NO was observed to oxidize the surface at room temperature. This suggested that NO reduction by NH_3 occurs by an Eley-Rideal type mechanism and V_2O_5 catalyst has an acid-redox function. Their findings did not give any support for the reaction between NO_2 and surface NH_4^+ as postulated by Takagi et al. (1976).

In 1996, Ramis et al. performed FT-IR studies for the selective catalytic reduction of NO_x by NH_3 reaction over the V_2O_5 based catalysts including pure V_2O_5. In their spectra they detected NH_2 vibrations while no adsorbed NO species vibration was observed. They suggested that the main mechanism that leads to reaction products water and N_2 was the reaction between pre-adsorbed ammonia, i.e. NH_2 species, and gaseous NO, via an Eley-Rideal type mechanism.

As in the case of the reaction mechanism, there is not a general agreement on the nature of the surface sites that involve in the selective catalytic reduction of NO by NH_3 over V_2O_5 catalytic surface. This is due to the surface characteristics of the vanadium pentoxide catalyst. The oxide surface is highly dynamic in nature under reaction conditions consisting of double-bonded oxygen sites, Brønsted acidic V-OH sites, and oxygen vacancies being created, used, or inter-converted to one another in the presence of water and the gas phase oxygen. So, for the reaction, there are three different types of adsorbed ammonia species that have been suggested by different researchers: **a)** $V-ONH_2$, **b)** $V-ONH_3$, **c)** $V-ONH_4$. Therefore, it can be concluded that ammonia adsorption over the V_2O_5 catalytic surface may occur either through a Lewis acidic adsorption (as coordinatively bonded NH_3 or NH_2 by abstracting one hydrogen) or by a Brønsted acidic adsorption (as adsorbed NH_4^+ ion) reaction.

Inomata et al. (1980) suggested from the TPD and IR studies that the active site for the ammonia activation is the Brønsted acidic V_s-OH site adjacent to $V^{5+}=O$

site. Ammonia is strongly adsorbed on this site as $NH_4^+(ad)$. Then, gas phase NO reacts with this species to form N_2 and H_2O by reducing the surface to V-OH. The V-OH species are then reoxidized to $V^{5+}=O$ by either gaseous O_2, or bulk V=O species. This suggests that $V^{5+}=O$ sites also play an essential role in the reaction. The mechanism suggested by Inomata et al. (1980) is summarized in Figure 2.1.
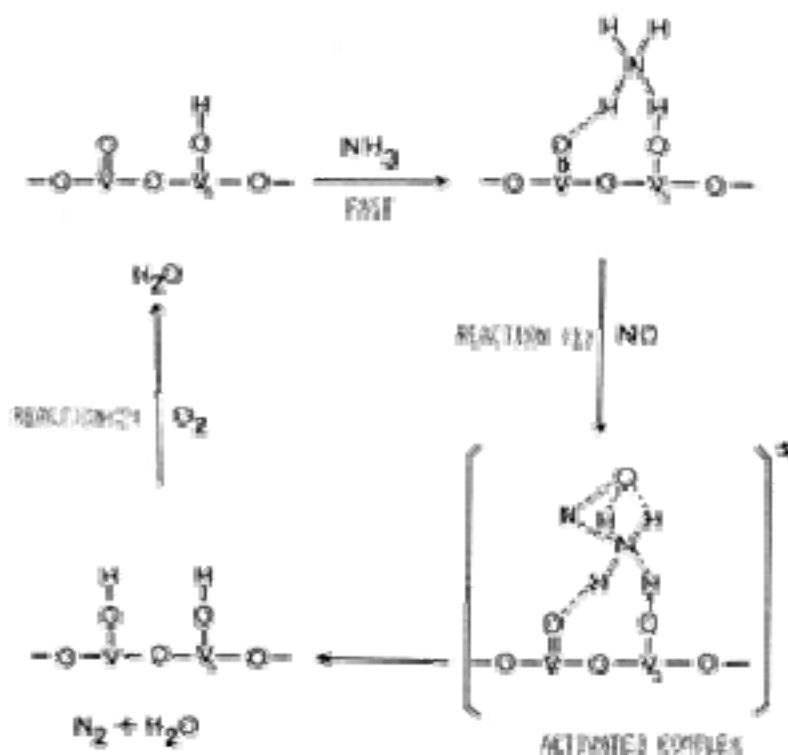
Figure 2.1. Mechanism of the NO-NH₃ reaction on vanadium oxide catalysts proposed by Inomata et al. (1980) in the presence of oxygen.

For the selective catalytic reduction reaction of NO by NH₃ over V_2O_5 catalytic surface, Janssen et al. (1987) found that at least two types of active sites were present on the surface of the catalyst and that these sites were probably due to the presence of vanadium species with valances of both +4 and +5. Two different reactions occur on these different sites: the oxidized sites could be reduced by

ammonia while re-oxidation can be brought about by ambient oxygen, by lattice oxygen from underlying layers, or by the oxygen of NO, depending on the reaction conditions. Therefore the V=O species was considered to be the active sites that were easily reduced. Accordingly, ammonia was adsorbed on this site as V-ONH$_2$ that is proposed as the key intermediate in the SCR reaction by reducing the adjacent V=O site to V-OH. The proposed reaction mechanism is given in Figure 2.2.

Nan-Yu Topsøe (1990) observed a slight intensity increase of the V=O band in the FTIR spectra when the catalyst was reduced by NH$_3$. This was considered as associated with a decrease in V-OH concentration on the surface. And also the IR spectra of ammonia adsorbed on V$_2$O$_5$ in its oxidized and reduced states showed distinct bands attributed to NH$_4^+$ species and weak bands due to the coordinated NH$_3$ species, which in turn suggested that predominantly Brønsted acid sites (V-OH) were present on the surface of oxidized V$_2$O$_5$. Therefore, ammonia was preferentially adsorbed on Brønsted acidic V-OH sites as NH$_4^+$ ion. Moreover, when NO was introduced to the system pretreated by NH$_3$, it was seen that NH$_4^+$ species were preferentially removed indicating that the reaction is predominantly between NO and surface NH$_4^+$ species, in agreement with the proposal of Gasior et al.(1988).
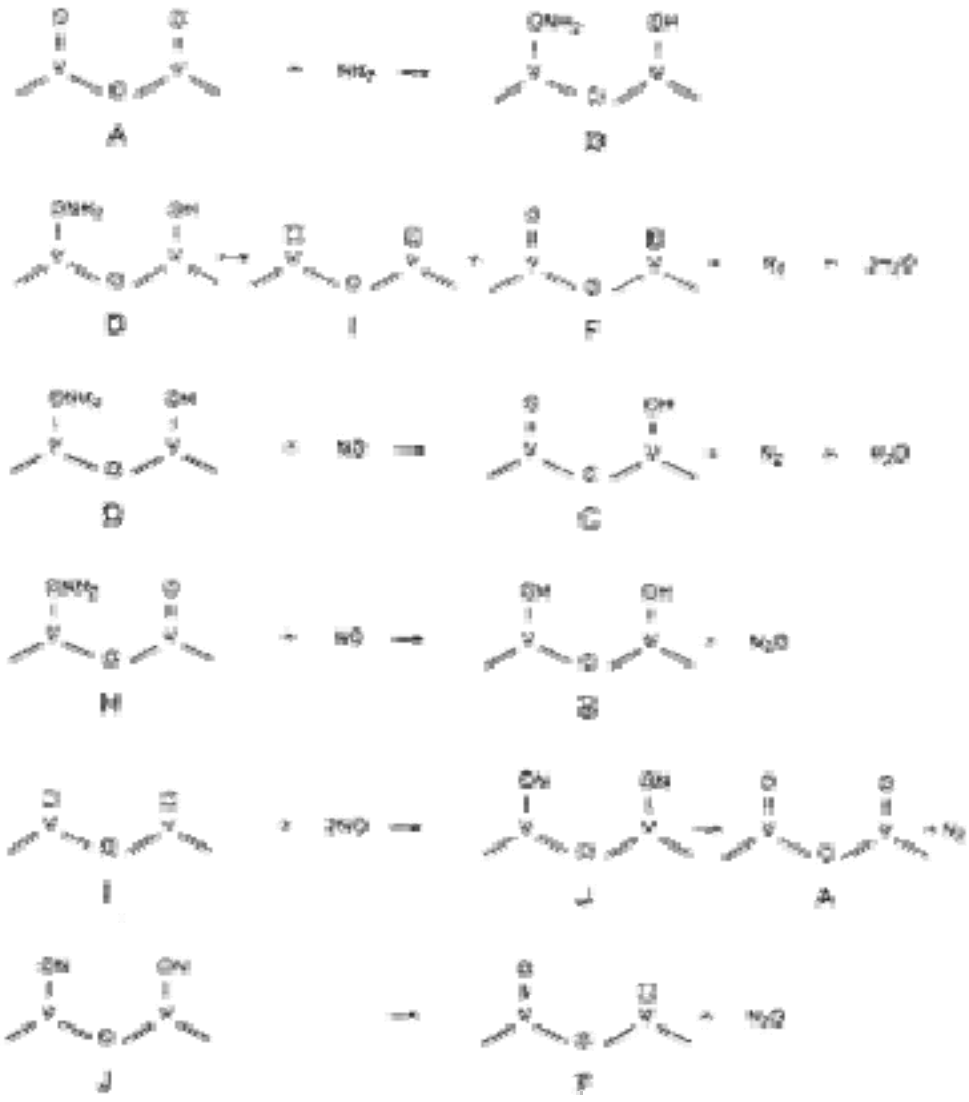
Figure 2.2. Reaction mechanism of the NO-NH$_3$ reaction on V$_2$O$_5$ surface proposed by Janssen et al. (1980).
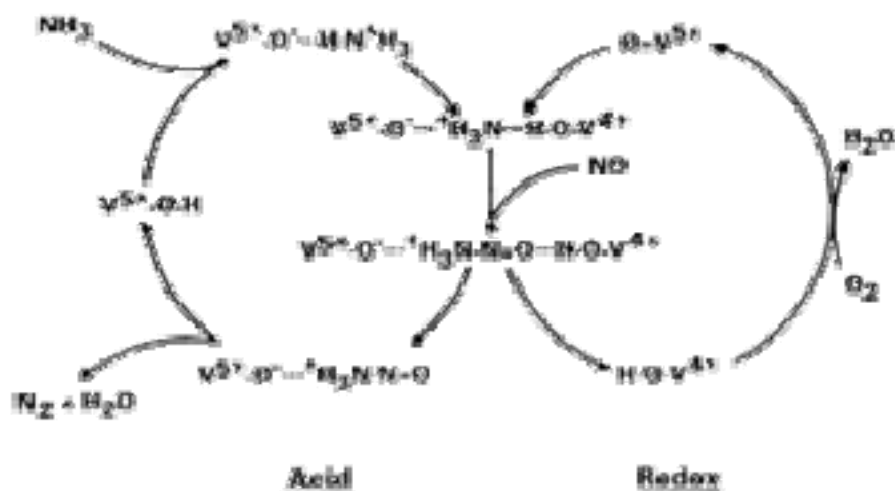
Figure 2.3. Illustration for the reaction mechanism for the SCR over V_2O_5 proposed by Topsøe et al. (1991)

In 1994, by means of the isotopic labeling studies using $^{18}O_2$, $^{15}NH_3$, ^{15}NO, and $^{15}N^{18}O$, Ozkan et al. suggested that ammonia adsorbs on at least three types of sites present on V_2O_5 catalyst surface, which were denoted as types A, B, and C. The type A sites were pairs of V=O centers located on the (010) planes that lead to dissociative adsorption of ammonia to give $V-ONH_2$ and V-OH species. The ammonia species thus created were believed to be short lived, converting quickly to NO and water with an oxygen vacancy and OH group left behind. The type B sites, which were also located on the (010) planes, were thought to be double-bonded oxygen sites neighboring a V-OH group, leading to the formation of $V-ONH_3$ species. These species appeared to have a longer "surface life" and had the ability to couple between themselves to form nitrogen and nitrous oxide or to react with NO to give nitrous oxide. The type C sites were thought to be located mainly on the side planes and to consist of pairs of V-OH groups, leading to the formation of surface ammonium ion species. From the structural specificity studies that link nitrogen selectivity in SCR reaction to the side planes, they

21

concluded that these sites (type C) were the primary sites that reduce NO selectively.

In contrast to these studies, Ramis et al. (1996) observed very intense bonds corresponding to the coordinatively bonded NH_3 mode in the NH stretching region of the adsorbed ammonia on V_2O_5 surface. This was considered to be sensitive to the strength of the Lewis acid-base interaction. Furthermore, they investigated the activity of CuO/TiO_2 catalyst for the SCR reaction and observed only species coordinated on Lewis acid sites. According to the similarity of the catalytic behavior of these materials (CuO/TiO_2 and V_2O_5) in the SCR reaction, they suggested that Brønsted acidity is not a necessary requirement for SCR activity. Ammonia is activated for SCR by coordination over Lewis acidic sites not on the Brønsted acidic V-OH sites and this activated ammonia is easily transformed to amide NH_2 species by the hydrogen abstraction. NH_2 species formed reacts with NO to give rise to reaction products nitrogen and water. The catalytic cycle is closed by re-oxidation of the reduced catalyst by gaseous oxygen. Since amide species is formed during the reaction as an intermediate, they referred to this mechanism as the "amide-nitrosamide" mechanism. The reaction mechanism of the selective catalytic reduction reaction of NO by NH_3 proposed by Ramis et al. (1996) is summarized in Figure 2.4.
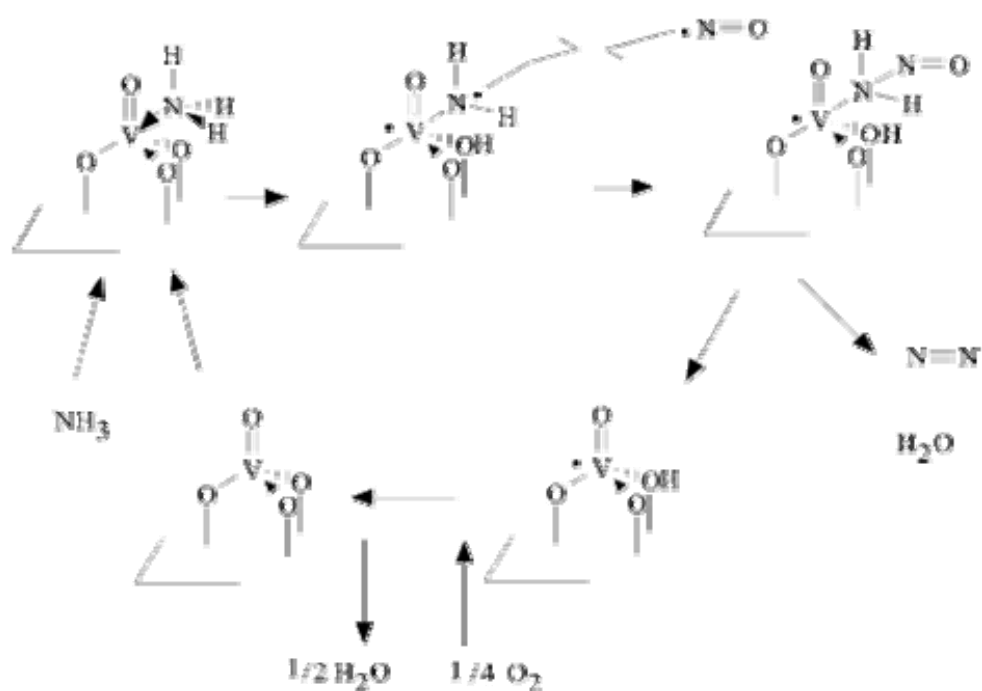
Figure 2.4. The proposed reaction mechanism of Ramis et al. (1996) for the SCR reaction of NO by NH_3.

2.1.2. Theoretical Studies

Although there are several experimental studies performed to elucidate the mechanism of the SCR reaction of NO by NH_3, there is still disagreement concerning the active sites involved in the SCR reaction. There are very few studies that have been carried out to obtain more detailed information about the nature of the active sites theoretically.

In the research carried out by Gilardoni et al. (1997) quantum chemical calculations by using density functional theory (BP86 method) are performed to model the mechanism of selective catalytic reduction of NO by NH_3 on vanadium oxide catalytic surface starting from the ammonia activation over Brønsted acidic

V-OH site. For the calculations a cluster with C_s symmetry was constructed as $V_2O_9H_6$-H with a Brønsted acidic V-OH site. During the study the following computational procedure was followed; the adsorbing molecule was located in the vicinity of the active site of the cluster and then one point equilibrium geometry calculations were performed. At the end of the calculations carried out for the first step of the reaction (Brønsted acidic ammonia adsorption), two different geometries were obtained. By comparing calculated total energies and calculated vibration frequency data, it was concluded that one of the geometries with higher energy and one imaginary frequency is a transition state structure. The other geometry was considered as the global minimum geometry, in other words, equilibrium geometry for the ammonia adsorption over Brønsted acidic V-OH site. The relative energy for this geometry was calculated as -25 kcal/mol. As the second step of the SCR reaction, NO molecule was introduced to the equilibrium geometry of the first step and equilibrium geometry calculation was performed by freezing the structural parameters of: **1.** the oxygen atom bridging the two vanadyl groups, **2.** the vanadium atoms, and **3.** the six O-H groups bonded to the vanadium centers. This led to the release of the adduct H_2NNO (N-nitrosamide) and the formation of two V-OH sites. The heat of this reaction was found to be +18.2 kcal/mol, corresponding to an endothermic process. Then the intermediate formed at the end of this step, undergoes a series of H atom migrations and some isomerisation reactions to yield reaction products N_2 and water. At the end of the DFT calculations carried out for the SCR reaction of NO by NH_3 starting from the NH_3 adsorption over Brønsted acidic V-OH site, Gilardoni et al. concluded that the adsorbed NH_3 (as NH_4^+) is activated by transferring an H to the V^{5+}=O site, which becomes partly reduced. Gaseous or weakly adsorbed NO subsequently reacts with this activated NH_3, leading to the formation of V^{4+}-OH and NH_2NO. In order to complete the catalytic cycle, it was suggested that V^{4+}-OH must be oxidized to V^{5+}=O at the end of the reaction.

Similarly, Anstrom et al. (2002) performed density functional theory (B3LYP method) calculations to probe various adsorption geometries and energies for the interaction of ammonia with hydrogen atoms present on clusters representing vanadium oxide, with the aim of addressing various factors involved in controlling the formation of Brønsted acid sites that interact with ammonia to form NH_4 species. For the calculations, several vanadium pentoxide clusters consisting of one to four vanadium atoms were constructed with different oxidation states of vanadium atoms, +4 and +5. While constructing these clusters, some angles and distances were kept constant. The computational procedure followed by Dumesic et al. was very close to what Gilardoni et al. followed. The adsorbing molecule was located in the vicinity of the active site of the cluster, and geometry optimization calculations were performed to obtain the equilibrium geometries. At the end of the calculations that were performed over the cluster with one vanadium atom (VO_4H_3), it was concluded that ammonia is adsorbed on the vanadia monomers as H-bonded NH_3 species, with an energy change of adsorption equals to -59 kJ/mol. The adsorption of ammonia calculations were also performed on the clusters with the formula of $H-V_2O_7H_4.(H_2O)_2$. As with the VO_4H_3 monomer, the calculations showed that ammonia is adsorbed on these clusters as H-bonded NH_3 species, with adsorption energy changes near -50 kJ/mol. Thus, it was observed that neither of these clusters led to the formation of NH_4^+ ion at the end of the adsorption of NH_3 reaction. In order to address the factors responsible for the adsorption of ammonia to form NH_4 species, they constructed several other clusters containing two to four vanadium atoms with different oxidation states. By means of the DFT calculations performed on these clusters it was concluded that ammonia adsorption as NH_4 is not possible in clusters where the formal oxidation state of the vanadium cations was 4+, over these type of clusters, ammonia is adsorbed as H-bonded NH_3. On the other hand, over the clusters $V_2O_9H_8$ and $V_4O_{16}H_{12}$ in which vanadium has an oxidation state of +5, the adsorbed ammonia forms NH_4 species between two V=O sites, with adsorption energy changes of -112 kJ/mol and -110 kJ/mol, respectively.

Moreover, the total Mulliken charge on the NH_4 species formed was calculated as +0.802 e, suggesting that ammonia was adsorbed as NH_4^+ species.

As a continuation of this work, Anstrom et al. published another article in 2003. In this article, the steps involved in the formation of the adsorbed NH_2NO on the $V_4O_{16}H_{12}$ cluster were investigated and the steps involved in the catalytic decomposition of NH_2NO to form reaction products N_2 and H_2O were addressed. Furthermore, ammonia adsorption energies over three different types of Brønsted acidic sites were calculated. To obtain three different types of the Brønsted acidic sites, hydrogen atom was placed either on the doubly bonded Oxygen atom (O1), or on the bridging oxygen atom between two vanadium atoms (O2), or on the bridging Oxygen atom between three vanadium atoms (O3). At the end of the calculations, it was concluded that the Brønsted acidic site located on the doubly bonded oxygen atom (O1-H site) is the most active site for the ammonia adsorption reaction. For the interaction of NO with the adsorbed ammonia species, Dumesic et al. performed a series of geometry optimization calculations where the N-N bond was constrained at successively shorter distances and all other atoms in the NH_4-NO complex were relaxed fully. Among the optimized geometries in this series, the one with the higher energy was considered as the approximate transition state. By means of the DFT calculations the energy of the approximate transition state was obtained as +4 kJ/mol, and that for the equilibrium geometry was calculated as -25 kJ/mol with respect to the $V_4O_{16}H_{12}$ cluster and gas phase NO and NH_3. From the adsorbed NH_3NHO species, the reaction was preceded by the transfer of two hydrogen atoms to the $V_4O_{16}H_{12}$ cluster which led to the formation of the NH_2NO intermediate. The energy of the approximate transition state was calculated as +48 kJ/mol and that for the adsorbed NH_2NO species on the $V_4O_{16}H_{12}$ cluster was obtained as -87 kJ/mol with respect to the $V_4O_{16}H_{12}$ cluster plus gas phase NH_3 and NO species. At the end of the DFT calculations, it was found out that to form the reaction products N_2 and H_2O, the NH_2NO reaction intermediate must undergo a series of hydrogen-transfer steps in a "push-pull"

manner on the vanadium cluster. In each of those steps, a hydrogen atom is transferred from a VOH group to an adsorbed species with NH_2NO stoichiometry, and a second hydrogen atom is simultaneously transferred from the NH_2NO-stoichiometric species to an adjacent V=O group.

There are few theoretical studies proposing vanadia/titania models. Kachurovskaya et al. (2002) considered cluster models of VO_x/TiO_2 catalytic system based on embedding process of V-ion in the anatase support and isomorphous substitution of two Ti-ions on V-ions are calculated by DFT methods. They concluded that embedding procedure increases the acidic power. The same group (Mikheeva et al., 2002) investigated the molecular structures of the active vanadium phase of the VO_x/TiO_2 supported catalyst by DFT. It is shown that vanadium can be stabilized on the anatase (001) surface both in the tetrahedral and octahedral coordinations with the formation of monoxo- and dioxovanadyl structures. Izumi et al. (2002) reported that the major local structure of low concentrations (1-3 wt% V) of vanadium on TiO_2 was determined to have two terminal oxo groups and in total five oxygen coordination by means of vanadium K-edge XANES and ab initio calculations of the XANES spectra.

Very recently, Jug et al. (2004) investigated the reaction mechanism of the selective catalytic reduction of NO with NH_3 and O_2 to N_2 and H_2O by semiemprical MSINDO calculations. The catalytic surface was modeled by a $V_2O_7H_4Ti_{33}O_{66}$ cluster and full reaction steps including intermediates and transition structures are obtained. Zhanpeisov et al. (2001) employed ab initio quantum chemical studies at the HF/Lanl2dz level to investigate ammonia, NO, and a mixture of the two with vanadia/titania (rutile). Highly dispersed vanadia on titania was simulated by model clusters obtained by the replacement of the six coordinated titanium atom by the six coordinated vanadium atom at the surface. In this way, V=O species having octahedral symmetry with the axial distortions are formed. It was reported in this study that the formation of an adsorbed ammonium

ion is an energetically unfavorable process. It was suggested that the SCR reaction products are formed through the reactions of both adsorbed NO and NH_2 via a Langmiur-Hinshelwood mechanism or the desorbed NH_2 group with NO in gas phase.

2.2. H_2O and NH_3 Adsorption on (101) and (001) Anatase Surfaces

Titanium oxides are used in a wide variety of technological applications where surface properties play a role. Titanium oxide is used in heterogenous catalysis; as a photocatalyst (Teramura et al., 2003 and 2004); in solar cells for the production of hydrogen and electrical energy; as a gas sensor; as a white pigment (e.g. in paints and cosmetic products); as a corrosion protective coating; as an optical coating; in ceramics; in electric devices such as varistors; is important in earth sciences; plays a role in the biocompatibility of bone implants; is being discussed as a gate insulator for the new generation of MOSFETs and as a spacer material in magnetic spin-vawe systems; and finds application in nanostructured form in Li-based batteries and electrochromic devices. It is hope that insight into surface properties on the fundamental level will help to improve materials and device performance in many of these fields. Second, TiO_2 is a preferred system for the experimentalists, because it can be prepared simply by sputtering and annealing. Polished crystals with a high surface quality can be purchased from various vendors. Samples can be reduced easily and the resulting increase in conductivity conveniently prevents charging of this wide-band-gap semiconductor (E_{gap}=3eV). Third, because there is already so much known about the surface of this material, it is a good system to test new techniques and approaches. In the experimental study of Hengerer et al. (2000) on (101) and (001) surfaces carried out by secondary-electron imaging and low energy electron diffraction (LEED) the stability of anatase surfaces are demonstrated and the feasibility of preparing and investigating clean surfaces of this important form of TiO_2 are illustrated.

Three different structures are encountered in the nature: anatase, rutile and brookite. In particular, theoretical calculations deal with the rutile (110) surface, which is the most stable polymorph of titanium dioxide, that is, in turn the most stable polymorph of titanium oxide. However, it is anatase, another polymorph of TiO_2, which is more efficient and more widely used in catalysis and (photo) electrochemistry. Specifically, anatase is thermodynamically stable up to 800°C, and crystallizes in a tetragonal lattice, being six and three the coordination numbers for titanium and oxygen respectively. This structure can be described as chains of TiO_6 octahedra having four common edges (Vittadini et al, 1998).

It is in general agreement that titanium dioxide support has anatase structure (Homann et al., 2004) under SCR conditions and the most stable surface of TiO_2 anatase is (001) surface (Beltran et al., 2001). In addition Kryukova et al. (1997) indicated by using high resolution electron microscopy that there is a good geometric complementary between (010) V_2O_5 and (001) TiO_2-anatase. Therefore, (001) anatase surface is used to model the support of V_2O_5/TiO_2 catalyst in this research and tested for the adsorption properties. The studies in the literature with regard to (mainly focused on (001) surface) the adsportion reactions on this surface are summarized below:

2.2.1. Experimental Studies

There are some experimental studies with regard to the surface properties and the adsorption reactions of titanium dioxide-anatase surface. Lin and Bai (2003) reported by using in situ diffuse reflectance infrared Fourier transform spectroscopy (DRIFTS) that anatase surface is Lewis acidic since V_2O_5 based catalysts and pure TiO_2 powder yield almost the same intensity of Lewis acidity. In addition they indicated that the formation of Brønsted acidity may be related to the existence of water vapor. Bredzona et al. (2004) carried out IR analysis of H-

bonded water on pure TiO$_2$ surface. In the same publication, it is indicated that water adsorption on TiO$_2$ occurs by several mechanisms as the surface is filled. As a first step, there occurs the dissociative adsorption of water which includes the destruction and formation of identical Ti-O and O-H bonds. Preferable sites for molecular water adsorption are Ti^{4+} ions. Adsorbed water molecules form additional H bond with surface OH groups. Primet et al. (1971) indicated molecular water adsorption takes place on anatase as Morterra et al. (1988) suggests a mixed type of adsorption. In the study of Srnak et al. (1992), desorption activation energies for water and ammonia adsorption reactions are estimated from vacuum TPD studies as 11, 18 kcal/mol and 14, 27 kcal/mol, respectively. A heat of desorption value of 50 kJ/mol for water adsorption was reported by Munuera et al. (1972). Sprinceana et al. (1999) carried out a calorimetric study of the acidity and interface effects of tin dioxide layers deposited on another metal oxide and reported a differential heat of 130-150 kJ/mol for ammonia adsorption on anatase. Topsøe et al. (1995) indicated that ammonia adsorbs on the titania surface mainly as coordinated ammonia reflecting predominantly Lewis acid sites are present on pure titania. On the other hand, Ramis et al. (1995, 1996) and Busca et al. (1998) reported that ammonia is activated by coordination over Lewis acidic sites on TiO$_2$ and this activated ammonia is easily transformed to amide NH$_2$ species by the hydrogen abstraction.

2.2.2. Theoretical Studies

There are few theoretical studies about the adsorption reactions and surface properties of anatase (101) and (001) surfaces.

Vittadini et al. (1998) studied the structure and the energetics of water adsorption on the (101) and (001) surfaces at various coverages by use of density functional theory calculations. They have found that on the (101) surface of TiO$_2$

30

nondissociative molecular water adsorption is favored however on the (001) surface for at low coverages, H_2O is adsorbed dissociatively while at high coverages, molecular water adsorption took place, but with a state with half of the H_2O is adsorbed dissocitively and the other half H bonded in a second layer. Previously, Bredow et al. (1995) investigated water adsorption on rutile (110) and anatase (001) surfaces theoretically by means of the semiemprical MO method SINDO1. Kachurovskaya et al. (2002) reported a molecular adsorption energy value on (001) anatase surface and did not study dissociation case. Fahmi et al. (1994) studied water adsorption on various crystallographic faces of TiO_2 anatase by using a periodic Hartree-Fock method. It is reported that titanium oxide is an amphoteric compound. Water adsorbs on the acidic site (the titanium atom), afterwards it dissociates to give hydroxyl groups. In both of these studies it is reported that dissociative water adsorption is favored on (001) anatase. On the other hand, Selloni et al. (1998) indicated by molecular dynamics that molecular adsorption of water is more favorable on (101) surface of anatase. Redfern et al. (2003) also agreed with this finding by using ab initio molecular orbital theory and density functional theory.

It should be noted that ammonia adsorption on (101) and (001) surfaces have not been studied theoretically in the literature.

31

CHAPTER 3

METHODOLOGY

3.1. Density Functional Theory (DFT)

Density functional theory (DFT) is one of the most powerful and elegant methods for calculating the ground state total energy which enables:

- Unique opportunity of investigating the catalytic surfaces at atomic level,
- Atomic level perspective of the catalyst surface leading to the identification of the surface intermediates which can not be detected by current experimental techniques,
- Determination of the energetics of various reactions and prediction of reliable reaction models (Gokhale et al., 2004).

In density functional theory the total energy of a system is expressed as a functional of the total electron density. Because of the crude treatment of the kinetic energy term, i.e. the absence of molecular orbitals, the accuracy of these early attempts was far from satisfactory. It was not until the 1960's that an exact theoretical framework called density functional theory (DFT) was formulated by Kohn and Sham (1965) that provided the foundation for accurate calculations. Earlier, motivated by the search for practical electronic structure calculations, Slater (1951) had developed an approach, later to become the Xα method, which was originally intended as an approximation to Hartree-Fock theory. Today, the Xα method is generally viewed as a simplified form or precursor of density functional theory.

DFT offers a powerful and elegant method for calculating the ground-state total energy and electron density of a system of interacting electrons. The system may range in complexity from a single atom to a complex system together with the atoms of the solid surface on which they are about to be adsorbed and where they will react with one another, guided by the total energy. The whole theory is based on *functional* (which means a function of a function) of the electron density, which therefore plays the central role. However, the key functional, which describes the total energy of the electrons as a functional of their density, is not known exactly: the part of it which describes electronic *exchange and correlation* has to be approximated in practical calculations.

The existence of correlations between the particles, the main formal difficulty encountered in treating a materials problem in quantum mechanics, is a familiar one in many contexts. The positions and motions of the particles that make up a molecule or material are correlated because the particles interact with each other and exert forces upon each other as they move. In quantum mechanics, the situation is further compounded by the mysterious forces that devolve from the Pauli Exclusion Principle governing electrons. This causes correlations to appear even between (fictitious) noninteracting particles that have no direct interaction with each other. Such forces are referred to as *exchange forces* because they have to do with the set of rules in quantum mechanics that govern what happens when the labels characterizing indistinguishable particles are exchanged.

Whether due to interactions (e.g., the Coulomb force) or exchange, correlations can be characterized as either long- or short-range. The former can be dealt with by averaging techniques and a mean-field or a self-consistent field (meaning that the field experienced by an atom depends on the global distribution of atoms). Short-range correlations involve the local environment around a particular atom, i.e., deviations of the local environment from average behavior, and are much more difficult to treat. In large part, the central problem of quantum methods in

chemistry and condensed matter physics has been the search for more and more accurate ways of incorporating short-range correlations into mean-field theory. The massive CPU requirement of codes that employ modern methods such as coupled clusters or Quantum Monte Carlo bear witness to the degree of difficulty of the problem. These methods are applicable only to relatively small molecules or very simple crystalline solids and their scaling properties as the system size increases are very unfavorable.

Fortunately, the fine details of short range correlations are often of only minor importance so that a theory based on the concept of a mean or self-consistent field is sufficiently accurate for many purposes. Where this is not the case, as in the high temperature ceramic superconductors, or valence-mixed solids, one refers to strongly correlated systems, implying that the short-range correlations between electrons due to exchange and their mutual Coulomb repulsions must be accounted for very accurately even if the qualitative features of observed behavior are to be reproduced.

Several promising methods of dealing with the problem of strong correlations have been developed in recent years but this is still at the cutting edge of research in condensed matter physics and none of these methods is quite ripe for inclusion for general software tools. An important advance in the calculation of the energy of collections of atoms and the forces on each atom was made by Kohn and Sham (1965), who showed how a mean-field theory could be applied to this problem. In their method, the electron density plays a crucial role so that, although the term has more general applicability, the Kohn-Sham method is commonly referred to as density functional theory (DFT). This has since advanced to become a very important method for determining the energy of many-electron, and therefore many-atom systems. In addition, Kohn-Sham density functional theory is equally applicable to molecules (bounded collections of atoms) and crystalline materials (where a specific unit cell is repeated throughout space).

In the density functional theory, the energy is not written in terms of the many-electron wavefunction as is conventional in quantum chemistry, but as a functional of the electron density. Kohn and Sham proposed that the total energy of an n-electron system can be written without approximations as:

$$E_{el} = -\frac{1}{2}\sum_i \int \phi_i(\vec{r}_1)\nabla^2\phi_i(\vec{r}_i)d\vec{r}_1 + \sum_A \int \frac{Z_A}{\left|\vec{R}_A - \vec{r}_1\right|}\rho(\vec{r}_i)d\vec{r}_1 + \frac{1}{2}\int \frac{\rho(\vec{r}_1)\rho(\vec{r}_2)}{\left|\vec{r}_1 - \vec{r}_2\right|}d\vec{r}_1 d\vec{r}_2 + E_{xc}$$

(3.1)

the first term in equation (3.1) represents the kinetic energy of n noninteracting electrons with the same density $\rho(\vec{r}_1) = \sum_i \phi_i(\vec{r}_1)\phi_i(\vec{r}_1)$ as the actual system of interacting electrons. The second term accounts for the electron-nucleus attraction and the third term for the Coulomb interaction between the two charge distributions $\rho(\vec{r}_1)$ and $\rho(\vec{r}_2)$. The last term contains the exchange-correlation energy and can be expressed in terms of the spherically averaged exchange-correlation hole functions $\overrightarrow{\rho}_x^{\gamma\gamma'}(\vec{r}_1,s)$ as:

$$E_{xc} = \sum_\gamma \sum_{\gamma'} -4\pi/2\int \frac{\overrightarrow{\rho}_1^{\gamma}(\vec{r}_1)\overrightarrow{\rho}_1^{\gamma\gamma'}(\vec{r}_1,s)}{s}d\vec{r}_1 s^2 ds$$

(3.2)

where the spin indices γ and γ' both run over a α-spin as well β-spin and $s = \left|\vec{r}_1 - \vec{r}_2\right|$ the one electron orbitals, $\left\{\phi_i(\vec{r}_1); i=1,...,n\right\}$ of equation (3.1) are solutions to the set of one-electron Kohn-Sham equations:

$$\left[-1/2 \nabla^2 + \sum_A \frac{Z_A}{\left| \vec{R}_A - \vec{r}_1 \right|} + \int \rho(\vec{r}_2) + V_{xc} \right] \phi_i(\vec{r}_1) = h_{KS} \phi_i(\vec{r}_1) = \varepsilon_i \phi_i(\vec{r}_1)$$

(3.3)

where the exchange-correlation potential V_{xc} is given as the functional derivative of E_{xc} with respect to the density:

$$V_{xc}[\rho] = \delta E_{xc}[\rho]/\delta\rho$$

(3.4)

the hole function $\overrightarrow{\rho_x^{\gamma\gamma'}}(\vec{r}_1, s)$ contains all information about exchange and correlation between the interacting electrons as well as the influence of correlation on the kinetic energy. The interpretation of $\overrightarrow{\rho_x^{\gamma\gamma'}}(\vec{r}_1, s)$ is that an electron at $\vec{r}_1$ to a larger or smaller extend will exclude the other electrons from approaching within a distance s. the extend of exclusion or screening increases with the magnitude of $\overrightarrow{\rho_x^{\gamma\gamma'}}(\vec{r}_1, s)$. Examples of the hole function are shown in Figure 3.1 for $\gamma = \gamma`$, part a, as well as $\gamma \neq \gamma`$, part b. The intricate function $\overrightarrow{\rho_x^{\gamma\gamma'}}(\vec{r}_1, s)$, can in practice only be obtained from an exact solution to the Schrödinger equation of our n-electron system. The set of one electron Kohn-Sham equations is a consequence of limited value for exact solutions to many-electron systems. They form, however, the starting point for an approximate treatment in which $\overrightarrow{\rho_x^{\gamma\gamma'}}(\vec{r}_1, s)$ is replaced by model hole functions. The form of the exact hole function $\overrightarrow{\rho_x^{\gamma\gamma'}}(\vec{r}_1, s)$ is not known in detail. Nevertheless, a number of properties of $\overrightarrow{\rho_x^{\gamma\gamma'}}(\vec{r}_1, s)$ can be deduced from general considerations. It can readily be shown that the spherically averaged (Coulomb) hole-correlation functions $\overrightarrow{\rho_x^{\gamma\gamma'}}(\vec{r}_1, s)$ have the following properties:

$$4\pi \int \vec{\rho}_x{}^{\gamma\gamma'} (\vec{r}_1, s)_1 s^2 ds = 0 \qquad\qquad \text{when } \gamma \neq \gamma` \qquad\qquad (3.5a)$$

whereas the corresponding (Fermi) functions $\overrightarrow{\rho}_x{}^{\gamma\gamma'} (\vec{r}_1, s)$ satisfy the normalization condition:

$$4\pi \int \vec{\rho}_x{}^{\gamma\gamma'} (\vec{r}_1, s)_1 s^2 ds = 1 \qquad\qquad \text{when } \gamma = \gamma` \qquad\qquad (3.5b)$$

Further, the Fermi contributions:

$$\vec{\rho}_x{}^{\gamma\gamma'} (\vec{r}_1, 0) = \vec{\rho}_1{}^{\gamma} (\vec{r}_1) \qquad\qquad (3.5c)$$

The two Coulomb functions $\vec{\rho}_x{}^{\alpha\beta} (\vec{r}_1, 0)$ and $\vec{\rho}_x{}^{\beta\alpha} (\vec{r}_1, 0)$ are in general considered to be smaller than $\vec{\rho}_x{}^{\gamma\gamma'} (\vec{r}_1, 0)$ although different from zero. They cannot be related to $\vec{\rho}_1{}^{\gamma} (\vec{r}_1)$ in a simpler way.

The model hole function are in general constructed in such a way that the constraints given in equations 3.5a to 3.5c are satisfied. Thus, the Fermi function of Figure 3.1 (a) with $\gamma = \gamma`$, is seen to satisfy the constraints of equations 3.5b & 3.5c, whereas the Coulomb Function of Figure3.1 (b) with $\gamma \neq \gamma`$ satisfies equation 3.5a.
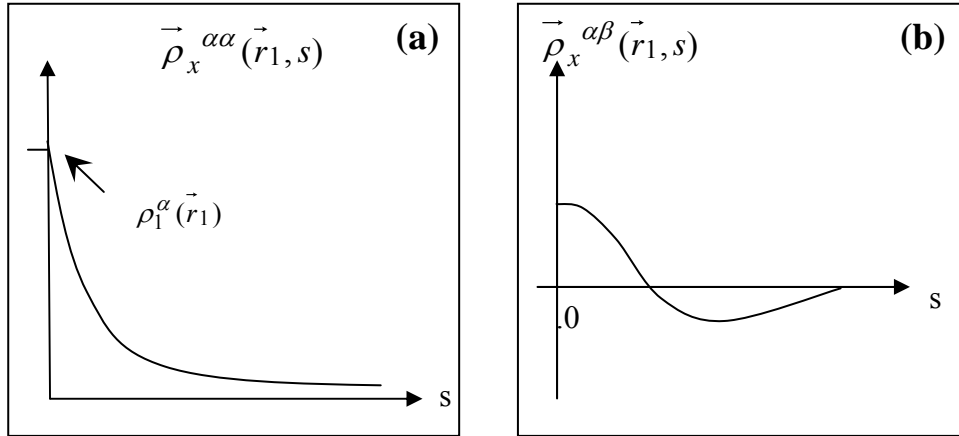
Figure 3.1. (a) Fermi hole function as a function of the interelectronic distance. **(b)** The Coulomb hole function as a function of the interelectronic distance.

3.1.1. Local Density Methods

In the Local Density Approximation (LDA) it is assumed that the density locally can be treated as a uniform electron gas, or equivalently that the density is a slowly varying function. The exchange-correlation energy for the homogeneous electron gas can be written as:

$$E_{xc}^{LDA} = E_x^{LDA} + E_c^{LDA} \tag{3.6}$$

the first term, representing the exchange energy, has the form:

$$E_x^{LDA} = -9/4\alpha_{ex}[3/4\pi]^{1/3}\sum_\gamma \int \left[\rho_1^\gamma(\vec{r}_1)\right]^{4/3} d\vec{r}_1 \tag{3.7}$$

where the electron gas value for the exchange scale factor α_{ex} is 2/3. The exact exchange energy in the Kohn-Sham theory is simply E_{xc} corresponding to single

determinantal wave function constructed from the exact Kohn-Sham orbitals. The second term, representing the correlation energy, has the form:

$$E_c^{LDA} = \int \rho_1(\vec{r}_1)\varepsilon_c\left[\rho_1^\alpha(\vec{r}_1)\rho_1^\beta(\vec{r}_1)\right]d\vec{r}_1 \qquad (3.8)$$

where $\varepsilon_c\left[\rho_1^\alpha,\rho_1^\beta\right]$ represents the correlation energy per electron in a gas with the spin densities ρ_1^α and ρ_1^β. The specific correlation energy, $\varepsilon_c\left[\rho_1^\alpha,\rho_1^\beta\right]$, is not known analytically. However, approximations of increasing accuracy have been developed.

Simplified versions of LDA were known long before the formal development of DFT. Of particular importance is Hartree-Fock-Slater, or Xα. This method is retains only the exchange part (see equation 3.7) of the total expression for the exchange-correlation energy given in equation 3.6 and adopts in many cases values for the exchange scaling factor that differs somewhat from 2/3.

The exchange-correlation hole functions for the homogeneous electron gas satisfy the general constraints given in equation 3.5 and can thus be used as models for calculations on atoms and molecules by substituting the corresponding (in homogeneous) electron densities into the expression for the exchange-correlation energy in equation 3.6.

The LSDA approximation in general underestimates the exchange energy by ~10%, thereby creating errors which are larger than the whole correlation energy. Electron correlation is furthermore overestimated. Despite the simplicity of the fundamental assumptions, LSDA methods are often found to provide results with accuracy similar to that obtained by wave mechanics HF methods.

3.1.2. Gradient Corrected Methods

Improvements over the LSDA approach have to consider a non-uniform electron gas. A step in this direction is to make the exchange and correlation energies dependent not on the electron density, but also on derivatives of the density. Such methods are known as Gradient Corrected or Generalized Approximation (GGA) methods (a straightforward Taylor expansion does not lead to an improvement over LSDA, it actually makes things worse, thus the name generalized gradient approximation). GGA methods are also sometimes referred to as non-local methods, although this somewhat misleading since the functionals since the functionals depend only on the density (and derivatives) at a given point, not on a space volume as for example the Hartree-Fock exchange energy.

Perdew and Wang (PW86) proposed modifying the LSDA exchange expression to that shown in equation 3.9, where x is a dimensionless gradient variable, and a, b, c being suitable constants (summation over equivalent expressions for the α and β densities is implicitly assumed).

$$\varepsilon_x^{PW86} = \varepsilon_x^{LDA}(1 + ax^2 + bx^4 + cx^6)^{1/15}$$
$$x = \frac{|\nabla\rho|}{\rho^{4/3}}$$
(3.9)

Becke proposed a widely used correction (B or B88) to the LSDA exchange energy, which has the correct $-r^{-1}$ asymptotic behavior for the energy density (but not for the exchange potential).

$$\varepsilon_x^{B88} = \varepsilon_x^{LDA} + \Delta\varepsilon_x^{B88}$$
$$\Delta_x^{B88} = -\beta\rho^{1/3}\frac{x^2}{1 + 6\beta x \sinh^{-1} x}$$
(3.10)

The β parameter is determined by fitting to known atomic data and x is defined in equation 3.10. Another functional form (not a correction) proposed by Becke and Roussel (BR) has the form:

$$\varepsilon_x^{BR} = -\frac{2 - 2e^{-ab} - abe^{-ab}}{4b}$$

$$a^3 e^{-ab} = 8\pi\rho$$

$$a(ab-2) = b\frac{\nabla^2\rho - 2D^2}{\rho} \qquad (3.11)$$

$$D = \sum_i^N |\nabla\phi_i|^2 - \frac{(\nabla\rho)^2}{4\rho}$$

This functional contains derivatives of the orbitals, not just the gradient of the total density, and is computationally slightly more expensive. Despite the apparent difference in functional form, exchange expressions 3.10 & 3.11 have been found to provide results of similar quality.

Perdew and Wang have proposed an exchange functional similar to B88 to be used in connection with the PW91 correlation functional given below.

$$\varepsilon_x^{PW91} = \varepsilon_x^{LDA}\left(\frac{1 + xa_1 \sinh^{-1}(xa_2) + (a_3 + a_4 e - bx^2)x^2}{1 + xa_1 \sinh^{-1}(xa_2) + a_5 x^2}\right) \qquad (3.12)$$

where $a_{1\text{-}5}$ and b again are suitable constants and x is defined in equation 3.9.

There have been various gradient corrected functional forms proposed for the correlation energy. One popular functional (not a correction) is due to Lee, Yang and Parr (LYP) and has the form:

$$\varepsilon_c^{LYP} = -a\frac{\gamma}{(1+d\rho^{-1/3})} - ab\frac{\gamma e^{-c\rho^{-1/3}}}{9(1+d\rho^{-1/3})\rho^{8/3}}$$

$$\times \begin{bmatrix} 18(2^{2/3})C_F(\rho_\alpha^{8/3} + \rho_\beta^{8/3}) - 18\rho t_w \\ + \rho_\alpha(2t_w^\alpha + \nabla^2\rho_\alpha) + \rho_\beta(2t_w^\beta + \nabla^2\rho_\beta) \end{bmatrix}$$

$$\gamma = 2\begin{bmatrix} 1 - \frac{\rho_\alpha^2 + \rho_\beta^2}{\rho^2} \end{bmatrix}$$

$$t_W^\sigma = \frac{1}{8}\left(\frac{|\nabla\rho_\sigma|^2}{\rho_\sigma} - \nabla^2\rho_\sigma \right)$$

(3.13)

where the a, b, c and d parameters are determined by fitting to data for the helium atom. The t_w functional is known as the local Weizsacker kinetic energy density. Note that the γ-factor becomes zero when all the spins are aligned ($\rho = \rho_\alpha$, $\rho_\beta = 0$), i.e., the LYP functional does not predict any parallel spin correlation in such a case (e. g. the LYP correlation energy in triplet He is zero).

Perdew proposed a gradient correction to the LSDA result. It appeared in 1986 and is known as by the acronym P86. Then the formalism proposed by Perdew was modified by Perdew and Wang in 1991, this modified form of the formalism is known as PW91 or P91.

It should be noted that several of the proposed functionals violate fundamental restrictions, such as predicting correlation energies for one-electron systems (for example P86 and PW91) or failing to have the exchange energy cancel the coulomb self-repulsion.

3.1.3. Hybrid Methods

Since the GGA methods give a substantial improvement over LDA, a generalized version of the Half-and-Half method may be defined by writing the exchange energy as a suitable combination of LSDA, exact exchange and a gradient correction term. The correlation energy may similarly be taken as the LSDA formula plus a gradient correction term.

$$E_{xc}^{B3} = (1-a)E_x^{LSDA} + aE_x^{exact} + b\Delta E_x^{B88} + E_c^{LSDA} + c\Delta E_x^{GGA} \tag{3.14}$$

Models which include exact exchange are often called hybrid methods, the names Adiabatic Connection Model (ACM) and Becke 3 parameter functional (B3) are examples of such hybrid models defined by equation 3.14. The a, b, c parameters are determined by fitting to experimental data and depend on the form chosen for E_c^{GGA}, typical values are a~0.2, b~0.7 and c~0.8. Owing to the substantially better performance of such parameterized functionals the Half-and-Half model is rarely used anymore. The B3 procedure has been generalized to include more fitting parameters; however, the improvement is rather small.

3.1.4. Applications of DFT

There are two general approaches for modeling surface chemistry with quantum mechanics: the cluster approach and the extended band surface (or slab) approach. In the cluster approach, the local molecular fragment orbitals are explicit, thus making the local chemical interaction, chemical bonding, and charge transfer mechanism between the adsorbate and the metal surface orbitals very easy to elucidate. This detailed level of focus, however, makes is difficult to treat the bulk electronic structure. The extended band surface approach provides a more accurate representation of the materials electronic structure. The cluster approach,

instead of a continuous conduction and valance bands, is based on discrete orbitals which have specific energy gaps.

Both cluster, as well as the slab approaches, will likely to play invaluable roles in the future toward the quantitative prediction of transition metal surface chemistry.

3.1.5. Assessment of DFT methods

The status of density functional calculations for solids, surfaces, and molecules can be characterized as follows.

3.1.5.1. Capability

Like Hartree-Fock methods, density functional calculations provide structural, energetic, and vibration properties. More than Hartree-Fock calculations, density functional calculations enable also the prediction of electronic, optical, and magnetic properties of condensed phases.

3.1.5.2. Generality

The density functional approach is applicable to all atoms of the periodic table, provided relativistic effects are taken into account for heavier elements such as third-row transition metals, rare-earths, and actinides. The approach can be used for metallic, covalent, and ionic bonds. Its greatest strength is metallic condensed systems, yet its range also includes organic molecules. With the inclusion of gradient corrections for the exchange-correlation term, even weaker interactions

such as hydrogen bonds can be reasonably well described. Furthermore, so-called "difficult" molecules such as ozone seem to be treated by density functional methods with the same level of accuracy as other molecules. Within molecular applications, the approach is particularly useful for organometallic systems. Thus, in terms of generality and robustness, density functional theory seems to be superior to the Hartree-Fock approach. Local density functional calculations do encounter problems for narrow-gap insulators and certain oxides. The LDA tends to overemphasize the metallic character and one needs to be careful in the interpretation of the density functional one-electron energies. Furthermore, weaker bonds such as hydrogen bonds are significantly overestimated in the LDA. The primary results of density functional calculations are the electron density, the spin density, the total energy, and the one-particle energies and wave functions. From these quantities, one can derive important electronic, optic and magnetic properties including dipole (and higher) moments, polarizabilities and hyper-polarizabilities, and magnetic moments. LDA calculations for systems in their electronic ground state can be used to estimate electronic excitation energies including work functions, optical and UV spectra, and core level spectra for solids, surfaces, and molecules.

3.1.5.3. Accuracy

Quite consistently, for a great number of strong bonds in solids, molecules, and surfaces, interatomic equilibrium distances are predicted by precise density functional calculations to within about 0.02 A of experiment; bond angles and dihedral angles are found within a few degrees of their experimental values. Within the local density approximation, binding energies are typically overestimated, sometimes by as much as a factor of two. Inclusion of non-local gradient corrections improves the values of binding energies and brings them to within about 10 kJ/mol of experiment. The results obtained at this level of theory

are comparable with sophisticated correlated quantum mechanical methods such as coupled cluster theory. Vibration frequencies are predicted to within 10-50 cm^{-1}. At present, there is no clear theoretical path that would allow the systematic improvement of the accuracy of density functional methods. This is a major conceptual difference to Hartree-Fock based methods, where at least in principle there is a way for systematic improvements. Practical density functional calculations involve numerical integrations in addition to the evaluation of analytical expressions. These numerical integrations introduce a numerical noise that can be noticed, for example, in geometry optimizations of highly flexible molecules. By increasing the size of the numerical grid, this numerical noise can be controlled, though at the expense of computational effort. This is in contrast to Hartree-Fock methods, which are usually implemented in a completely analytical way. Thus, the numerical precision of Hartree-Fock calculations is limited by the machine precision (typically 14 decimal figures) whereas the precision of density functional calculations is governed by the grid resolution. One could argue that if a theory has a certain inherent error compared with experiment, any computational approach that gives results within that error range is acceptable and any improvement in numerical precision has no physical meaning. On the other hand, it can be desirable, for example in the investigation of subtle trends, to have a high numerical precision.

3.1.5.4. System Size

Density functional calculations are possible for systems of the order of 100 atoms. By exploring point-group symmetry, calculations for clusters of over 1000 atoms have been demonstrated for fixed geometries. While the self-consistent-field procedure converges typically in 10-20 iterations for organic materials and semiconductors, metallic systems and especially magnetic transition metals such

as Fe and Ni are very difficult to converge. In practice, this limits the size of systems that can be treated to perhaps less than 60 atoms per unit cell or cluster.

3.1.5.5. Tractable Time Scale

Recently, Density functional calculations have become possible for studying dynamic phenomena. However, for a system with about 100 atoms, accurate density functional calculations are about 1000 times slower than force field calculations, thus reducing the accessible time scales to the range of picoseconds. In practice, the Car-Parrinello method is presently used for structure optimizations by simulated annealing rather than for dynamic simulations, which has been done so far only for a few cases.

3.1.5.6. Computational Efficiency

Depending on the system under investigation, for example a metallic alloy or a molecular crystal, density functional theory can be implemented in quite different ways thus leading to efficient methods for particular materials. On the other hand, practical Hartree-Fock methods require the use of Gaussian basis functions, which can be fairly inefficient, for example for close-packed systems. Thus, in general, density functional theory tends to be computationally more efficient than Hartree-Fock calculations. Without doubt, compared with correlated post-Hartree-Fock methods, density functional calculations are by far more efficient computationally, scaling at worst with a third power in the number of basis functions. In fact, significant effort is dedicated to the development of so-called order-N methods, i.e. methods for which the computational effort increases linearly with system size. Such methods have been successfully demonstrated, yet the pre-factor is

rather large so that these methods are competitive with conventional density functional implementations only for systems with several hundred atoms. In molecular calculations it can be important to calculate vibration frequencies in order to determine ground state structures, transition states, and to predict infrared spectra. In Hartree-Fock theory, this approach is well established, whereas the evaluation of vibration frequencies (i.e. the calculation of the second derivatives of the total energy with respect to nuclear displacements) for molecular density functional is been done by a finite difference technique using analytic first derivatives. This is computationally not very efficient compared with analytical methods. While this type of calculation has been used for density functional methods within the pseudopotential plane wave approach for some time, the implementation of analytic second derivatives in localized orbital density functional calculations is a fairly recent development. However, this type of calculation is quite time consuming and may require supercomputer resources for larger molecules.

3.2. Surface Model and Calculation Method

Quantum chemical calculations employing DFT (Kohn and Sham, 1965) were conducted to investigate the energetics of the reaction of ammonia with nitric oxide over a finite vanadium oxide cluster ($V_2O_9H_8$) representing the (010) surface of V_2O_5. To investigate the role of TiO_2 support on the SCR, (001) and (101) surfaces of TiO_2 are represented by relaxed and fixed $Ti_2O_9H_{10}$ clusters and studied for the adsorption of small molecules. In addition a model for vanadia/titania catalyst surface is proposed by a $V_2TiO_{14}H_{14}$ cluster. This cluster approach is a well known and successful approach applied in quantum chemical calculations (van Santen et al. 1995). DFT calculations were conducted using Becke's (Becke 1988, 1989) three-parameter hybrid method involving the Lee, Yang, and Parr (1988) correlation functional (B3LYP) formalism. The basis set

employed in the DFT calculations was 6-31G** provided in SPARTAN'04 (Wavefunction Inc.).

A $V_2O_9H_6$ cluster was first obtained from (010) surface by cutting out V_2O_9 part and saturating all of the peripheral oxygen atoms by hydrogen atoms as described by Uzun (2003). This cluster size is significantly larger than the molecular sizes of ammonia, nitric oxide, and SCR products, so that the chemisorption properties of the surfaces should be minimally altered. Moreover, Michalak et al. (1997) showed that this size of the cluster gives a very reasonable description of the local electronic structure near the V_2O_5 (010) surface. A similar approach was also applied by Anstrom et al. (2002, 2003).

Both Lewis and Brønsted acid sites of the vanadia cluster were studied following the above methods for ammonia adsorption. Neutral clusters are employed in DFT computations. Lewis acidic $V_2O_9H_8$ cluster is formed by adding two hydrogen atoms to the peripheral oxygen atoms to obtain a neutral charged cluster (Figure 3.2).

For the Brønsted acidic ammonia adsorption calculations a Brønsted acidic site (V1-O1H) is created by adding one H atom to the V1-O1 site of the $V_2O_9H_6$ cluster to provide charge neutrality (Figure 3.3). The location of the Brønsted acidic site is selected as doubly bonded O1 atom since this site was considered as the most active site of the V_2O_5 cluster in the literature. Anstrom et al. (2003) performed DFT B3LYP calculations on V_2O_5 clusters by locating hydrogen atom on different oxygen sites and concluded that the interaction of hydrogen with O1 site was the strongest in agreement with what Hermann et al. (1999) suggested. Also, Gilardoni et al. (1997) selected O1-H as the Brønsted acidic site. The optimized geometries of the Lewis and the Brønsted acidic clusters used in the DFT calculations are shown in Figures 3.2 and 3.3, respectively. In all of the

calculations, V1=O1 site, V2-O1'H site, and the bridge oxygen (O2), were relaxed while the rest of the cluster atoms were kept fixed.

Wyckoff Parameters are also employed in the modeling of titanium dioxide anatase surface. From these parameters, cartesian coordinates are calculated and finally the unit cell of TiO_2 surface is obtained. Titanium dioxide unit cell (Ti_2O_4) is illustrated in Figure 3.4 while Wyckoff parameters and cartesian coordinates of TiO_2-anatase are given in Table 3.1.
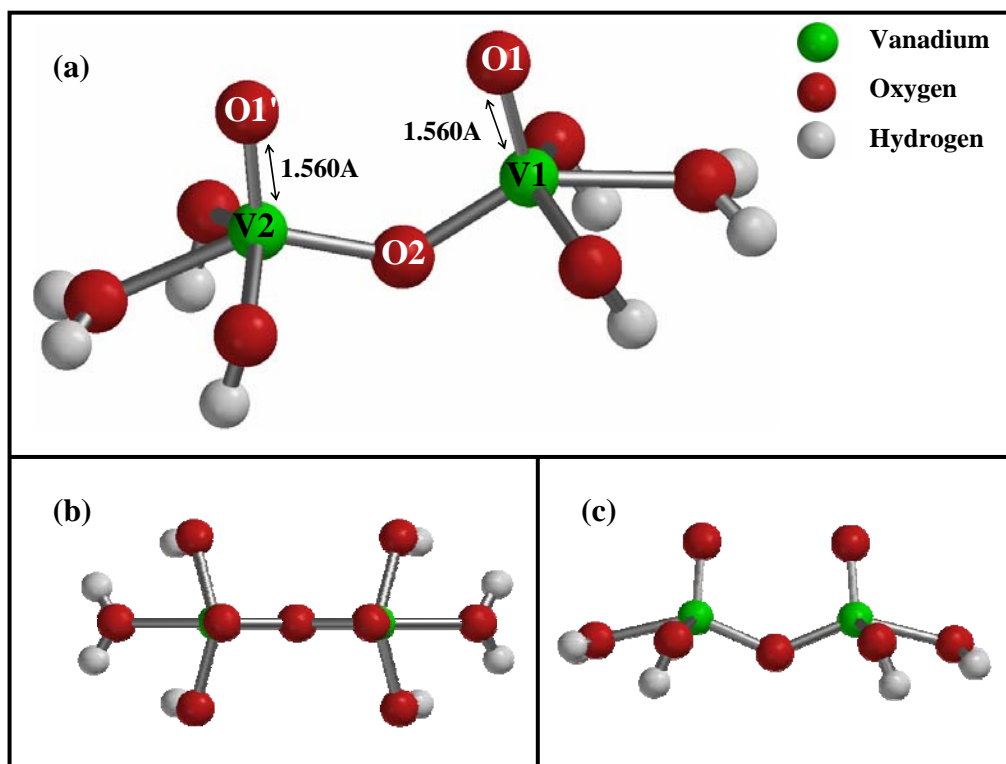
Figure 3.2. (a) The structure of the optimized Lewis acidic $V_2O_9H_8$ cluster, **(b)** Top view, **(c)** Side view.
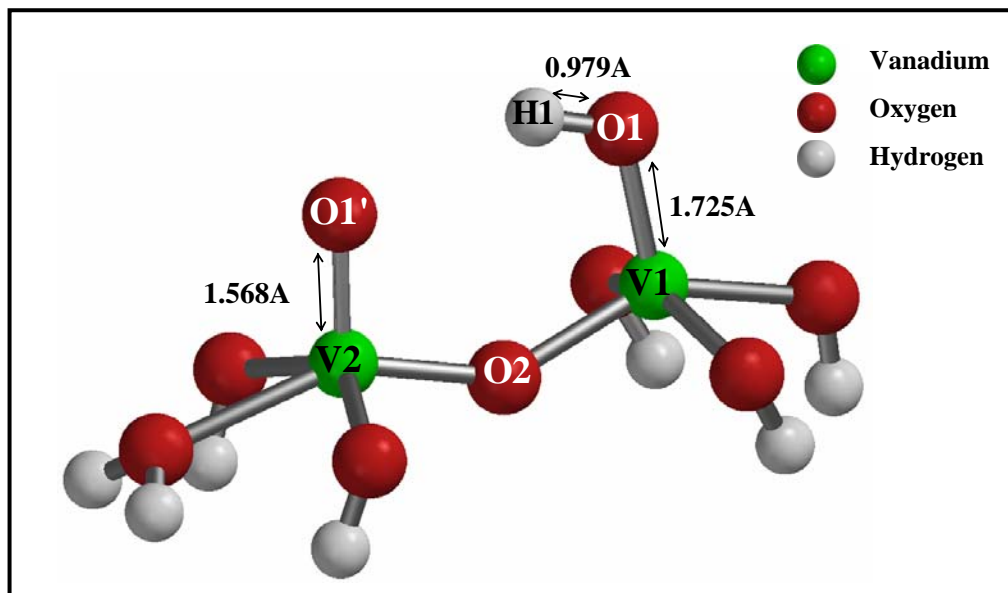
Figure 3.3. The structure of the optimized Brønsted acidic $V_2O_9H_8$ cluster.
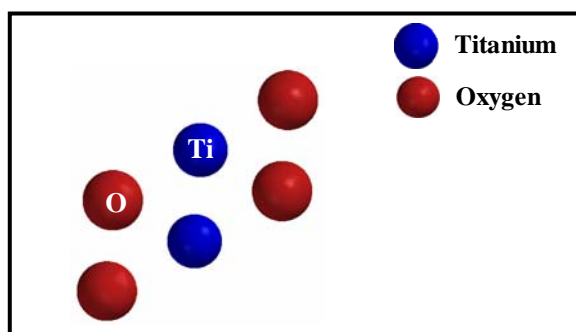
Figure 3.4. The unit cell of titanium oxide (Ti_2O_4).

Table 3.1. Wyckoff parameters and cartesian coordinates of TiO_2.

		Wyckoff Parameters	Cartesian Coordinates		
Ti	1	$(0, 0, 0)$	0.000000	0.000000	0.000000
Ti	2	$(0, a^*/2, c^*/4)$	0.000000	1.892500	2.378500
O	1	$(0, 0, -u^*c)$	0.000000	0.000000	- 1.965590
O	1	$(0, 0, +uc)$	0.000000	0.000000	1.965992
O	3	$(0, a/2, c/4-uc)$	0.000000	1.892500	0.412908
O	4	$(0, a/2, c/4+uc)$	0.000000	1.892500	4.344092

*a=b= 3.785, c=9.514, u=0.2066

Enlarging the unit cell obtained in x,y, and z coordinates (101) and (001) surfaces of titanium dioxide shown in Figure 3.5 are obtained. (101) face represents the most probable anatase surface and (001) surface is considered to be the most stable surface of TiO_2 anatase (Beltran et al., 2001). In addition Kryukova et al. (1997) indicated by using high resolution electron microscopy that there is a good geometric complementary between (010) V_2O_5 and (001) TiO_2-anatase for SCR reaction.
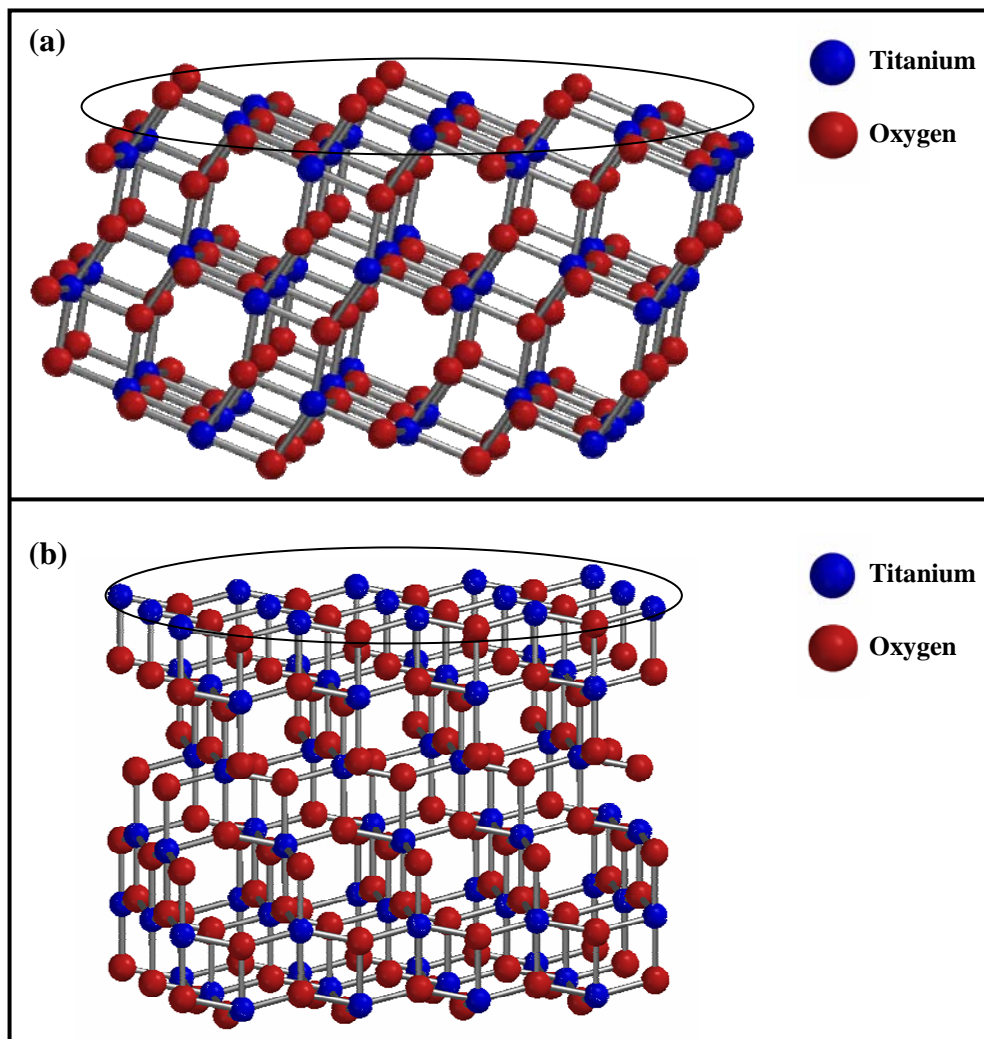
Figure 3.5. (a) (101) surface and **(b)** (001) surface of TiO$_2$ anatase (Marked with circle).

The cluster models are obtained from this enlarged surface by saturating the peripheral oxygen atoms with hydrogen atoms and also by providing the charge neutrality. The optimized geometries of the cluster models representing the physical and chemical properties of the TiO_2 (101) and (001) surfaces are shown in Figure 3.6. The computations are carried out for two types of cluster representations: **1.** All of the atoms are fixed and **2.** Partial relaxation is practiced where some of the atoms are relaxed. For the cluster representing (101) surface (Figure 3.6 (a)) five-coordinated Ti1 atom and the bridge oxygen atom (O1) are relaxed while for (001) cluster (Figure 3.6 (b)) Ti1, Ti2 and O1 atoms are relaxed. The rest of the atoms are kept fixed in both clusters. In Figure 3.6 the bond lengths are for optimized geometries of the relaxed clusters while the values given in parentheses belong to the totally fixed cluster models.
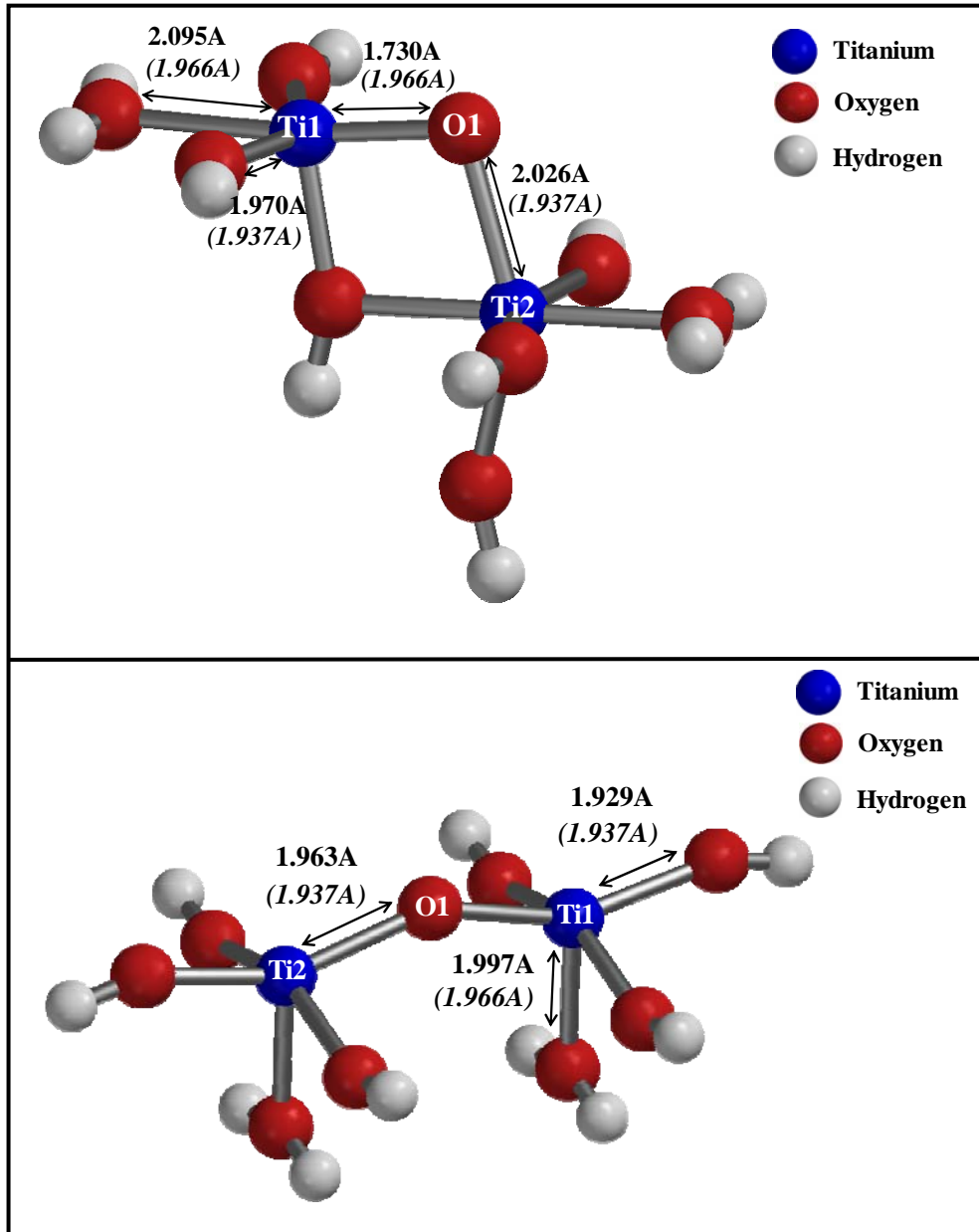
Figure 3.6. Optimized geometries of relaxed and fixed **(a)** (101) $Ti_2O_9H_8$, and **(b)** (001) $Ti_2O_9H_8$ cluster surfaces of titanium dioxide–anatase (Bond lengths without parentheses belong to the partially relaxed clusters, while the values given in parentheses are for fixed clusters).

In this research, a vanadia/titania cluster model is also proposed and studied for ammonia adsorption. It is indicated by experimentally that there is a good geometric complementary between (010) vanadium oxide and (001) titanium dioxide surfaces. Searching the suitable model describing this geometry, suitable positions of the $V_2O_9H_6$ cluster on (001) anatase surface is investigated. This cluster was previously obtained by Uzun (2003) from (010) V_2O_5 surface by cutting out V_2O_9 part and saturating all of the peripheral oxygen atoms by hydrogen atoms, and adding one hydrogen atom to create a Brønsted acidic site. It is found that $V_2O_9H_6$ cluster should either stand along (010) or (100) direction of the (001) anatase surface (see Figure 3.7).
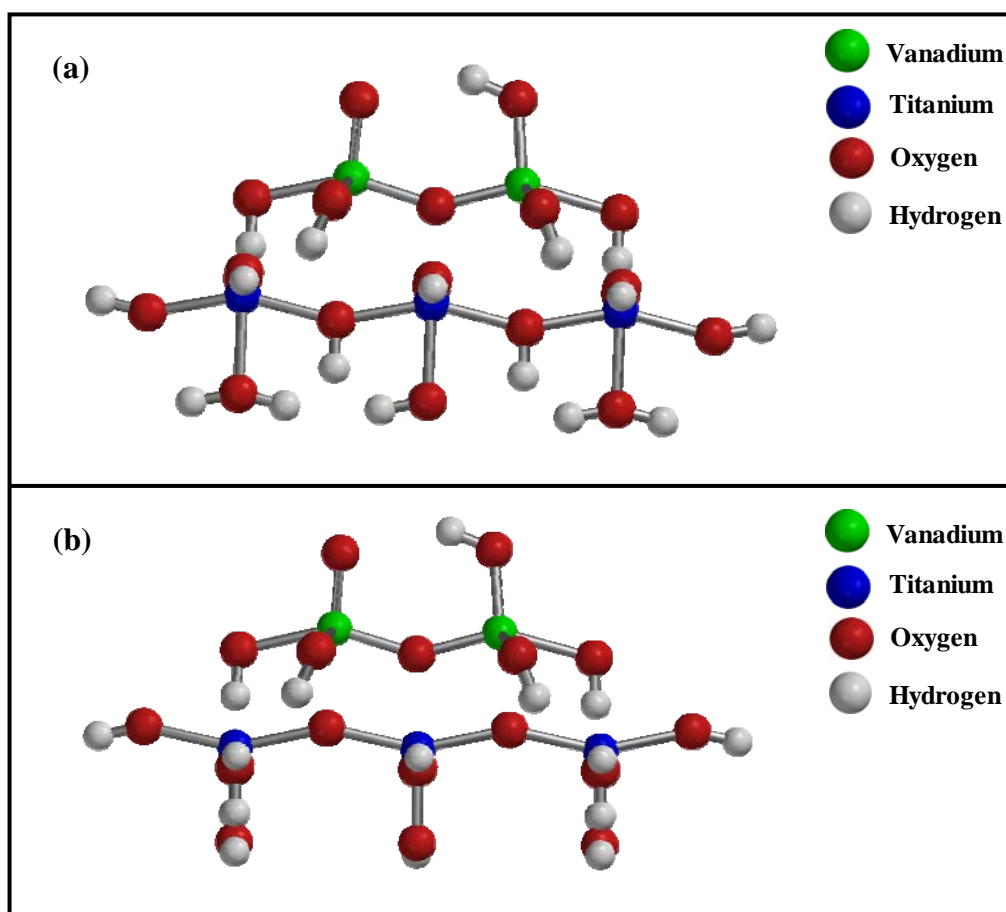
Figure 3.7. Two alternatives of (010) V_2O_5 cluster on (001) anatase: **(a)** Along (010) direction or **(b)** Along (100) direction of anatase surface.

By the single point energy calculations carried out on $V_2Ti_3O_{22}H_{22}$ clusters shown in Figure 3.7, it is found that the configuration along (100) direction has a lower energy than that along (010) direction. Therefore, a vanadia/titania cluster model is obtained by the previous methods starting from Figure 3.7 (a). The optimized geometry of the resulting $V_2TiO_{14}H_{14}$ cluster is illustrated in Figure 3.8. This equilibrium geometry structure is obtained by relaxing the positions of V1=O1 site, V2-O1'H site, and the bridge oxygen (O2) while keeping the rest of the cluster atoms fixed
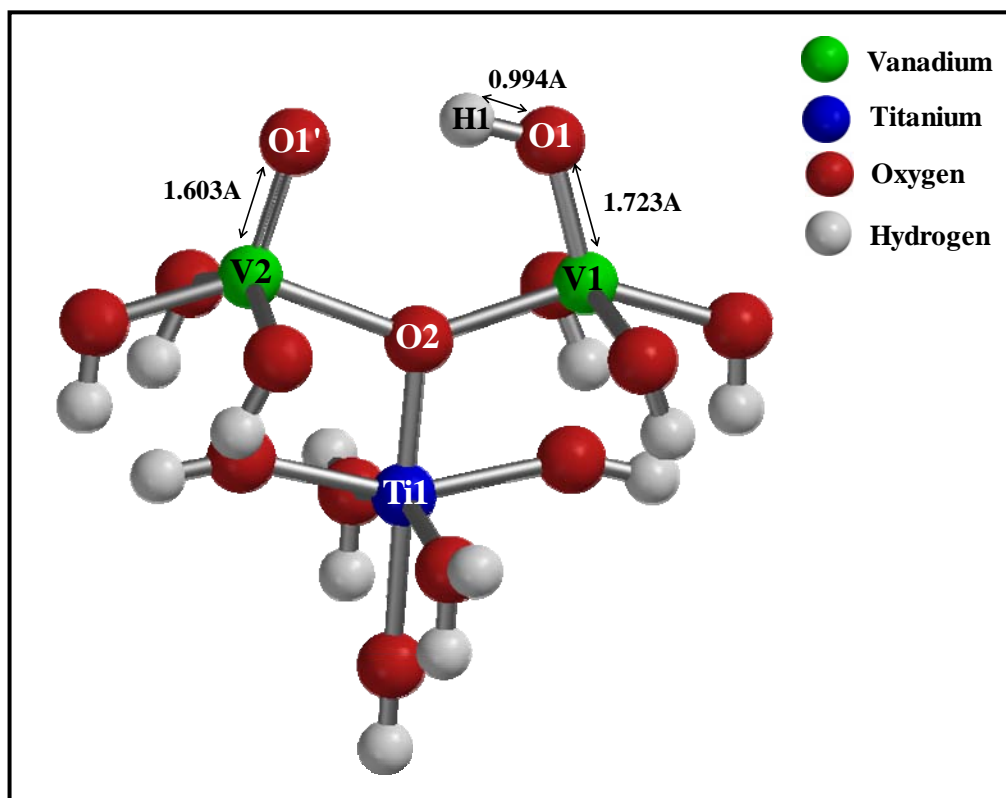
Figure 3.8. The structure of the optimized Brønsted acidic $V_2TiO_{14}H_{14}$ cluster.

The following general computational procedure was followed in the calculations of this reasearch: Initially, both the cluster and the adsorbing molecules are fully optimized geometrically by means of the equilibrium geometry calculations. Then, the adsorbing molecule is located over the active site of the cluster at a selected distance and a coordinate driving calculation[*] is performed by selecting a reaction coordinate in order to obtain the variation of the relative energy with a decreasing reaction coordinate to get an energy profile as a function of the selected reaction coordinate distance. Single point equilibrium geometry calculations were also performed where necessary by locating the adsorbing molecule in the vicinity of the catalytic cluster. The relative energy is defined as:

$$\Delta E = E_{System} - (E_{Cluster} + E_{Adsorbate}) \qquad (3.15)$$

where E_{System} is the calculated energy of the given geometry containing cluster and the adsorbing molecule at any interatomic distance, $E_{Cluster}$ is the energy of the cluster itself and $E_{Adsorbate}$ is that of the adsorbing molecule.

After having obtained the energy profile for the desired reaction, the geometry with the minimum energy on the energy profile is re-optimized by means of the equilibrium geometry calculations to obtain the final geometry for the reaction. For the calculated final geometry, vibration frequencies and atomic charges are computed by single point energy calculations. Furthermore, from the energy profile, the geometry with the highest energy is taken as the input geometry for the transition state geometry calculations. Starting from these geometries, the transition state structures with only one negative eigenvalue in hessian matrix are obtained. If a successful transition state geometry can not be achieved, the geometry with the maximum energy in the energy profile is reported as the approximate transition geometry.

---

[*] Detailed information on performing a reaction coordinate calculation is given in Uzun (2003).

CHAPTER 4

RESULTS AND DISCUSSION

4.1. SCR Reaction on V_2O_5 Catalyst Surface

Before performing mechanism calculations over the catalytic surface represented by the $V_2O_9H_8$ cluster, the reactants (NH_3 and NO) were initially optimized by means of the equilibrium geometry calculations. Then the computational procedure described previously was applied for investigating the SCR reaction mechanism, and through these calculations it has been established that SCR reaction consists of three main parts:

- Part I: Brønsted acidic ammonia adsorption
- Part II: NH_2NO formation reactions
- Part III: NH_2NO decomposition reactions

4.1.1. Part I: Initiation Step

It is generally agreed that the SCR reaction is initiated with the activation of ammonia which is strongly adsorbed over the catalytic surface, and it then proceeds by the interaction of NO with pre-adsorbed ammonia, suggesting an Eley-Rideal type mechanism. Therefore, ammonia activation over the (010) V_2O_5 catalytic surface was considered as the initiation reaction of the SCR of nitric oxide by ammonia. Ammonia activation may occur through two different mechanisms: ammonia can be adsorbed on vanadium catalyst either through

Lewis-type interaction as molecularly adsorbed ammonia, or over a Brønsted acidic site as ammonium ion. These two possibilities were considered separately and a comparison between them was made to select the most favorable one.

4.1.1.1. Lewis Acidic Ammonia Adsorption

Ammonia adsorption through a Lewis acidic interaction is one of the possible activation modes of ammonia over V_2O_5 surface. This interaction type was investigated over the optimized Lewis Acidic $V_2O_9H_8$ cluster (Figure 3.2). For this type of ammonia activation mode, coordinate driving calculations were performed by selecting four different reaction coordinates as the distances between: **1.** one of the hydrogen atoms of ammonia and O1 site of the $V_2O_9H_8$ cluster, **2.** one of the hydrogen atoms of ammonia and V site of the $V_2O_9H_8$ cluster, **3.** the nitrogen of the ammonia and the O1 site of the cluster, and **4.** the nitrogen atom of the ammonia and O1 site of the cluster. Since the total energy of the system shows a continuous rise as ammonia gets close to O1 or V active sites in the resultant energy profiles for all of the above calculations, it is concluded that Lewis acidic NH_3 adsorption is an unfavorable reaction for the initiation step.

4.1.1.2. Brønsted Acidic Ammonia Adsorption

Another possible activation mode of ammonia on V_2O_5 catalytic surface is the adsorption over Brønsted acidic V1-O1H1 site of the $V_2O_9H_8$ cluster as shown in Figure 3.3. In order to investigate the Brønsted acidic ammonia adsorption over the cluster, the distance between the nitrogen atom of ammonia and Brønsted acidic O1-H1 site of the cluster is selected as the reaction coordinate for a coordinate driving calculation and decreased in a stepwise manner. The system is

taken as neutral and with singlet spin multiplicity in this calculation. The energy profile obtained accordingly shows that ammonia activation over Brønsted acidic V-OH site occurs through a non-activated process (Figure 4.1).
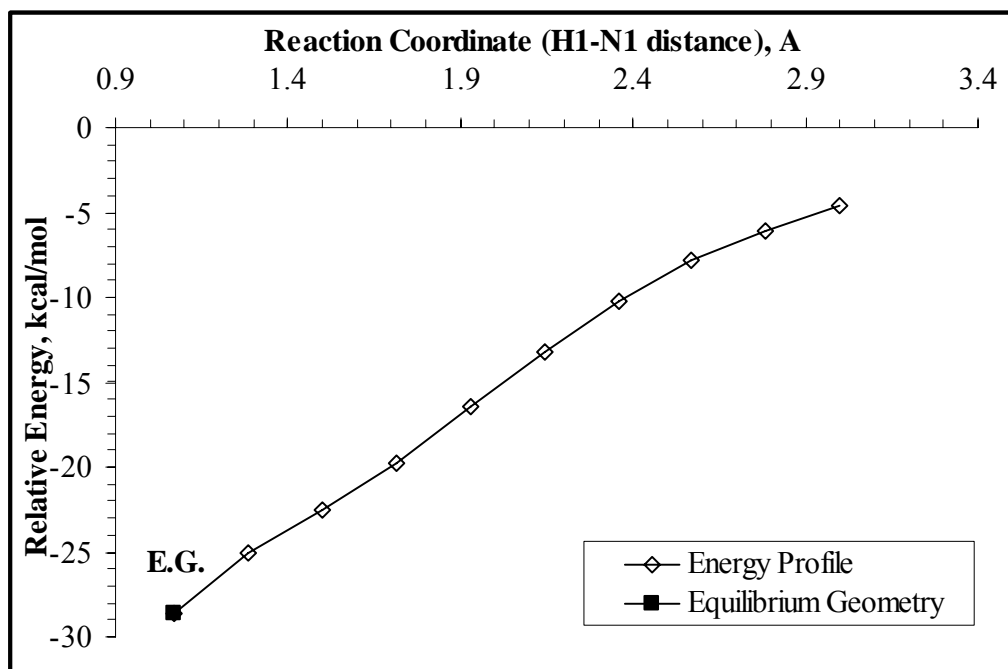
Figure 4.1. Energy profile for the Brønsted acidic ammonia activation.

The equilibrium geometry[*] of this interaction is given in Figure 4.2. where ammonia is adsorbed over the Brønsted acidic site of the cluster symmetrically forming NH_4 species over the catalytic surface with an exothermic energy difference of 28.65 kcal/mol with respect to $V_2O_9H_8$ cluster and NH_3 (g) molecule. In Figure 4.2. (a), N1-H3 and N1-H4 bond distances are 1.019A as the N1-H1 and N1-H2 distances being 1.071A and 1.072A, respectively, suggesting a symmetrical configuration. The findings in this part are in agreement with what Srnak et al. (1992) observed via TPD experiments and what Anstrom et al. (2003)

---

[*] Input and output files of this calculation are given in detail in Appendix B.

and Gilardoni et al. (1997) reported by DFT calculations. Srnak et al. (1992) estimated the enthalpy for ammonia desorption over Brønsted acidic V-OH site on pure V_2O_5 as between 18 kcal/mol and 26 kcal/mol via TPD experiments. Moreover, Anstrom et al. (2003) and Gilardoni et al. (1997) calculated the relative energy of the adsorbed NH_3 species over Brønsted acidic V-OH site of the V_2O_5 catalyst as -26 kcal/mol and -25 kcal/mol, respectively. Moreover, the Mulliken charge calculated for the equilibrium geometry of the Brønsted acidic NH_3 adsorption reaction is +0.787 e.

For the optimized geometry of Brønsted acidic NH_3 adsorption reaction, single point energy calculations are carried out to obtain vibration frequencies and Mulliken charges. The calculated vibration frequencies which are contributed by symmetric and asymmetric bending and stretching frequencies of NH_4, are compared with the experimental values available in the literature as given in Table 4.1.
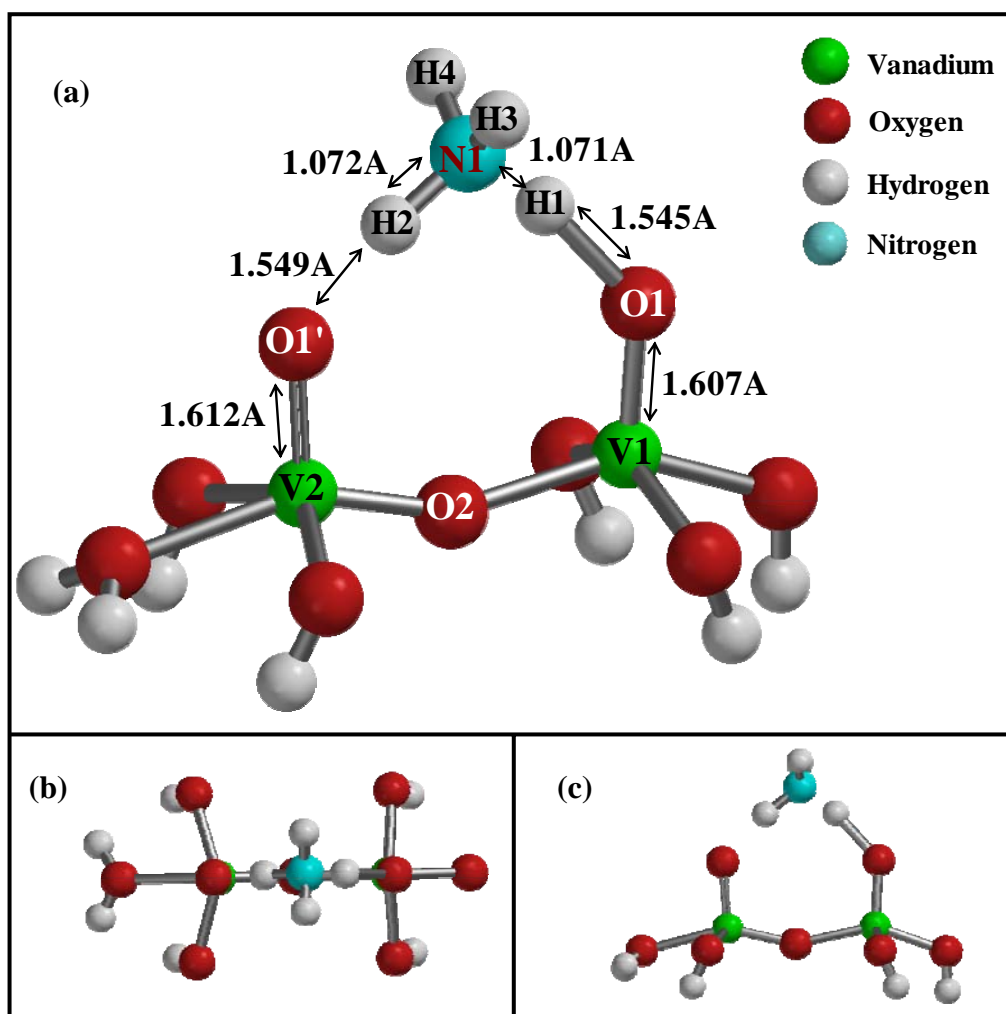
Figure 4.2. **(a)** Equilibrium geometry of Brønsted acidic NH_3 adsorption on $V_2O_9H_8$ cluster, **(b)** Top view, **(c)** Side view.

Table 4.1. Comparison of the calculated vibration frequency (cm^{-1}) data for the optimized geometry of Brønsted acidic NH$_3$ adsorption reaction with experimentally obtained ones.

Frequency, cm^{-1}	This Work	Experimental Literature
NH$_4$ bend. (asym.)	1392 (unscaled) 1514 (scaled by 1.0873)	1425 [a], 1417 [b]
NH$_4$ bend. (sym.)	1528 (unscaled) 1661 (scaled by 1.0873)	1680 [a], 1670 [b]
NH$_4$ stret. (asym.)	2593 (unscaled) 2819 (scaled by 1.0873)	2850 [a]
NH$_4$ stret. (sym.)	2754 (unscaled) 2994 (scaled by 1.0873)	3000 [a]

[a] Ramis et al. (1995)
[b] Topsøe (1991)

Vibration frequency values calculated also provide good agreement with the experimental data for both bending and stretching frequencies of NH$_4^+$ ion as shown in Table 4.1. A scaling factor of 1.0873 was obtained through a least squares fit of the experimental data. It should be also noted here that there is no reported theoretical vibration frequency data in the literature with regard to any of the steps of SCR reaction taking place on pure vanadia surface. +0.787 e of Mulliken charge calculated for the equilibrium geometry of the Brønsted acidic NH$_3$ adsorption reaction suggests that NH$_4^+$ ion formation occurs at the end of the NH$_3$ adsorption on Brønsted acidic V-OH site. .This result is very close to what Anstrom et al. (2003) calculated (+0.808 e) and suggests that NH$_4^+$ ion formation occurs at the end of the NH$_3$ adsorption on Brønsted acidic V-OH site.

As a result of these calculations, it is concluded that the SCR reaction is initiated more favorably by the strong nonactivated ammonia adsorption mechanism on

Brønsted acidic V-OH site and the adsorbed ammonia forms NH_4^+ ion over the catalytic surface. Since the favorable activation mode of the ammonia over the catalytic surface was Brønsted acidic adsorption, the second part of the SCR reaction was investigated by introducing nitric oxide to the final geometry of the Brønsted acidic ammonia adsorption.

4.1.2. Part II: Formation of NH$_2$NO Species

As the second part of the SCR reaction, nitric oxide interaction with the pre-adsorbed ammonia species is investigated. For this purpose a coordinate driving calculation is performed by considering the distance between the nitrogen atom (N1) of the NH_4^+ ion formed at the end of part I and that of NO (N2) as the reaction coordinate. The system is considered as neutral and with doublet spin multiplicity for all of the calculations in this part. An approximate transition state and the equilibrium geometry are derived by use of an energy profile (see Figure 4.3) for the formation of NH$_3$NHO adduct as shown in Figures 4.4 (a) and 4.4 (b), respectively.
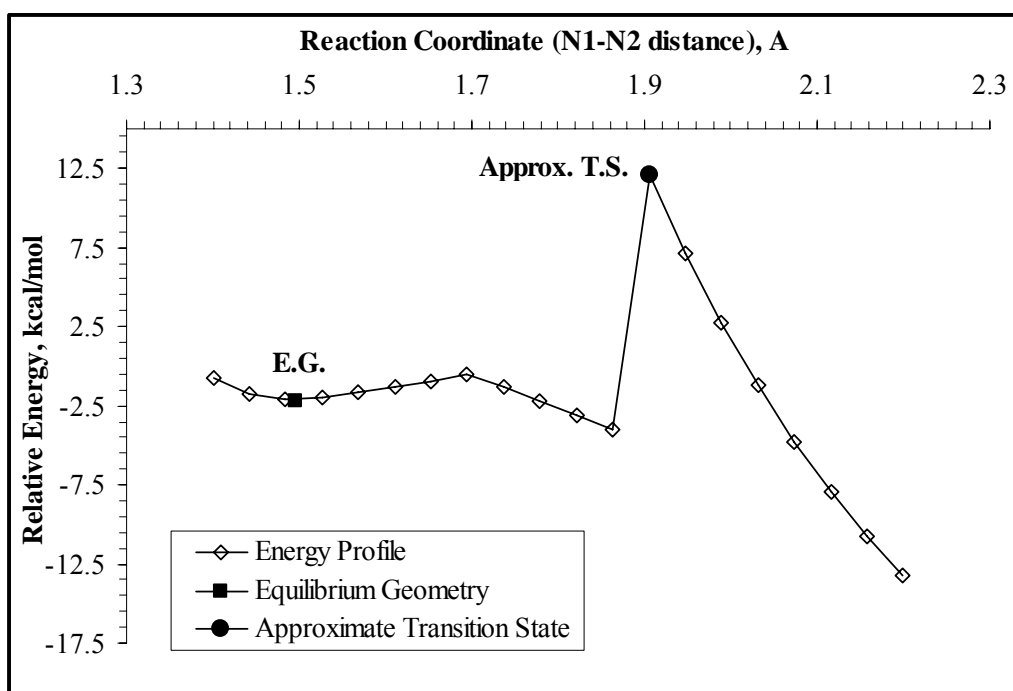
Figure 4.3. Energy profile obtained for the interaction of gas phase NO with the preadsorbed NH_4 species.
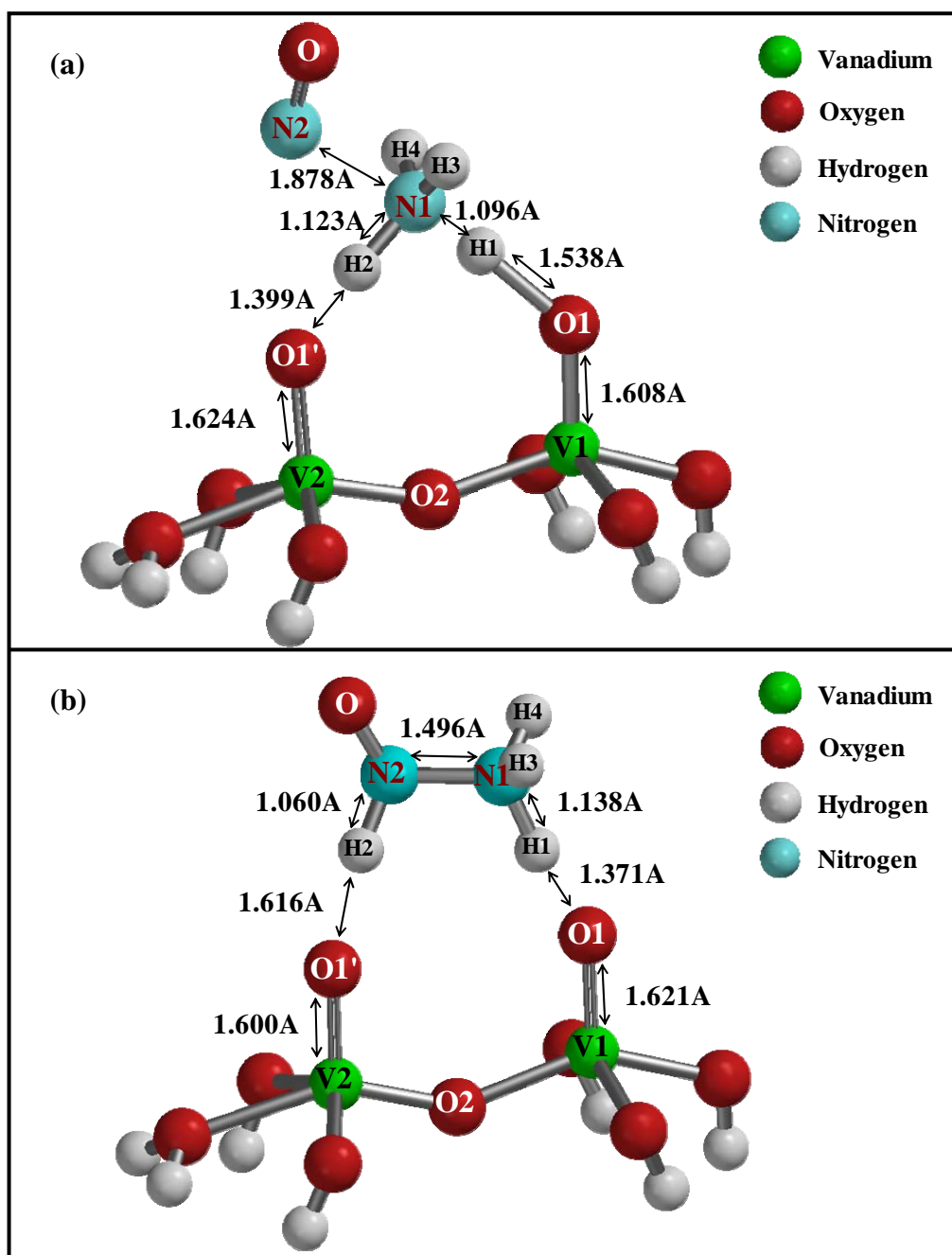
Figure 4.4. (a) Approximate transition state and **(b)** Equilibrium geometry obtained for the interaction of gas phase NO with the pre-adsorbed NH_4 species to form NH_3NHO adduct.

After the formation of NH_3NHO species, to achieve the migrations of H1 and H2 atoms of this species towards the O1 and O1' sites of the cluster two separate reaction coordinates of O1-H1 and O1'-H2 are selected to perform a coordinate driving calculation. The energy profile obtained accordingly is illustrated in Figure 4.5. As a result of this calculation NH_2NO is formed with an exothermic relative energy of 14.08 kcal/mol. An approximate transition state and the equilibrium geometry for this reaction step are given in Figures 4.6 (a) and (b), respectively. Since both of the oxygen sites of the cluster are saturated with hydrogen atoms by NH_2NO formation reaction, a new cluster will be employed in the next part of the SCR reaction.
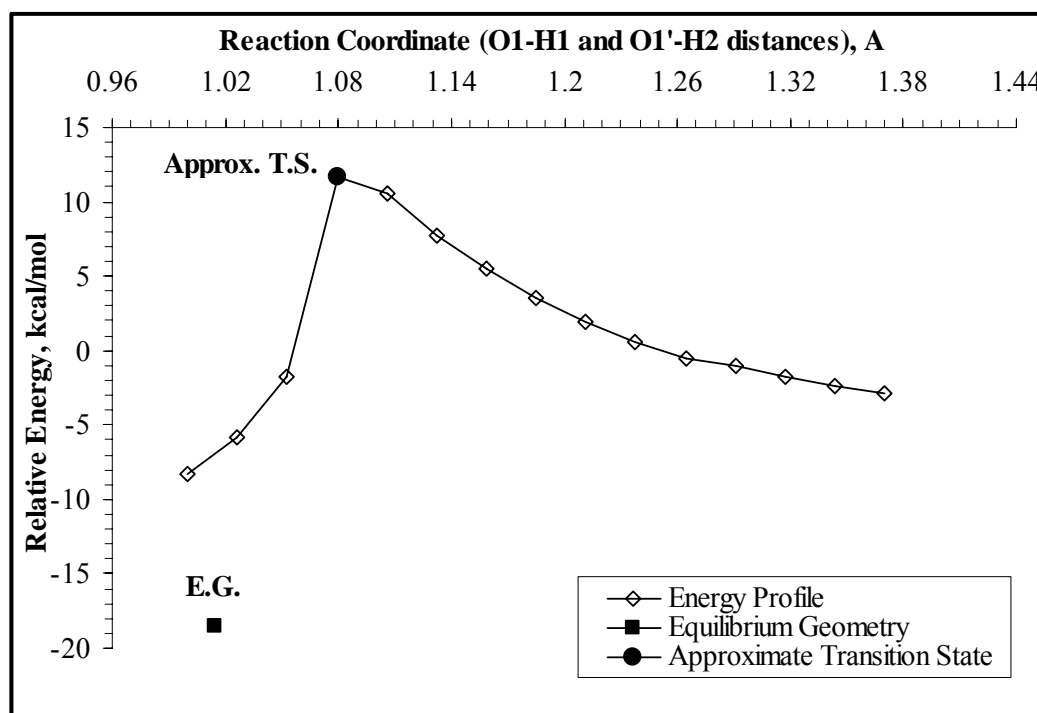
Figure 4.5. Energy profile obtained for NH_2NO formation reaction.
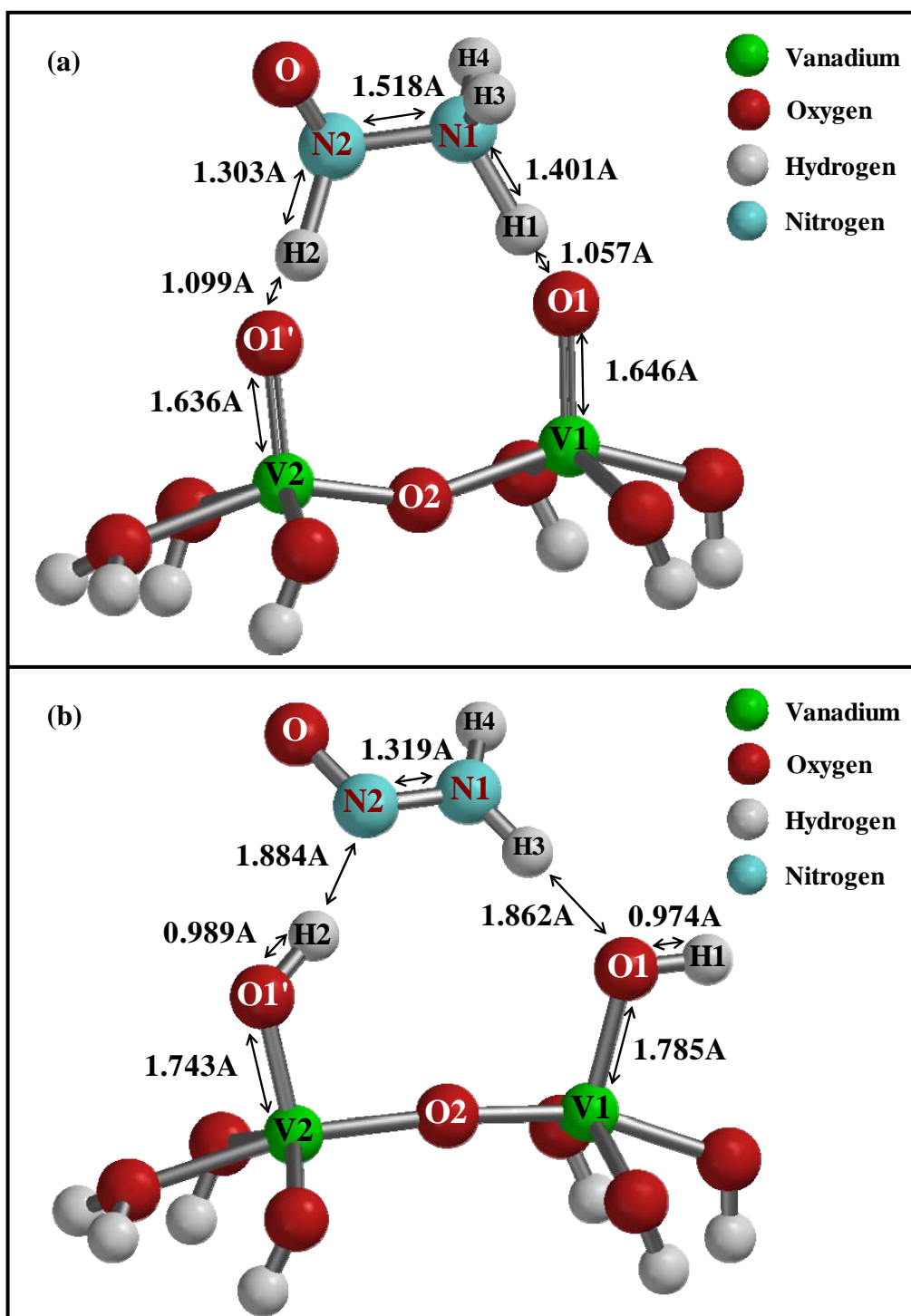
Figure 4.6. **(a)** Approximate transition state geometry and **(b)** Equilibrium geometry for NH_2NO formation reaction from NH_3NHO adduct.

A summary of the reaction steps of parts I and II are illustrated in Figure 4.7 in terms of relative potential energies. The relative energy values in this part are calculated with respect $V_2O_9H_8$ cluster and gas phase energies of ammonia and nitric oxide at infinite separation. It should be noted that the rate limiting step of the SCR reaction can be identified as NH_3NHO formation reaction with a high activation barrier of about 43.99 kcal/mol; however, it must be cautioned that it is only an approximate transition state.
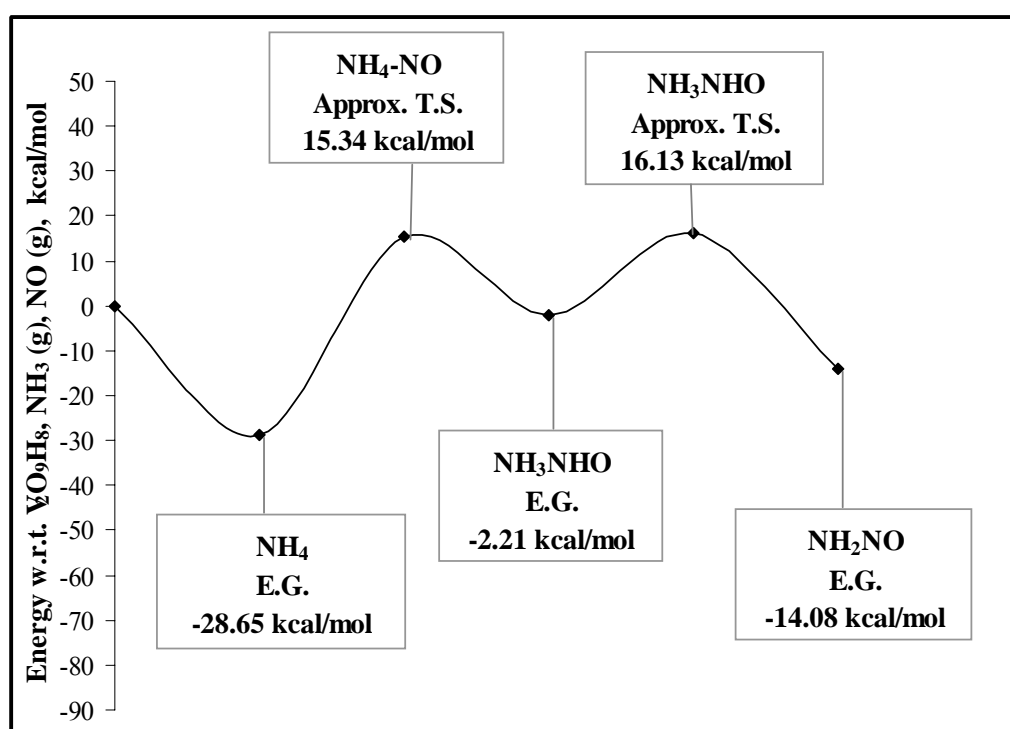
Figure 4.7. Potential energy profile for the first and second parts of SCR reaction. (Approx. T. S. represents the approximate transition states, while E. G. stands for the equilibrium geometries)

4.1.3. Part III: Decomposition of NH_2NO Species on V_2O_5

The reaction steps of this part are given in Figure 4.8 as a relative potential energy diagram. The relative energy values in this part are calculated with respect to $V_2O_9H_8$ cluster and gas phase energy of NH_2NO species.
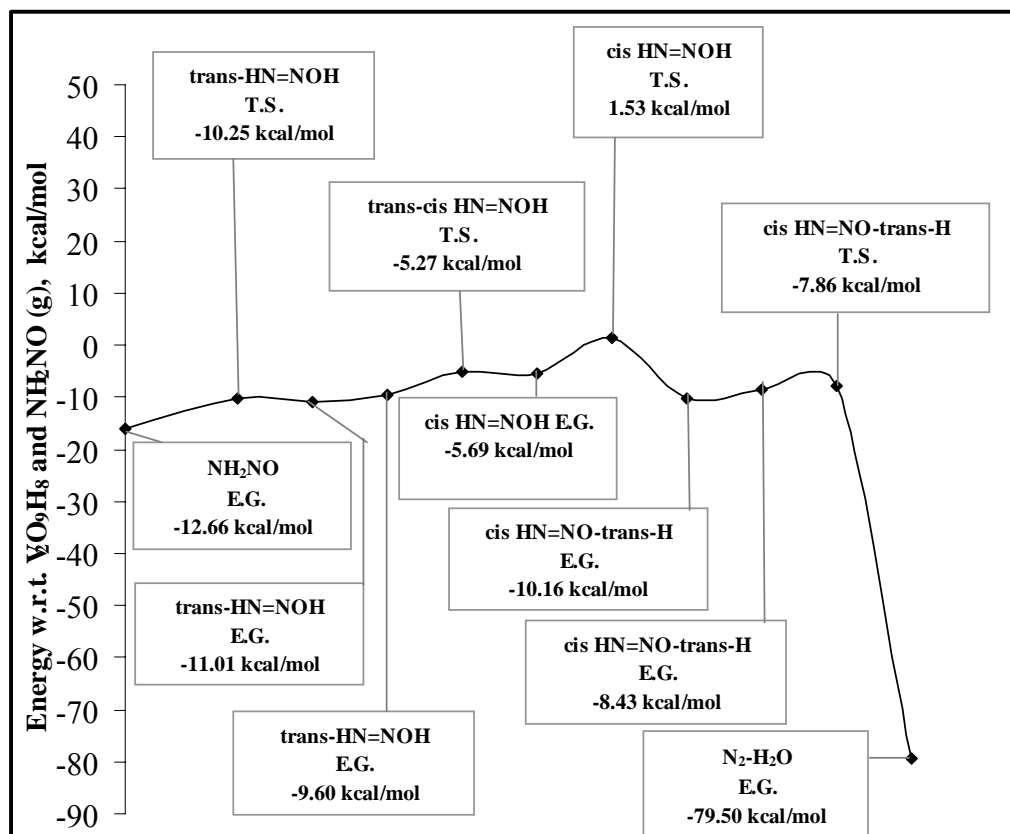
Figure 4.8. Potential energy profile for the third part of SCR reaction (T. S. represents the transition states, while E. G. stands for the equilibrium geometries).

The reaction series for the decomposition of NH_2NO species on the cluster start with the re-adsorption of nitrosamide species on a new Brønsted acidic $V_2O_9H_8$ cluster by a single point equilibrium geometry calculation. The system is taken as neutral and with singlet spin multiplicity in all of the calculations involving this

part. The equilibrium geometry of re-adsorbed NH_2NO species having a relative energy of -12.66 kcal/mol is given in Figure 4.9. As it is seen in the figure, nitrosamide species is adsorbed on the cluster having N1-N2 distance of 1.299 A, H1-O distance of 1.455 A and O1'-H4 distance of 1.966 A.
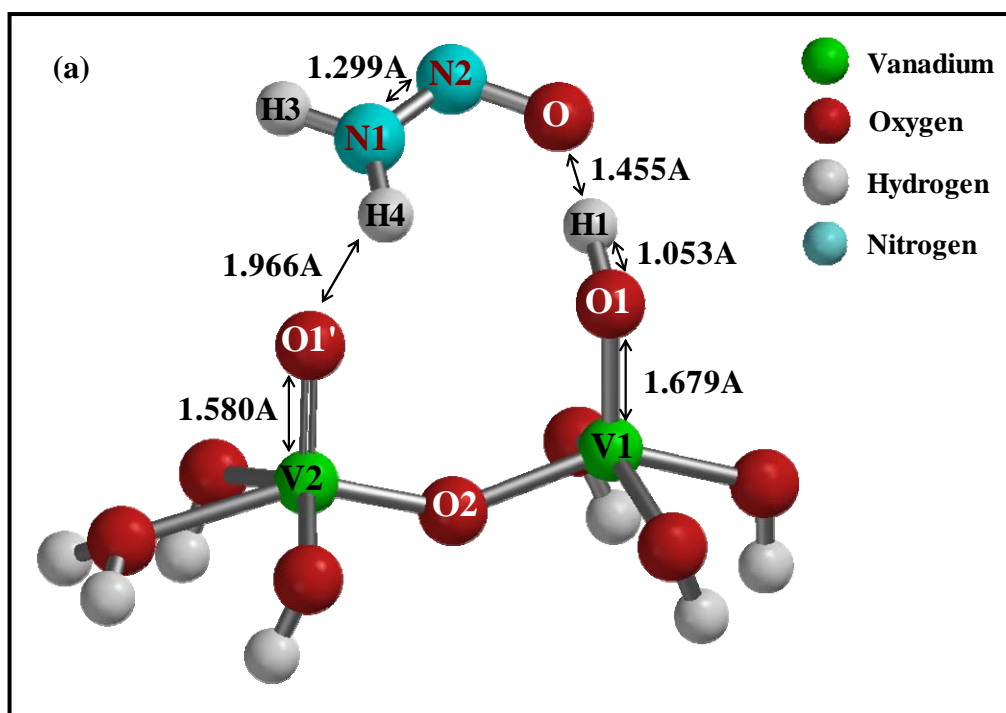
Figure 4.9. Equilibrium geometry of nitrosamide species re-adsorbed on a new Brønsted acidic $V_2O_9H_8$ cluster.

In order to accomplish the decomposition of this product to the final reaction products N_2 and H_2O, a series of many different reaction steps have been energetically investigated and the most favorable reaction path combination involving a push-pull mechanism of hydrogen transfer is obtained. The transition states and equilibrium geometries pertaining to each one of these reaction steps are given separately in Figures 4.10 to 4.19.

The reaction series for the decomposition of NH_2NO species on the cluster start with the adsorption of nitrosamide species on a new Brønsted acidic $V_2O_9H_8$ cluster by a single point equilibrium geometry calculation. The system is taken as neutral and with singlet spin multiplicity in all of the calculations involving this part. The equilibrium geometry of re-adsorbed NH_2NO species having a relative energy of -12.66 kcal/mol is given in Figure 3.9. As it is seen in the figure, nitrosamide species is adsorbed on the cluster having N1-N2 distance of 1.299 A, H1-O distance of 1.455 A and O1'-H4 distance of 1.966 A. One should notice that nitrosamide species was not observed experimentally under typical SCR conditions. This may be due to very fast decomposition of NH_2NO to the SCR reaction products N_2 and water.

In order to accomplish the decomposition of this product to the final reaction products N_2 and H_2O, a series of many different reaction steps have been energetically investigated and the most favorable reaction path combination involving a push-pull mechanism of hydrogen transfer is obtained. The transition states and equilibrium geometries as well as the energy profiles pertaining to each one of these reaction steps are given separately in Figures 4.10 to 4.15.

A coordinate driving calculation is first performed by selecting the distance between H4 atom of the nitrosamide species and the O1' site of the cluster surface as the reaction coordinate. This enables hydrogen transfer to the oxygen atom of the nitrosamide molecule as follows: It is observed by means of the energy profile (Figure 4.10) that as the distance between H4 and O1' atoms decreases, H1 moves apart from O1 atom. H1 atom is finally captured by the O atom. The transition state and equilibrium geometry of this interaction are shown in Figure 4.11.

73
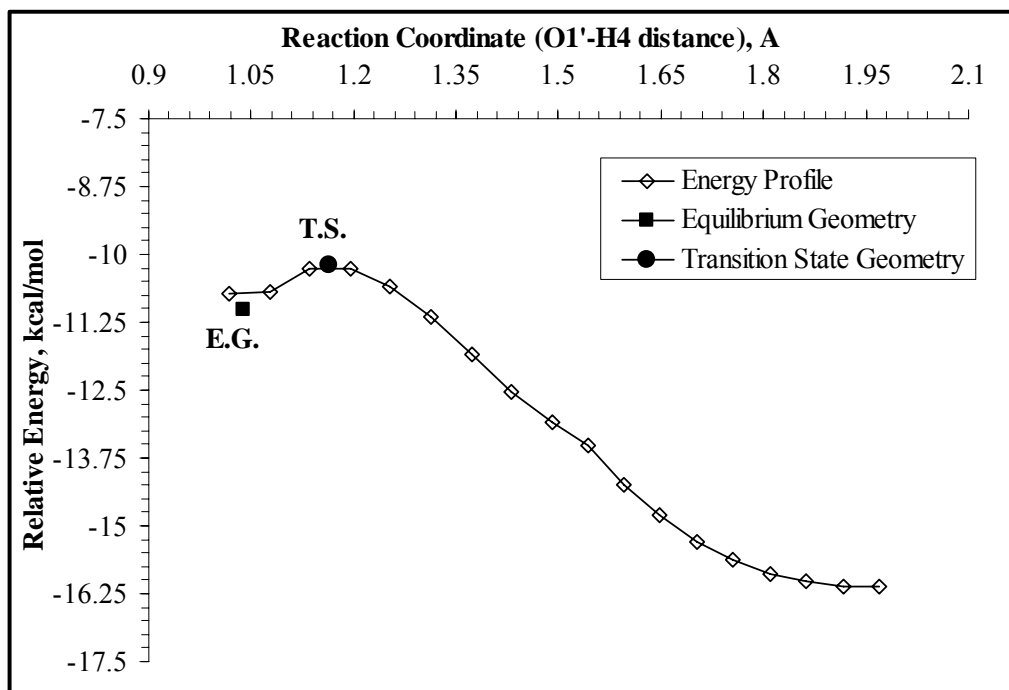
Figure 4.10. Energy profile obtained for the interaction of NH_2NO species with the oxygen site (O1') of the cluster.

The trans-HN=NOH species shown in Figure 4.11 (b) is further rotated on the cluster surface by a single point equilibrium geometry calculation as given in Figure 4.12. At this stage a coordinate driving calculation is employed by selecting a reaction coordinate between O1 and H3 atoms in order to provide cis-HN=NOH formation. Using the resultant energy profile given in Figure 4.13, the transition state geometry and equilibrium geometry of this interaction are obtained as shown in Figure 4.14. For the transition state geometry, N1-H4 bond is about to be formed as H3 atom of the trans H-N=NOH species is about to be captured by V1=O1 site.
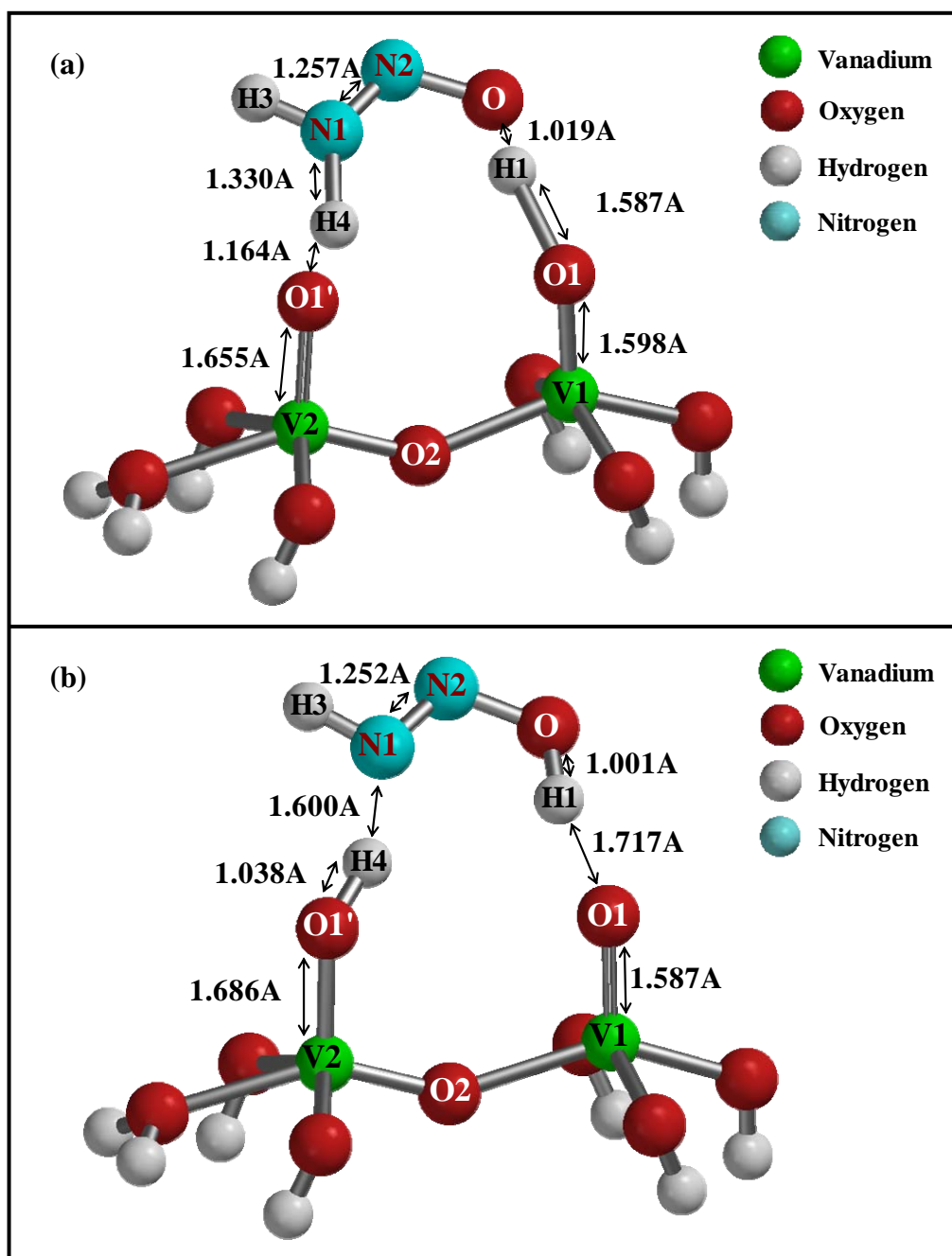
Figure 4.11. **(a)** Transition state geometry and **(b)** Equilibrium geometry structures for trans-HN=NOH formation reaction from NH_2NO species.
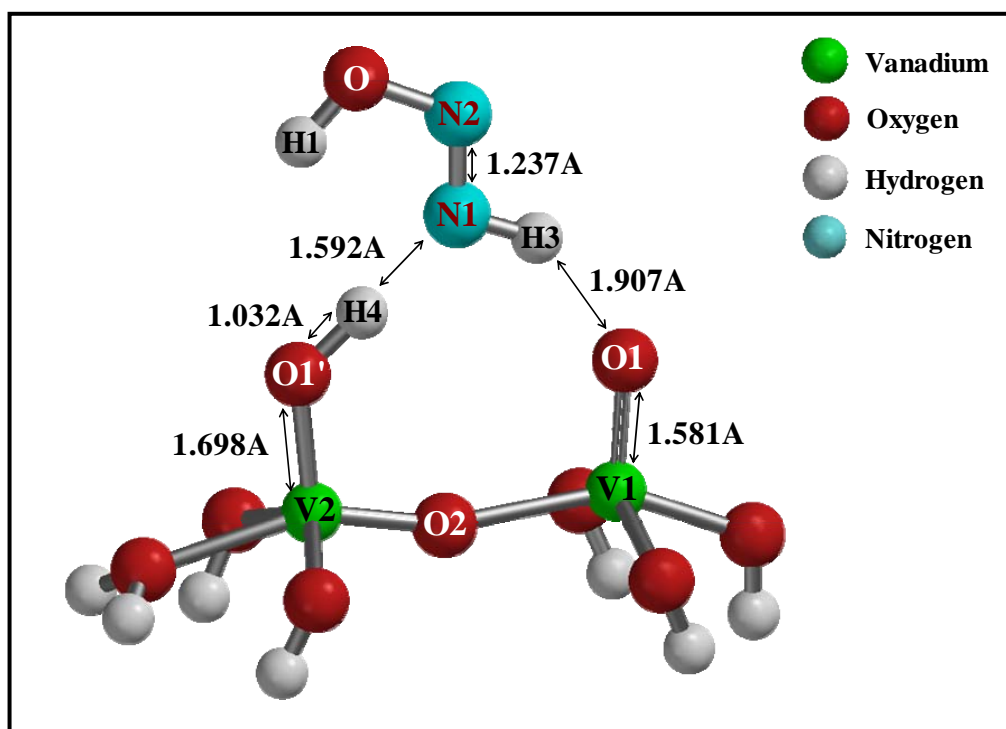
Figure 4.12. Equilibrium geometry of the rotated trans-H-N=NOH species on $V_2O_9H_8$ cluster.

At this stage a coordinate driving calculation is employed by selecting a reaction coordinate between O1 and H3 atoms in order to provide cis-HN=NOH formation. Using the resultant energy profile (Figure 4.13), the transition state geometry and equilibrium geometry of this interaction are obtained as shown in Figure 4.14. For the transition state geometry, N1-H4 bond is about to be formed as H3 atom of the trans H-N=NOH species is about to be captured by V1=O1 site.
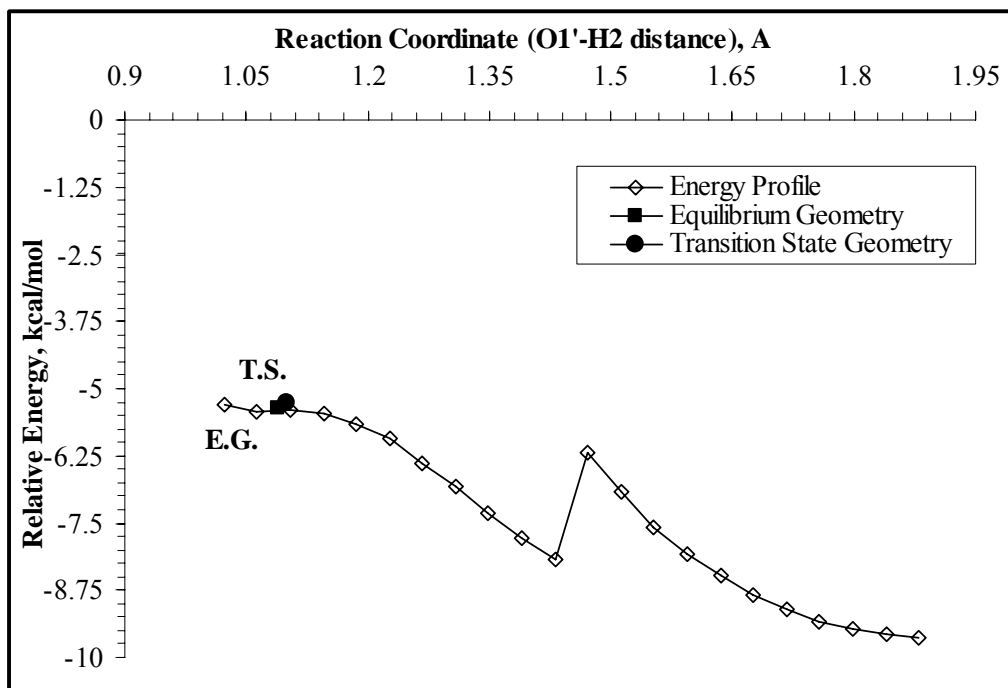
Figure 4.13. Energy profile obtained for the interaction of trans H-N=NOH species with the oxygen site (O1') of the cluster to form cis-HN=NOH species.

The next step for the SCR of NO by NH_3 is the isomerization of the cis-HN=NOH species (see Figure 4.14b) to form cis-HN=NO-trans-H species. For this purpose N1N2O-H1 dihedral angle is chosen as the reaction coordinate. The transition state and equilibrium geometry obtained accordingly by use of an energy profile (Figure 4.15) are illustrated in Figure 4.16. At the transition state geometry N1N2O-H1 dihedral angle is 77.67° indicating that the H1 atom is about to rotate to form cis-HN=NO-trans-H species.

In the third part of the SCR reaction, comprising the decomposition of nitrosamide species, this reaction step has the highest activation barrier value among all of the steps involved in this part (see Figure 4.8) as previously pointed out by Anstrom et al. (2003).
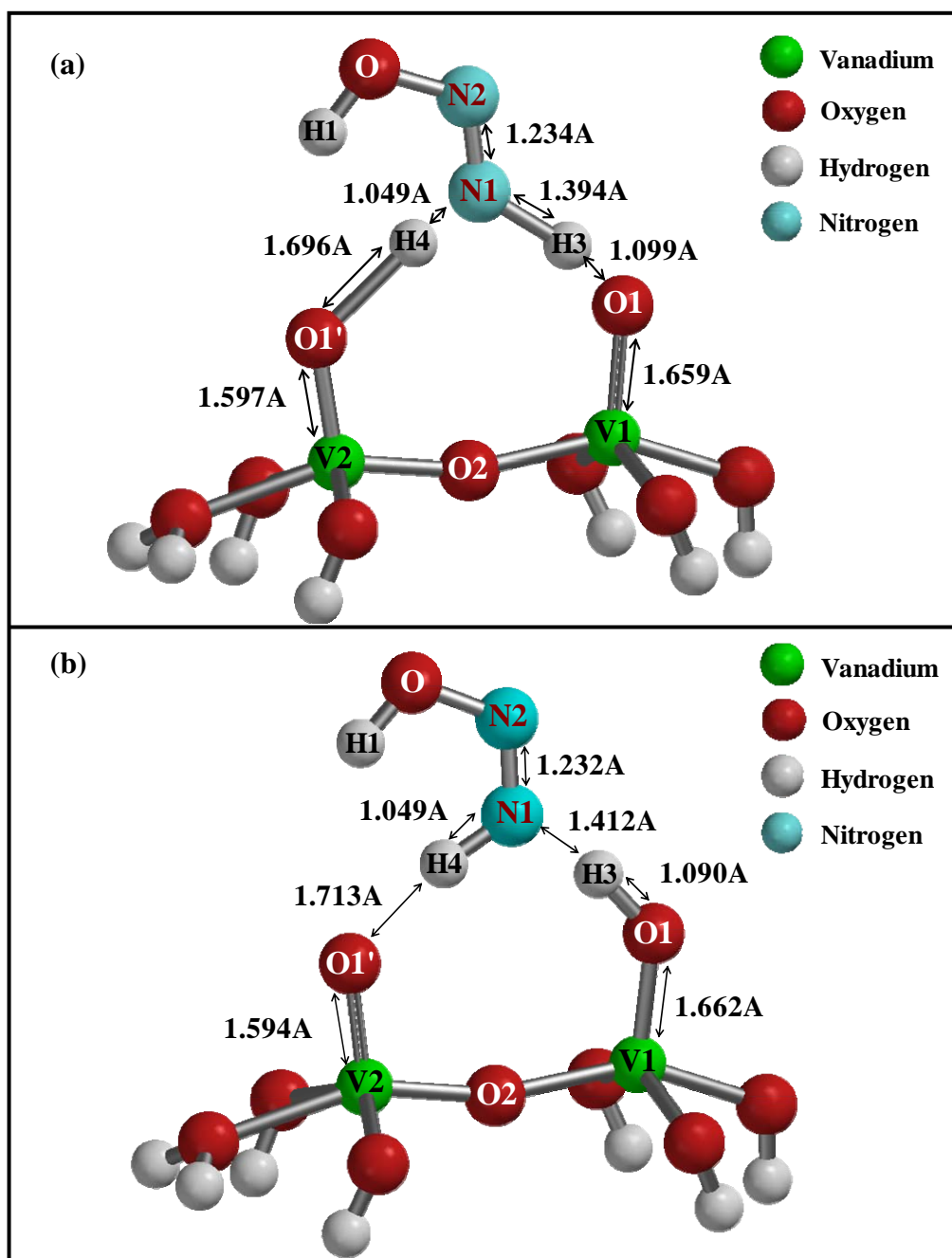
Figure 4.14. (a) Transition state geometry for the reaction of formation of cis-HN=NOH species from trans H-N=NOH species, **(b)** Equilibrium geometry of the adsorbed cis-HN=NOH species.
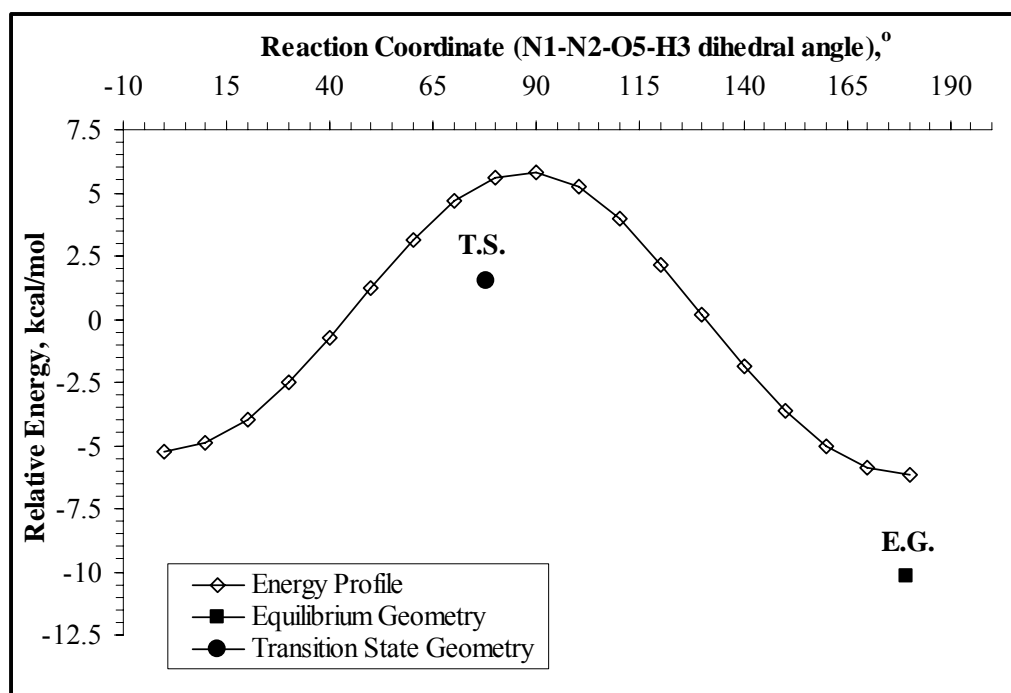
Figure 4.15. Energy profile for the isomerization reaction of the cis-HN=NOH species to form cis-HN=NO-trans-H species.
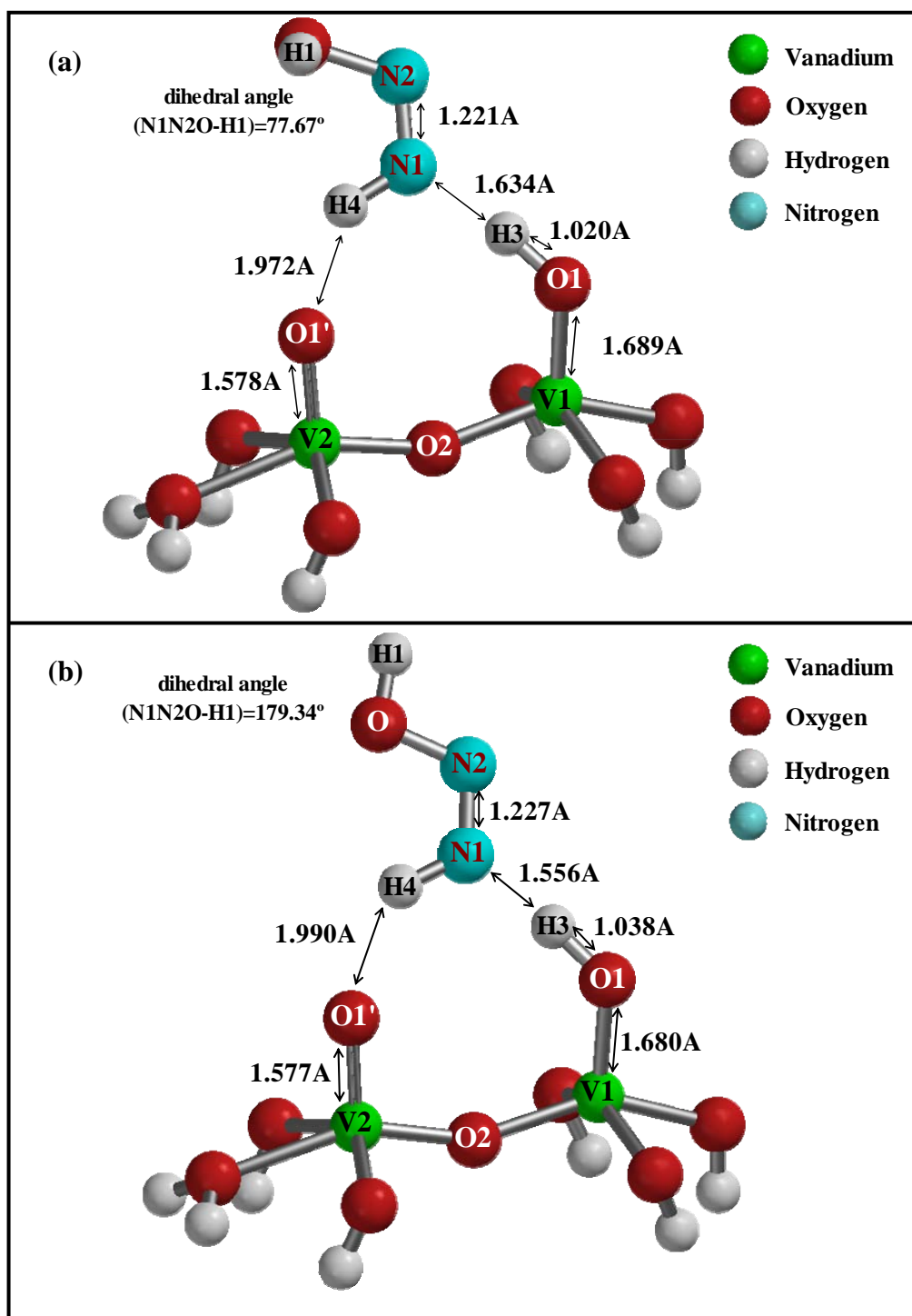
Figure 4.16. (a) Transition state geometry for the isomerization reaction of the adsorbed cis-HN=NOH species to form cis-HN=NO-trans-H species, **(b)** Equilibrium geometry of the adsorbed cis-HN=NO-trans-H species.

Cis-HN=NO-trans-H species is rotated again on the cluster in order to take advantage of the hydrogen atom push pull capability of the catalyst surface (see Figure 4.17). A coordinate driving calculation is finally performed for H_2O and N_2 formation reaction by selecting the distance between H3 and O atoms as a decreasing reaction coordinate and energy profile which is illustrated in Figure 4.18 is obtained. The transition state of this interaction having a relative energy difference of -7.86 kcal/mol is illustrated in Figure 4.19 (a). Searching for the equilibrium geometry of this interaction, it is found that formation of water and nitrogen occurs as shown in Figure 4.19 (b) with an exothermic relative energy difference of 79.50 kcal/mol. The catalytic cycle can then be completed by the oxidation of the V-OH site formed during the last step in part II (NH_2NO formation reactions).
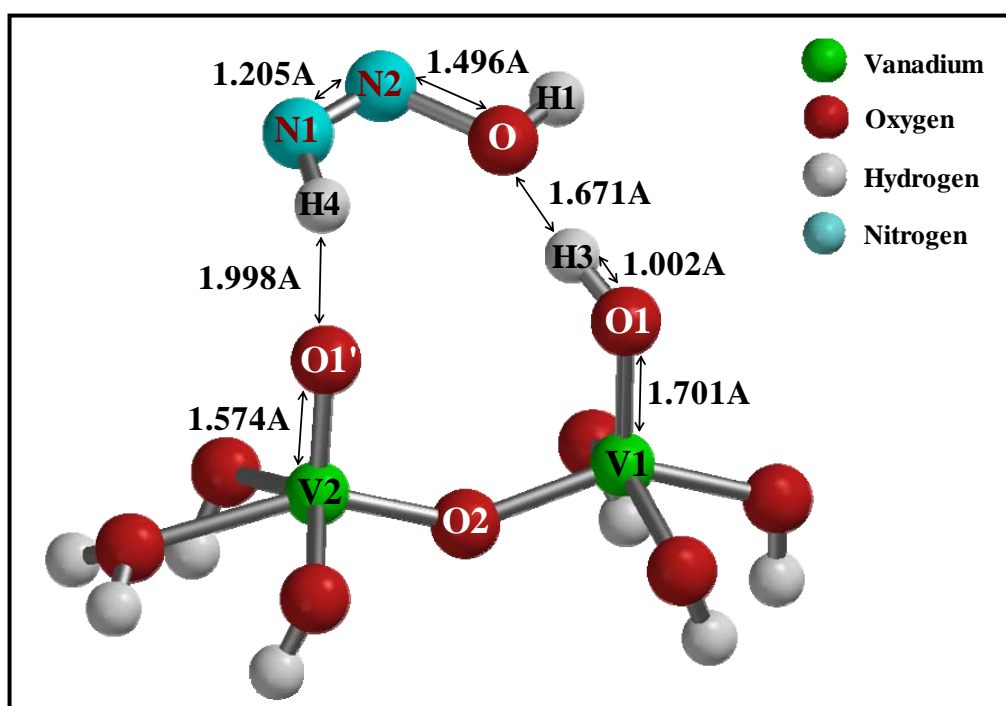
Figure 4.17. Equilibrium geometry of the rotated cis-H-N=NO-trans-H species on $V_2O_9H_8$ cluster.
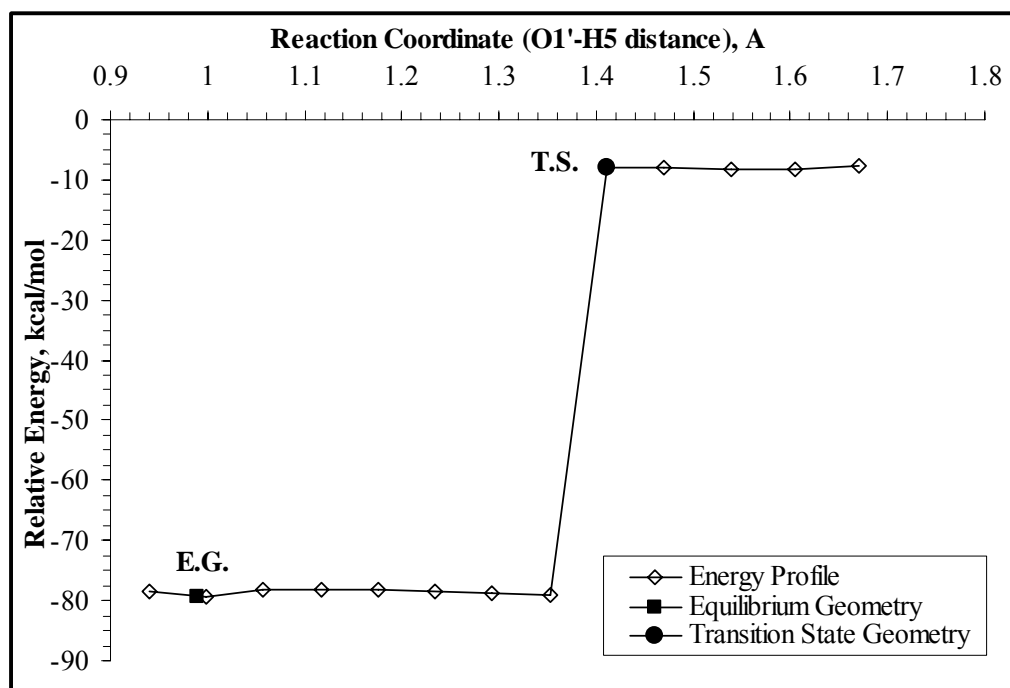
Figure 4.18. Energy profile for H_2O and N_2 formation reaction from cis-HN=NO-trans-H species.

An important point about the calculations in this part is that, as mentioned before a new cluster is employed to be able to decompose NH_2NO species into H_2O and N_2. Because by the formation of this molecule, the oxygen sites of the $V_2O_9H_8$ cluster are saturated with the hydrogen atoms (Part II). However, Anstrom et al. (2003) performed all of the reactions on a cluster consisting of four vanadium atoms and calculating the relative energy with respect to $V_2O_9H_8$ cluster, NH_3 (g) and NO (g). In this research NH_2NO decomposition reaction is accomplished on a new $V_2O_9H_8$ cluster and the relative energy values in this part are calculated with respect to the cluster and NH_2NO (g). Moreover, the work of Anstrom et al. (2003) the vanadium atoms were kept fixed while here, the vanadium atoms of the cluster are relaxed. It should be also noted that due to the complexity of the reaction, a successful transition state geometry with regard to SCR reaction steps has not yet been reported in the theoretical literature using DFT method.

However, in this research the transition state geometries for all of the reaction steps involved in the third part of the SCR reaction are the results of the successful transition state geometry calculations, not the approximate transition state values.

An alternative to this part was the gas phase decomposition of NH_2NO. In Uzun (2003) and in the work of Onal et al. (2005) the energetics of the gas phase decomposition reaction of NH_2NO into nitrogen and water are summarized by a potential energy profile including relative energies of transition and equilibrium geometries as shown in Figure 4.20.
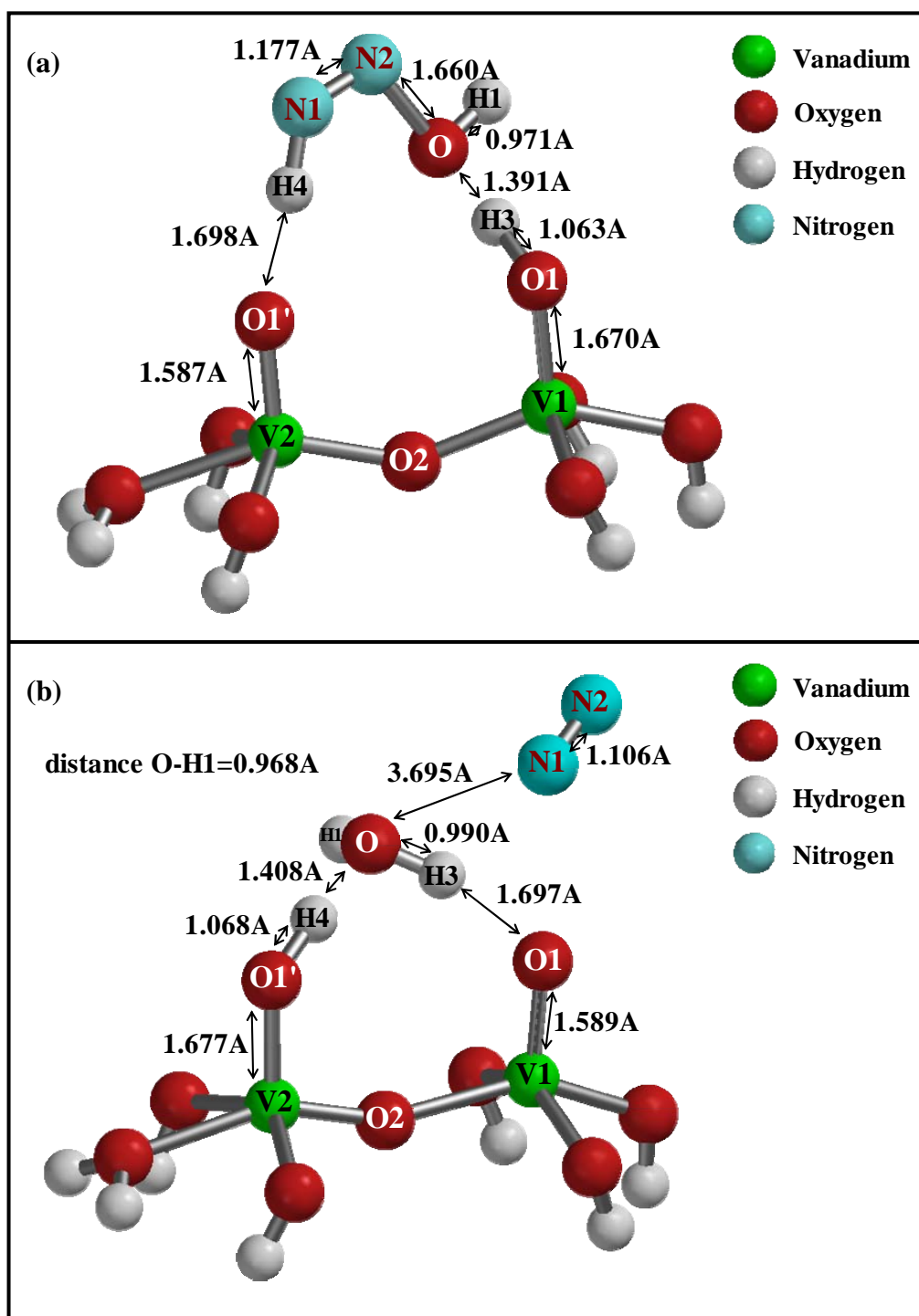
Figure 4.19. (a) Transition state geometry and **b)** Equilibrium geometry for N_2 and H_2O formation reaction from the re-adsorbed cis-H-N=NO-trans-H species.
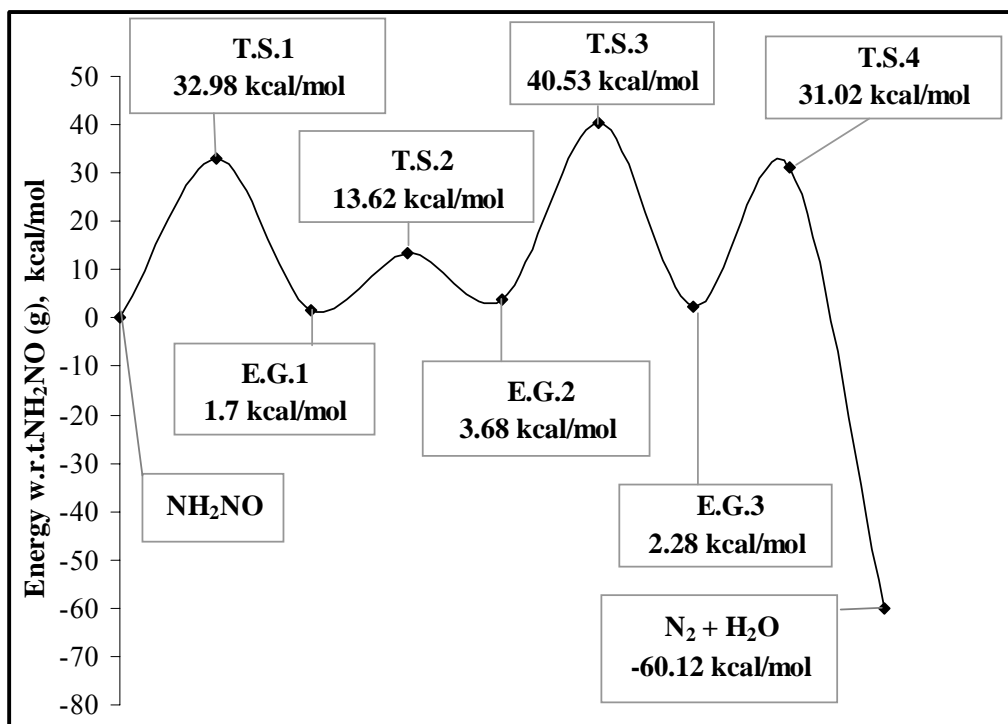
Figure 4.20. Potential energy profile for the gas phase NH_2NO decomposition reaction (T. S. represents the transition states, while E. G. stands for the equilibrium geometries) (Uzun, 2003; and Onal et al., 2005).

As it is evident from the figure the activation barriers of the reaction steps of the gas phase NH_2NO decomposition are quite high values ranging from 11.92 to 36.85 kcal/mol. On the other hand, the activation barriers for the catalytic NH_2NO decomposition range from 0.57 to 7.22 kcal/mol (Figure 4.8). Therefore, it is concluded that the gas phase NH_2NO decomposition reaction is energetically a much less favorable reaction in the SCR process as compared to the catalytic decomposition of this species on the cluster surface and the beneficial effect of the vanadia surface providing a hydrogen transfer mechanism through oxygen sites is quite apparent in these calculations.

4.2. Adsorption Reactions on (101) and (001) TiO$_2$-Anatase Surfaces

Before performing the adsorption calculations over fixed and relaxed (101) and (001) anatase surfaces, both represented by Ti$_2$O$_9$H$_{10}$ clusters (Figure 3.6), the reactants (H$_2$O and NH$_3$) were initially optimized by means of the equilibrium geometry calculations. The energies of the fixed clusters are obtained by single point geometry calculations. Computational procedure described previously is then applied. All of the adsorption calculations in this part are carried out by considering the system as neutral and with singlet spin multiplicity.

4.2.1. H$_2$O Adsorption

4.2.1.1. H$_2$O Adsorption on (101) TiO$_2$ Surface

For molecular water adsorption, a reaction coordinate is selected as the distance between the oxygen atom of the water molecule and the titanium atom of the cluster for both fixed and relaxed clusters. The energy profiles obtained are shown in Figure 4.21. Molecular water adsorption occurs on partially relaxed cluster (Ti1 and O1 are relaxed) with an exothermic relative energy difference of -25.08 kcal/mol through a non-activated process. As shown in the same figure, on totally fixed (101) cluster the adsorption energy of molecular water adsorption comes out to be -28.97 kcal/mol. Moreover the energy points of the energy profile obtained for molecular water adsorption on fixed cluster are lower than those on relaxed cluster. The equilibrium geometries of this interaction are given in Figure 4.22. As seen in the figure water is molecularly adsorbed on the clusters with Ti1-O2 distance of 2.237 A in the case of relaxing the cluster and with Ti1-O2 distance of 2.222 on fixed cluster.
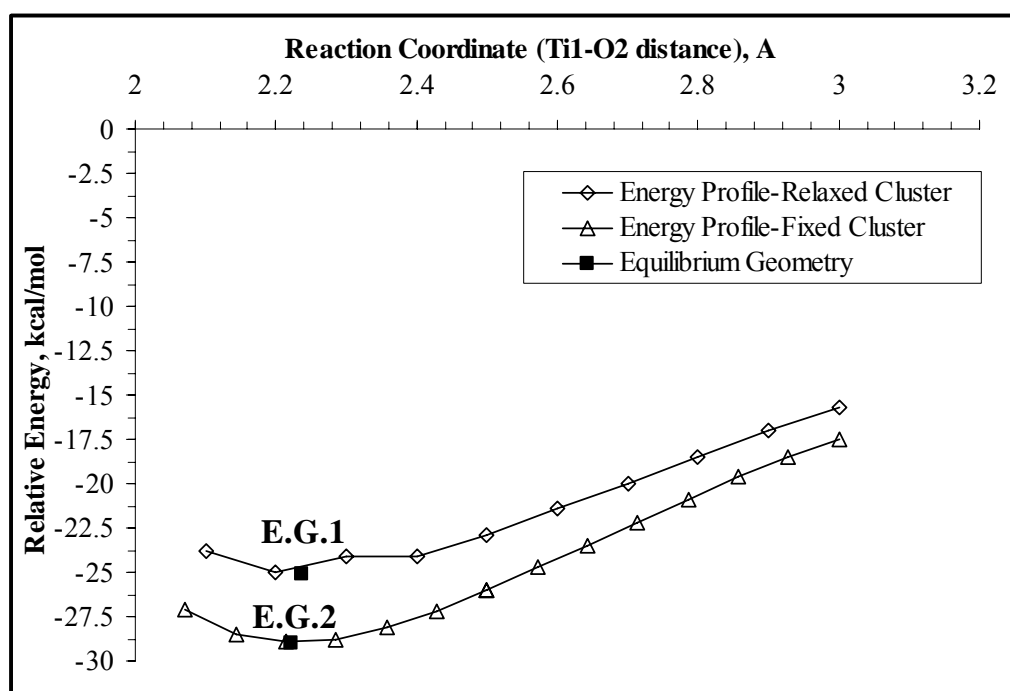
Figure 4.21. Energy profile for molecular H_2O adsorption on partially relaxed and fixed (101) $Ti_2O_9H_{10}$ clusters (E.G.1 and E.G.2 represents equilibrium geometries for relaxed and fixed clusters, respectively.)

Dissociative water adsorption is also considered on (101) anatase clusters starting from the optimized geometries of molecular water adsorption. For this purpose, for both clusters, a reaction coordinate is selected as the distance between the oxygen atom of the water molecule (H1) and the bridge oxygen (O1) of the cluster. As it is evident from the energy profiles obtained (see Figure 4.23), water dissociatively adsorbs on relaxed (101) cluster by an activation barrier of 18.76 kcal/mol with an endothermic relative energy difference of 5.87 kcal/mol, while on the fixed (101) cluster water dissociates with an activation barrier of 5.22 kcal/mol with an exothermic relative energy of 5.81 kcal/mol. It is seen that the activation barrier and adsorption energy for water dissociation on fixed cluster are

both much lower than the values obtained on relaxed cluster. The transition state and equilibrium geometries of this interaction are illustrated in Figure 4.24.
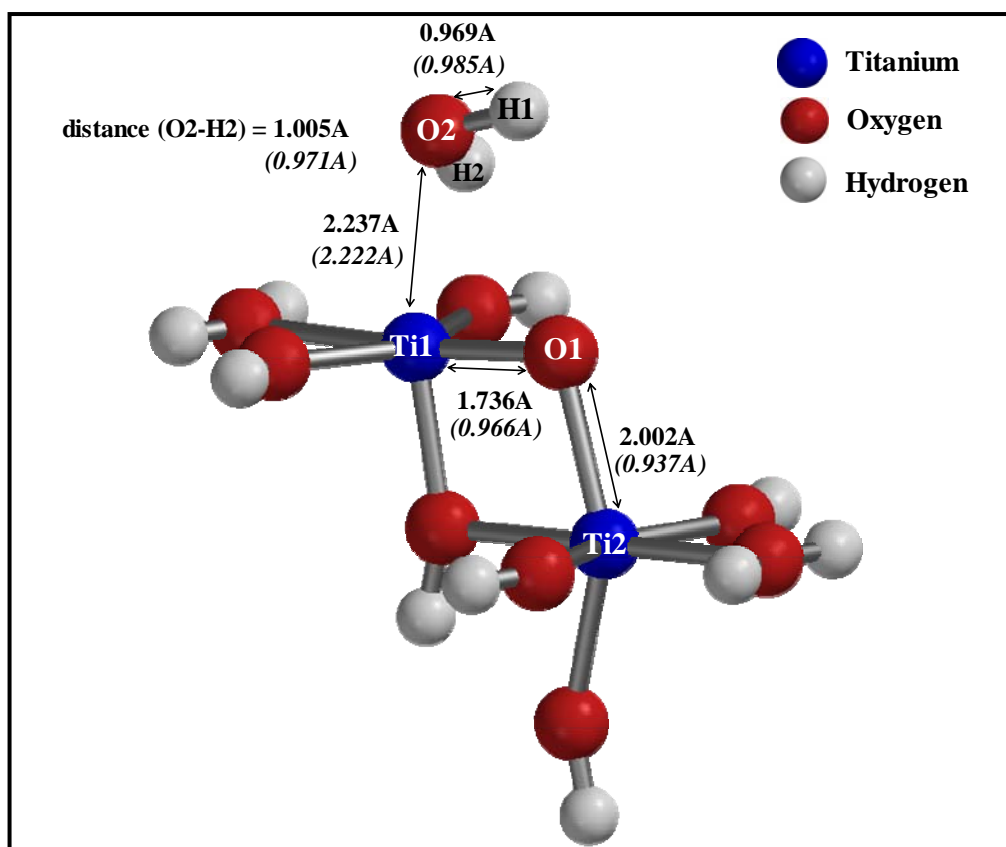
Figure 4.22. Equilibrium geometry of molecular H_2O adsorption on partially relaxed and fixed (101) $Ti_2O_9H_{10}$ clusters (Bond lengths without parentheses belong to the partially relaxed (101) cluster, while the values given in parentheses are for the fixed cluster).
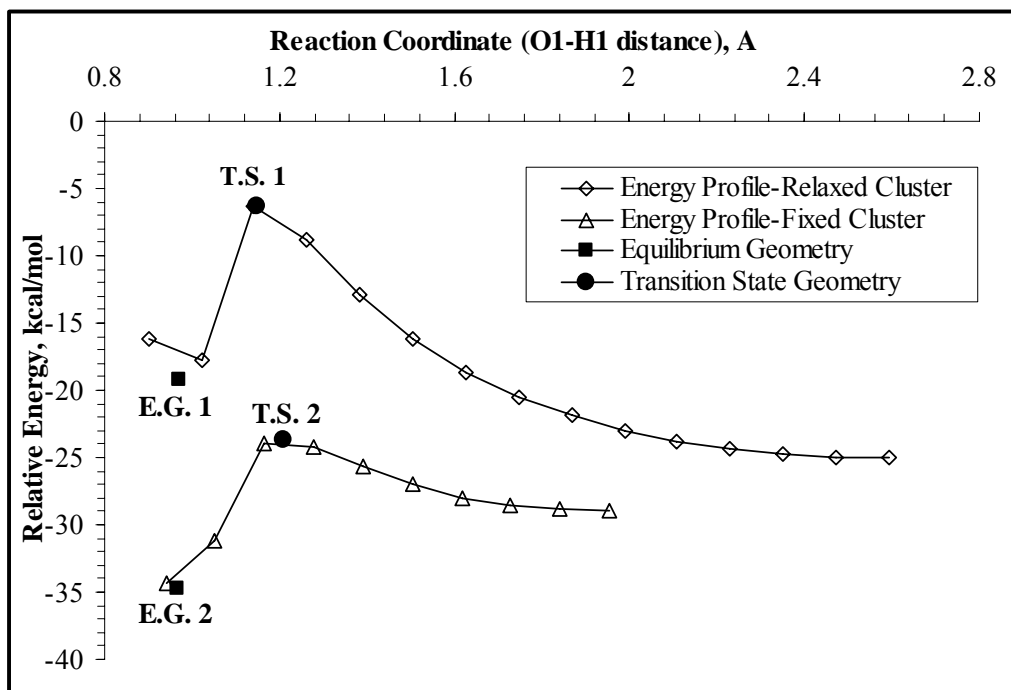
Figure 4.23. Energy profiles for dissociative H_2O adsorption for partially relaxed and fixed (101) $Ti_2O_9H_{10}$ clusters. (E.G.1 and E.G.2 represent equilibrium geometries; T.S.1 and T.S.2 stands for the transition state geometries calculated on relaxed and fixed (101) clusters, respectively).

The water adsorption energies calculated on relaxed and fixed (101) surfaces are compared with the available theoretical information in Table 4.2. It is found by the DFT calculations that molecular water adsorption is more favorable than dissociative adsorption (-25.08 kcal/mol vs -19.26 kcal/mol for relaxed (101) $Ti_2O_9H_{10}$ cluster while dissociative water adsorption is more favorable (-34.78 kcal/mol vs -28.97 kcal/mol) on fixed (101) $Ti_2O_9H_{10}$ cluster. All of the theoretical literature agrees that molecular water adsorption is more favorable on (101) anatase. However, by the calculations carried out on fixed (101) cluster the situation is the opposite case. The trend in the theoretical literature is met by the results obtained on the relaxed cluster.
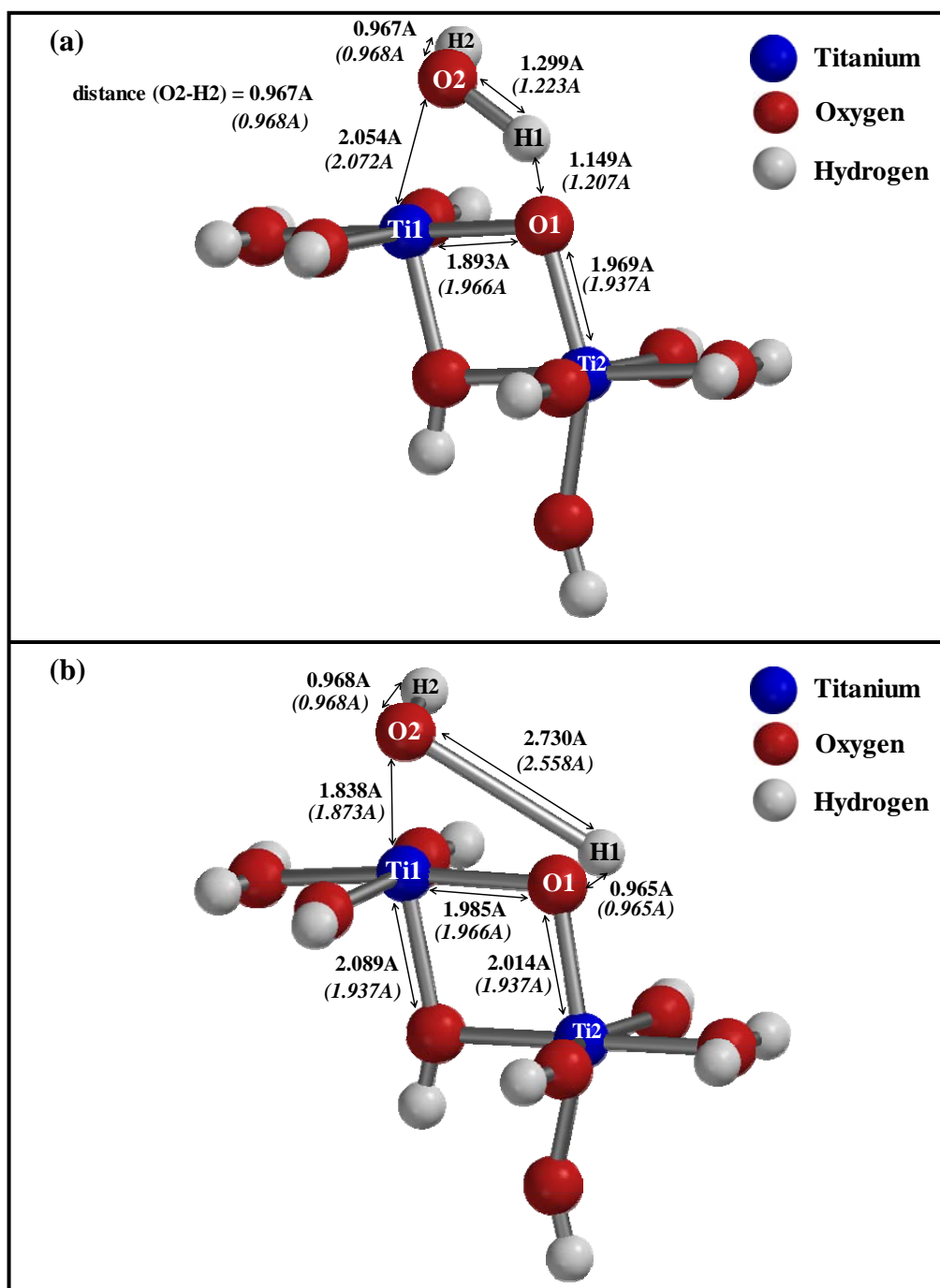
Figure 4.24. (a) Transition state and **(b)** Equilibrium geometries of dissociative H$_2$O adsorption on partially relaxed and fixed (101) Ti$_2$O$_9$H$_{10}$ clusters (Bond lengths without parentheses belong to the partially relaxed (101) cluster, while the values given in parentheses are for the fixed cluster).

Table 4.2. Comparison of the calculated H_2O adsorption energies on (101) surface with the theoretical values in the literature.

Method	Surface	Adsorption Energy (kcal/mol)	
		Molecular	Dissociative
DFT B3LYP/6-31G**	101 Anatase Relaxed $Ti_{12}O_9H_{10}$ Cluster	-25.08	-19.26
	101 Anatase Fixed $Ti_{12}O_9H_{10}$ Cluster	-28.97	-34.78
DFT	101 Anatase Slab	-16.60 ($\theta=1$)	-10.15 ($\theta=1$)
DFT	101 Anatase	-29.5	-11.7
B3LYP/6-31G*//B3LYP/6-31G*	TiO_5H_6 Cluster	(-31.1)[a]	(-11.5)[a]
Molecular Dynamics	101 Anatase Surface	-17.30	-6.92, -8.76

[a]Values in parentheses are calculated by MP2/6-31G*//MP2/6-31G*

In the experimental literature it is indicated that after water dissociates on titanium dioxide surface and then water molecules could form hydrogen bonds with the surface hydroxyl groups (Bredzona et al. (2004)). This case is also simulated on relaxed and fixed (101) clusters by single point equilibrium geometry calculations. Water molecule forms hydrogen bonding with pre-water dissociated system on fixed and relaxed (101) $Ti_2O_9H_8$ clusters (see Figure 4.25) with exothermic relative energy differences of 18.12 and 18.72 kcal/mol, respectively. As seen in Table 4.3, the adsorption energies of H-bonded water molecule on relaxed and fixed cluster models (18.12 and 18.72 kcal/mol) agree well with the experimental estimate of -18 kcal/mol (Srnak et al. (1992)). Therefore, our results indicate that the experimentally indicated value of 18 kcal/mol could be belonging to the H-bonded water molecule on (101) surface. In obtaining this result the fact that (101) face is exposed in anatase samples in majority could have played a role.
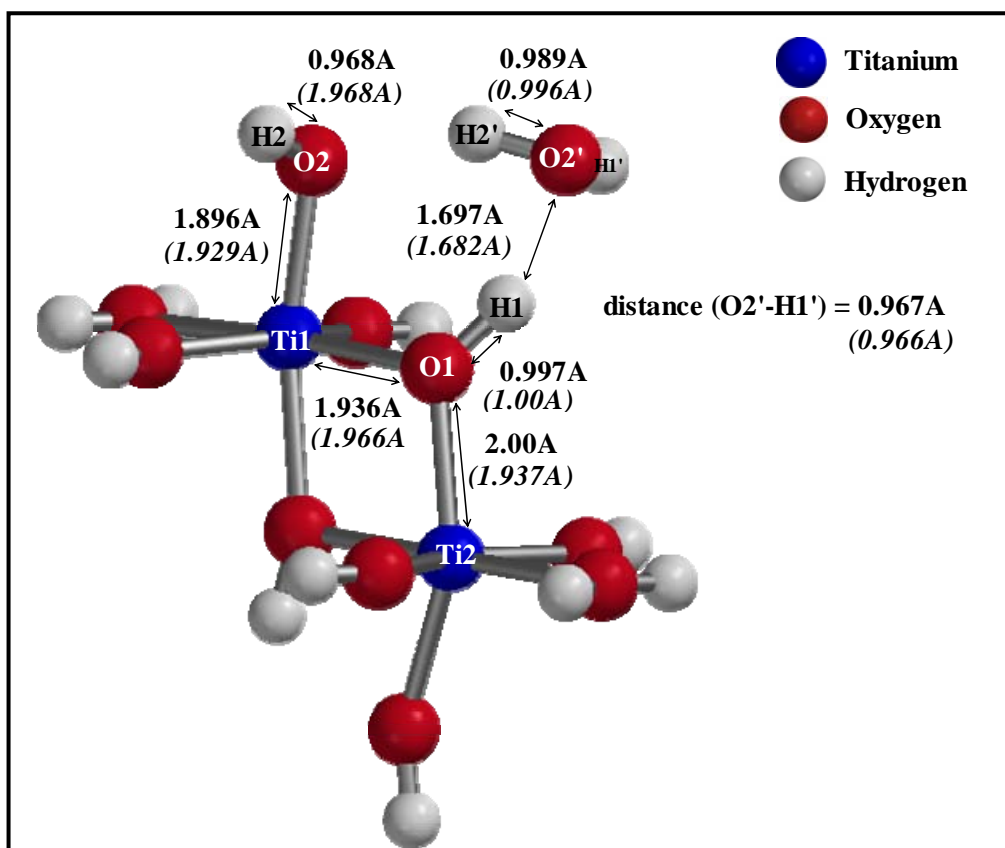
Figure 4.25. Optimized geometries of H-bonded H_2O adsorption on partially relaxed and fixed (101) $Ti_2O_9H_{10}$ clusters (Bond lengths without parentheses belong to the partially relaxed (101) cluster, while the values given in parentheses are for the fixed cluster).

Table 4.3. Comparison of the calculated adsorption energy of H_2O by H-bonding on (101) and (001) surfaces with the experimental values in the literature.

	Method	Surface	Adsorption Energy (kcal/mol)
Theoretical Values			
This Work	DFT B3LYP 6-31G**	101 Anatase Relaxed $Ti_2O_9H_{10}$ Cluster	-18.12
		101 Anatase Fixed $Ti_2O_9H_{10}$ Cluster	-18.72
		001 Anatase Relaxed $Ti_2O_9H_{10}$ Cluster	-11.47
Experimental Values			
Srnak et al. (1992)	TPD	TiO_2 Anatase	-11, -18
Munuera et al. (1972)	TPD	TiO_2 Anatase	-12

4.2.1.2. H_2O Adsorption on (001) TiO_2 Surface

Firstly, molecular water adsorption is aimed to be studied on a partially relaxed $Ti_2O_9H_{10}$ cluster (Ti1, Ti2, and O1 are relaxed) representing (001) surface (see Figure 3.6 (b)). As previously described methods, a coordinate driving calculation is performed by selecting the reaction coordinate as the distance between the oxygen of the water molecule and one of the Ti atoms of the cluster. As a result of the energy profile given in Figure 4.26, it is seen that water molecule is dissociated on the cluster surface by a non-activated process with an exothermic relative energy difference of 54.12 kcal/mol. The equilibrium geometry of this interaction including the bond lengths is shown in Figure 4.27. The water molecule is dissociated on this surface by destroying the oxygen bride structure of the cluster geometry. By this interaction, two inequivalent hydroxyls terminally bound to adjacent Ti sites along (100) direction are formed. The equilibrium geometry obtained (Figure 4.27) is similar to what Vittadini et al. (1998) previously reported by DFT method on (001) anatase slab.
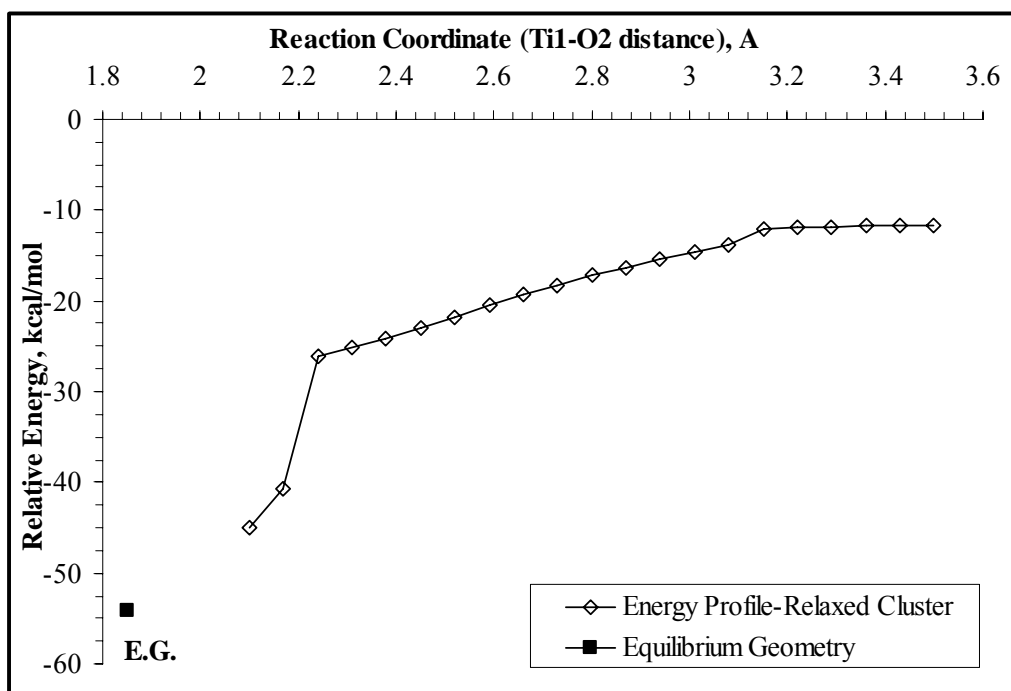
Figure 4.26. Energy profile for dissociative H_2O adsorption on (001) $Ti_2O_9H_{10}$ cluster.
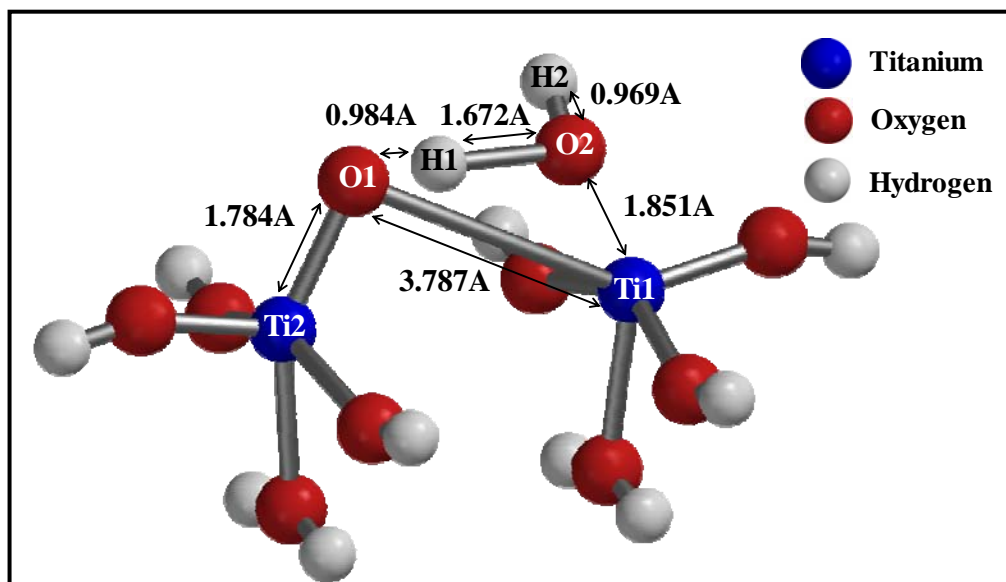
Figure 4.27. Equilibrium geometry for dissociative H_2O adsorption on (001) $Ti_2O_9H_{10}$ cluster.

By a single point equilibrium geometry calculation, water adsorption by hydrogen bonding on the system obtained in Figure 4.27 is also studied. Water adsorption by hydrogen bonding occurs with an exothermic relative energy difference of 11.47 kcal/mol. The optimized geometry of this event is illustrated in Figure 4.28. The adsorption energy calculated for H-bonded water on (001) anatase cluster is compared with the experimental values in Table 4.3. As it is evident from the figure the computed value provides agreement with the experimental data. It can be conjectured by this finding that second TPD site (-11 and -12 kcal/mol) can be represented by (001) surface.
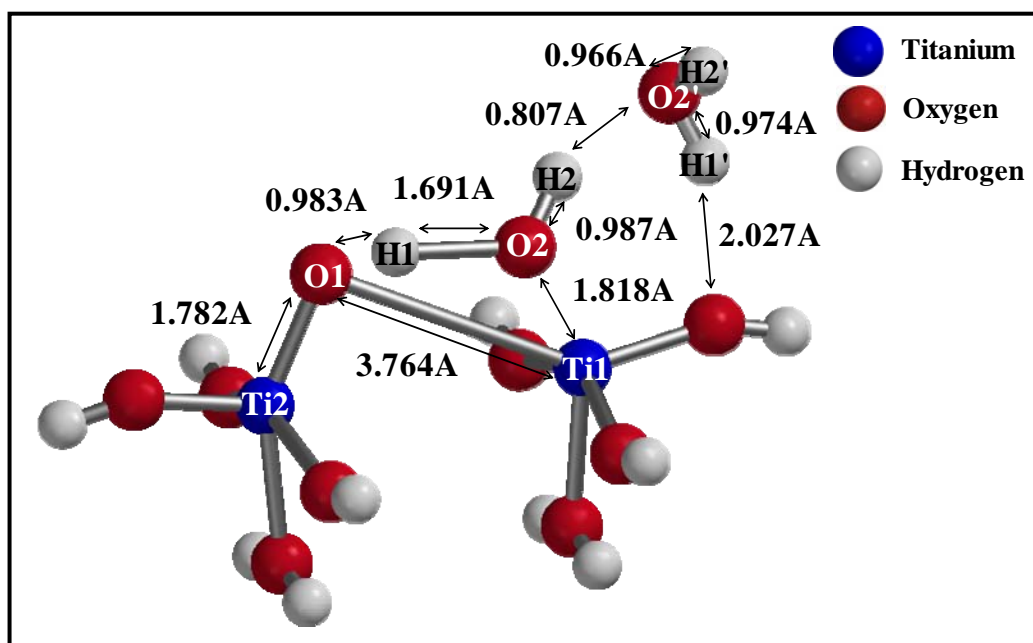
Figure 4.28. Equilibrium geometry for H-bonded water adsorption on relaxed (001) $Ti_2O_9H_{10}$ cluster.

As it is evident from Figure 4.27, water dissociates by a non-activated process destroying the bridge oxygen structure of the surface on the cluster representing (001) surface in contrary to (101) surface. By the dissociative adsorption of water

on (001) relaxed cluster surface two OH groups, T1-O2H2 and Ti2-O1H1, are formed (Figure 4.27). Therefore, according to DFT computations it is shown that if only one water molecule is present on the cluster it dissociates. Then, the situation when two H_2O molecules are approaching to the cluster is also investigated. For this purpose, two separate reaction coordinates are selected: the distances between the titanium atoms and the oxygen atoms of the two H_2O molecules. The resultant energy profile (Figure 4.29) shows that water molecules are adsorbed molecularly on the cluster with an exothermic relative energy of 49.85 kcal per two moles of H_2O or -24.93 kcal/mol. The equilibrium geometry of this interaction is illustrated in figure 4.30.
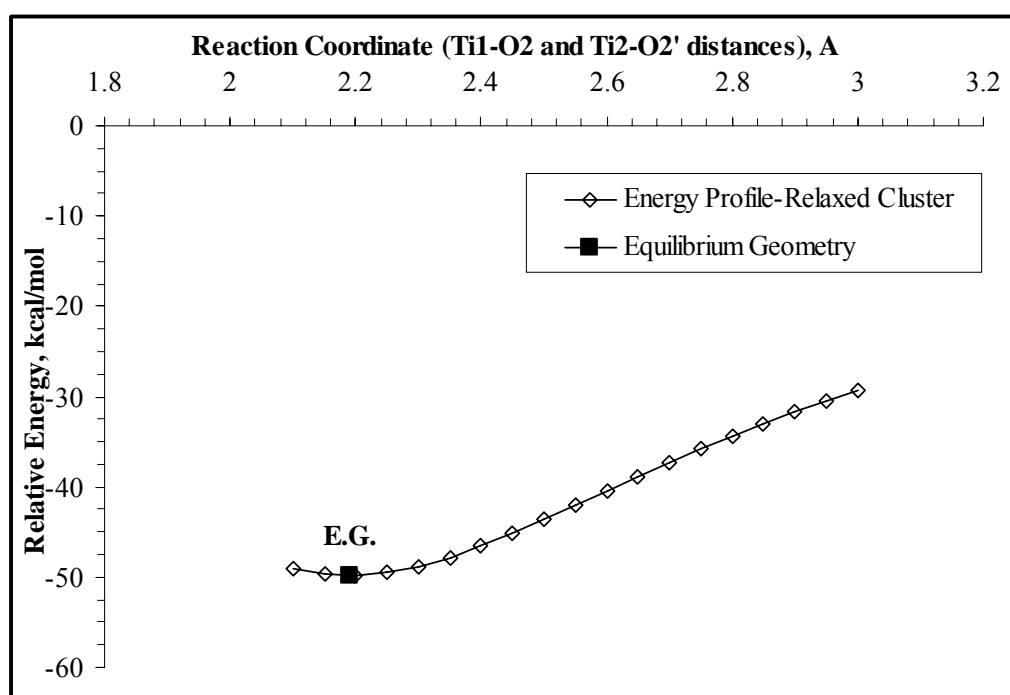
Figure 4.29. Energy profile for molecular adsorption of two H_2O molecules on relaxed (001) $Ti_2O_9H_{10}$ cluster.
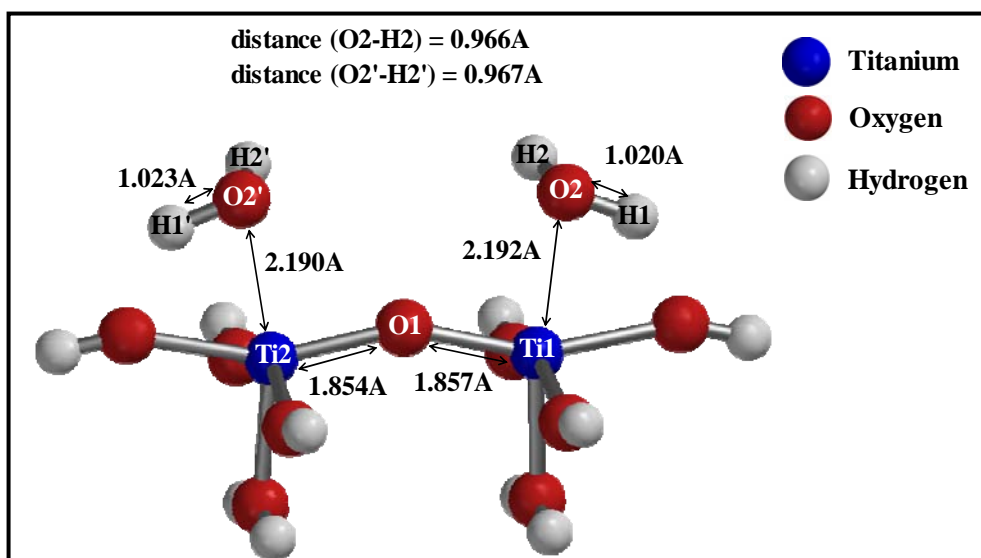
Figure 4.30. Equilibrium geometry for molecular adsorption of two H_2O molecules on relaxed (001) $Ti_2O_9H_{10}$ cluster.

If molecular water adsorption is simulated on a fixed $Ti_2O_9H_{10}$ cluster, by choosing a reaction coordinate as the distance between the oxygen of the water molecule (O2) and one of the Ti atoms of the cluster (Ti1), energy profile obtained is given in Figure 4.31. It can be concluded that water molecule is adsorbed on the cluster surface by a non-activated process with an exothermic relative energy difference of 23.46 kcal/mol with Ti1-O2 distance of 2.230 A (Figure 4.32).
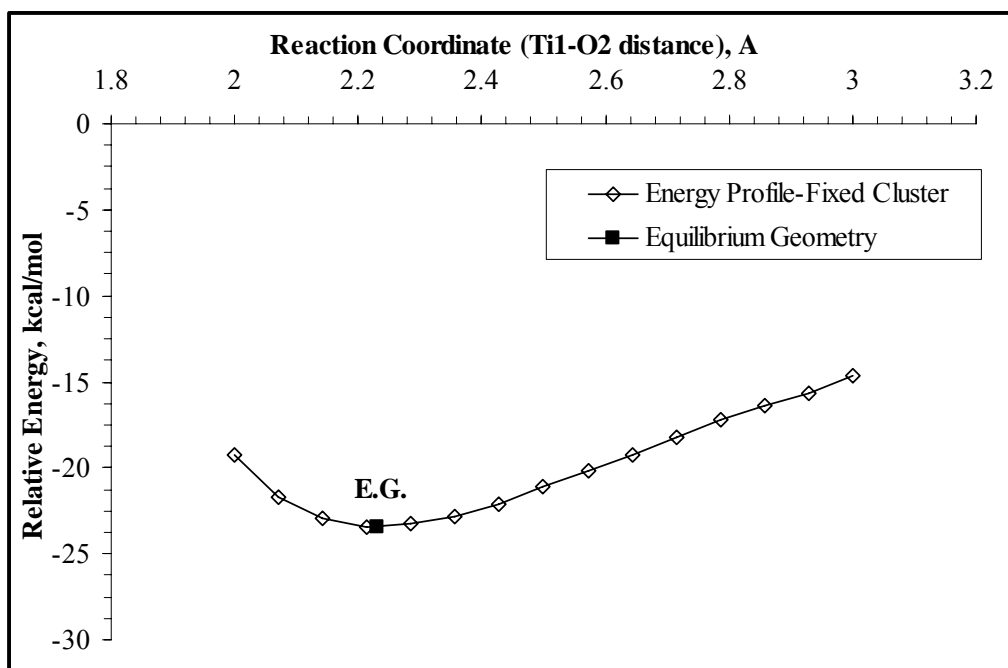
Figure 4.31. Energy profile for molecular H_2O adsorption on fixed (001) $Ti_2O_9H_{10}$ cluster.

Starting from the molecularly adsorbed water given in figure 4.32, water dissociation is studied by a coordinate driving calculation selecting the distance between O1-H1 atoms as the reaction coordinate. The resulting energy profile (Figure 4.33) shows that water dissociates on the fixed $Ti_2O_9H_{10}$ cluster with an endothermic relative energy difference of 12.25 kcal/mol by an activation barrier of 12.92 kcal/mol. Transition state and equilibrium geometry of water dissociation on (001) fixed cluster are given in Figure 4.34.
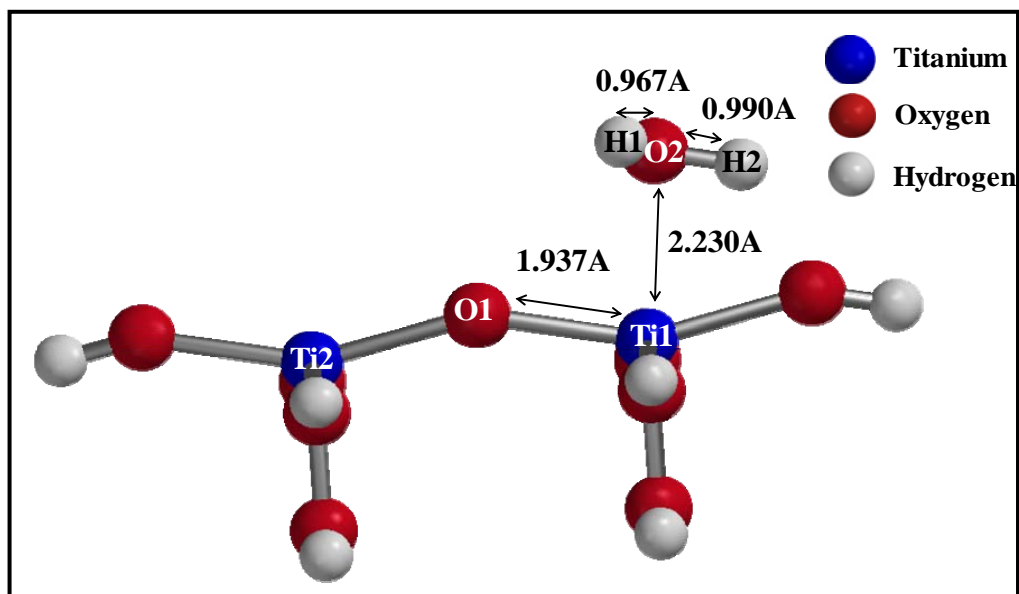
Figure 4.32. Equilibrium geometry for molecular H_2O adsorption on fixed (001) $Ti_2O_9H_{10}$ cluster.
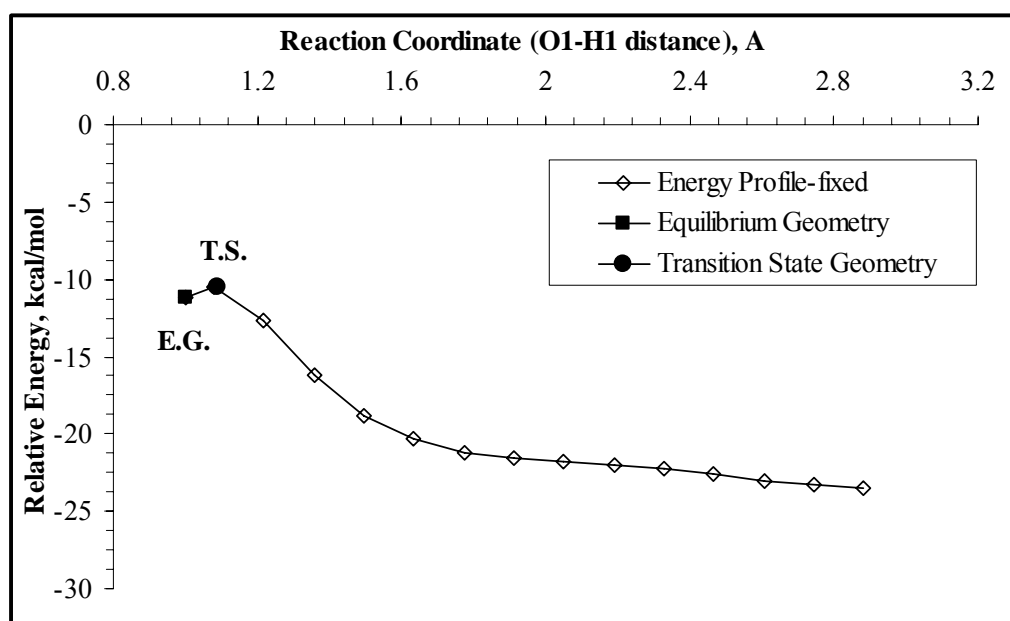
Figure 4.33. Energy profile for dissociative H_2O adsorption on fixed (001) $Ti_2O_9H_{10}$ cluster.
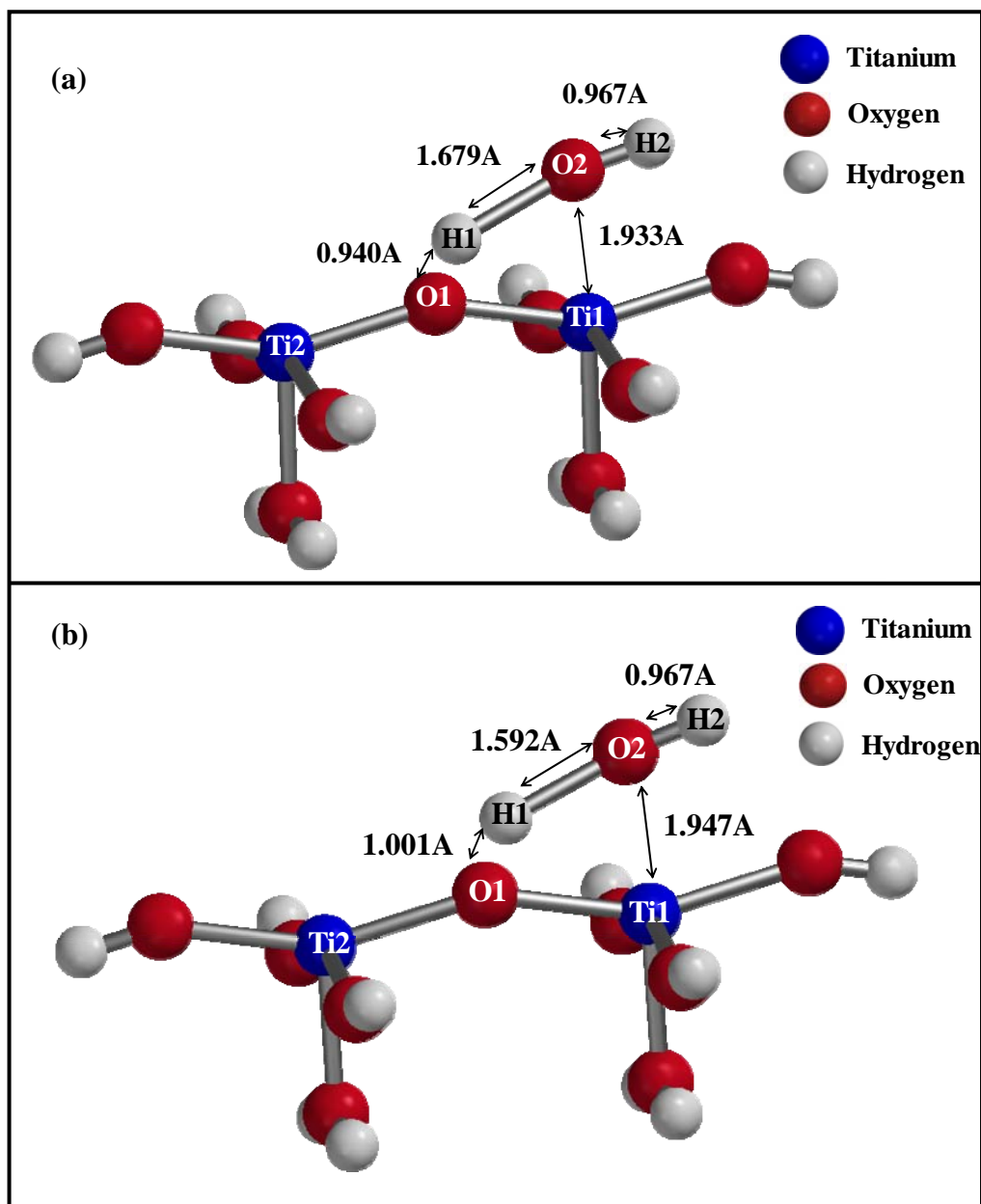
Figure 4.34. (a) Transition state and (b) Equilibrium geometry for dissociative H_2O adsorption on fixed (001) $Ti_2O_9H_{10}$ cluster.

The comparison of the water adsorption energetics on (001) surface with the available theoretical literature is given in Table 4.4. It is found that when the partial relaxation is applied on the cluster, dissociative water adsorption is more favorable than molecular adsorption (-54.12 kcal/mol vs -24.93 kcal/mol). However, the calculations carried out on the fixed cluster showed the reverse situation. The agreement with the theoretical literature in terms of the favorable adsorption mode of water is satisfied by relaxed (001) cluster model.

The vibration frequencies for water adsorption on (101) and (001) cluster surfaces are calculated by single point energy calculations. The results are compared with the relevant experimental information in Table 4.5. As seen in the table O-H stretching vibration data of 3666, 3713 cm^{-1} and 3657, 3711 cm^{-1} computed for dissociative water adsorption on relaxed and fixed (101) surfaces, respectively agree very well with the experimental values of 3665, 3715 cm^{-1}. However, the same frequencies calculated on (001) anatase clusters for dissociative water adsorption shows some discrepancies with the experimental data. Stretching frequencies of 3331 and 3035 cm^{-1} for relaxed and fixed (001) surfaces are out of the experimentally predicted range (3600-3800 cm^{-1}). To sum up the findings given in Table 4.5, it can be concluded that calculated vibration frequency data for dissociative water adsorption on (101) surface agree better with the experimental data than those on (001) anatase surface. This could be an expected result since (101) surface is statistically more exposed on TiO_2 than (001) surface.

Table 4.4. Comparison of the calculated H_2O adsorption energy on (001) surface with the theoretical information in the literature

	Method	Surface	Adsorption Energy(kcal/mol)	
			Molecular	Dissociative
Theoretical Values				
This Work	DFT B3LYP/6-31G**	001 Anatase Relaxed $Ti_2O_9H_{10}$ Cluster	-24.93	-54.12
		001 Anatase Fixed $Ti_2O_9H_{10}$ Cluster	-23.46	-11.21
Bredow et al. (1995)	MO/SINDO	001 Anatase 2X2X3 Cluster	-35.61	-52.82
		001 Anatase 3X3X3 Cluster	-32.50	-38.72
		001 Anatase 4X4X3 Cluster	-25.33	-31.79
Vittadini et. al. (1998)	DFT	001 Anatase	-18.68 (θ=0.5)[a]	-33.21 (θ=0.5)[a]
			-18.91 (θ=1)[a]	-(θ=1)[a]
Kachurovskaya et al. (2002)	DFT	001 Anatase $Ti_6O_{19}H_{12}$ Cluster	-13.6	-
Fahmi et al. (1994)	Periodic	001 Anatase	-14.34	-28.68

[a] θ is the surface coverage for H_2O on TiO_2 (001) surface

103

Table 4.5. Comparison of the vibrational frequencies (cm^{-1}) of H$_2$O adsorbed on (101) and (001) Ti$_2$O$_9$H$_{10}$ clusters with literature values.

| H$_2$O Adsorption on 101 Anatase Ti$_2$O$_9$H$_{10}$ Cluster[a] | | | | H$_2$O Adsorption on 001 Anatase Ti$_2$O$_9$H$_{10}$ Cluster[a] | | | | Experimental Values |
| Relaxed Cluster | | Fixed Cluster | | Relaxed Cluster | | Fixed Cluster | | |
Molecular	Dissociative	Molecular	Dissociative	Molecular	Dissociative	Molecular	Dissociative	Dissociative
3005, 3661	3666, 3713	3381, 3634	3657, 3711	2753, 3692	3331, 3656	3256, 3692	3035, 3681	3600-3800 [b] (O-H stret.)
1605		1622		1532		1543		3665, 3715 [c] (O-H stret.)

[a] Calculated values are scaled by 0.9613 (Ming et al., 1996)
[b] Morterra (1988)
[c] Primet et al. (1970)

The vibrational frequencies (cm^{-1}) of H-bonded H_2O molecule adsorbed on (101) and (001) $Ti_2O_9H_{10}$ clusters are compared with the experimental values in Table 4.6. As seen in the table, symmetric stretching frequency of H_2O calculated on (101) relaxed cluster (3299 cm^{-1}) is within 3200-3550 cm^{-1} range. On the other hand, asymmetric stretching frequency of 3679 cm^{-1} is a bit out of the experimentally estimated range of 3200-3500 cm^{-1}. Deformation frequency of water molecule (1666 cm^{-1}) adsorbed on Ti^{4+} cation of relaxed (101) cluster compare with the experimental value of 1600 cm^{-1}. The symmetric and asymmetric stretching frequency computed for fixed (101) surface comes out to be slightly out of the experimentally reported range of 3200-3500 cm^{-1}. Similar to relaxed (101) surface the deformation frequency value on this surface (1672 cm^{-1}) compares with the experimental value. For the relaxed (001) cluster, the H-bonded water molecule has symmetric and asymmetric OH stretching frequencies of 3295, 3352 cm^{-1} which agree well with the experimentally predicted range of 3200-3500 cm^{-1}. 1635 cm^{-1} of deformation frequency also compares with the experimental values. Moreover, another deformation mode of water at 1024 cm^{-1} is in good agreement with what Bredzona et al. (2004) reported as 1048 cm^{-1} for H-bonded water molecule on TiO_2. In brief, experimental TPD results are met by H-bonded water adsorption on fixed and relaxed (101), and on relaxed (001) $Ti_2O_9H_{10}$ clusters (Table 4.3). The interesting point is that the vibration frequency calculations for these geometries showed agreement with the experimentally reported values as given in Table 4.6.

Table 4.6. Comparison of the vibrational frequencies (cm^{-1}) of H-bonded H_2O molecule adsorbed on (101) and (001) $Ti_2O_9H_{10}$ clusters with the experimental values.

H_2O Adsorption on 101 Anatase $Ti_2O_9H_{10}$ Cluster[a]		H_2O Adsorption on 001 Anatase $Ti_2O_9H_{10}$ Cluster[a]	Experimental Values
Relaxed Cluster	Fixed Cluster	Relaxed Cluster	
3299, 3679 (O-H stret.)	3199, 3688 (O-H stret.)	3295-3352 (O-H stret.)	3350-3500 [b] 3200-3550 [c] (O-H stret.)
1666, 1145 (O-H deform.)	1672 (O-H deform.)	1635, 1024 (O-H deform.)	1640 [b], 1600-1630 [c] (O-H deform.) 1048, 1137, 1222 [c] (O-H deform.)

[a] Calculated values are scaled by 0.9613 (Ming et al., 1996)
[b] Morterra (1988)
[c] Bezrodna et al. (2004)

106

4.2.2. NH$_3$ Adsorption

Ammonia adsorption is also studied on fixed and relaxed Ti$_2$O$_9$H$_{10}$ clusters for both molecular and dissociative adsorption reactions. It is an important point that, to the best of our knowledge there is no theoretical study for ammonia adsorption on (101) and (001) anatase surfaces.

4.2.1.1. NH$_3$ Adsorption on (101) Surface

For both clusters, a reaction coordinate is selected as the distance between the nitrogen atom of the ammonia molecule (N1) and the titanium atom (Ti1) of the fixed and relaxed cluster surfaces. The resultant energy profile given in Figure 4.35 shows that NH$_3$ molecule is adsorbed on Ti^{4+} site exhibiting a non-activated mode with adsorption energies of -25.66 kcal/mol and -30.78 kcal/mol on relaxed and fixed Ti$_2$O$_9$H$_{10}$ clusters, respectively. The equilibrium geometry of this interaction is given in Figure 4.36. Ammonia molecule is adsorbed on the relaxed (Ti1 and O1 atoms are relaxed) and fixed cluster models representing the surface of (101) anatase with N1-Ti1 distances of 2.272 A and 2.257A, respectively.

Ammonia dissociation reaction is also studied following molecular NH$_3$ adsorption. For this purpose the distance between H1 and O1 (in Figure 4.36) is selected as the reaction coordinate for both clusters. According to the resulting energy profile given in Figure 4.37, it is seen that ammonia dissociates on relaxed and fixed Ti$_2$O$_9$H$_{10}$ clusters with endothermic relative energy differences of 22.02 and 13.58 kcal/mol; having activation barriers of 31.52 and 18.01 kcal/mol, respectively. Transition state and equilibrium geometries of this reaction are illustrated in Figure 4.38 including the distances between the atoms.
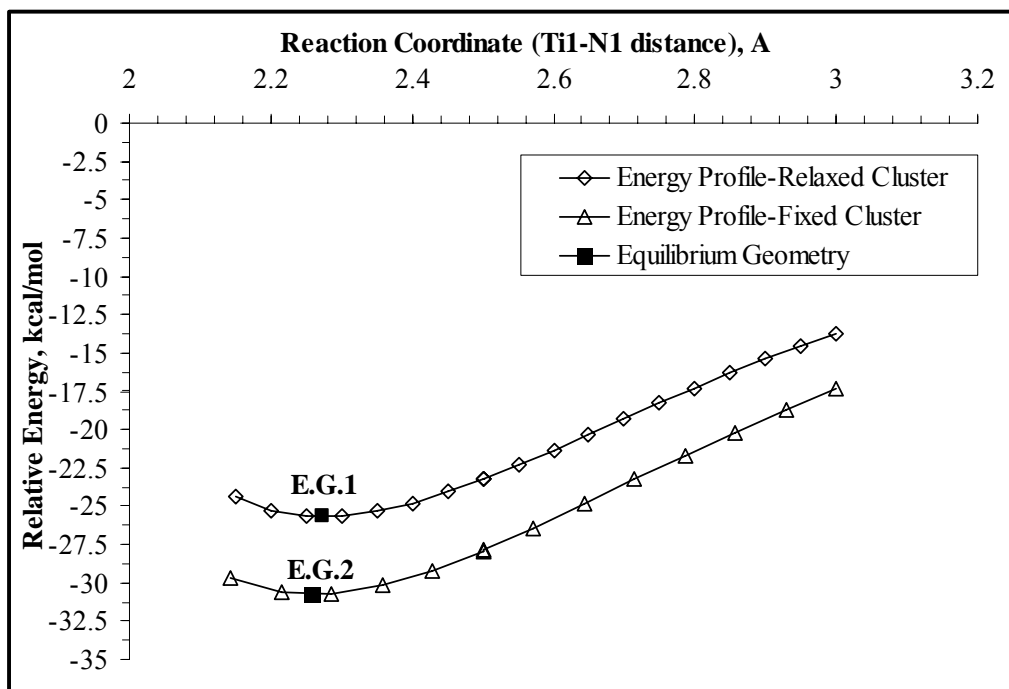
Figure 4.35. Energy profile for NH_3 adsorption on fixed and relaxed (101) $Ti_2O_9H_{10}$ clusters (E.G.1 and E.G.2 represent equilibrium geometries on relaxed and fixed (101) clusters, respectively).
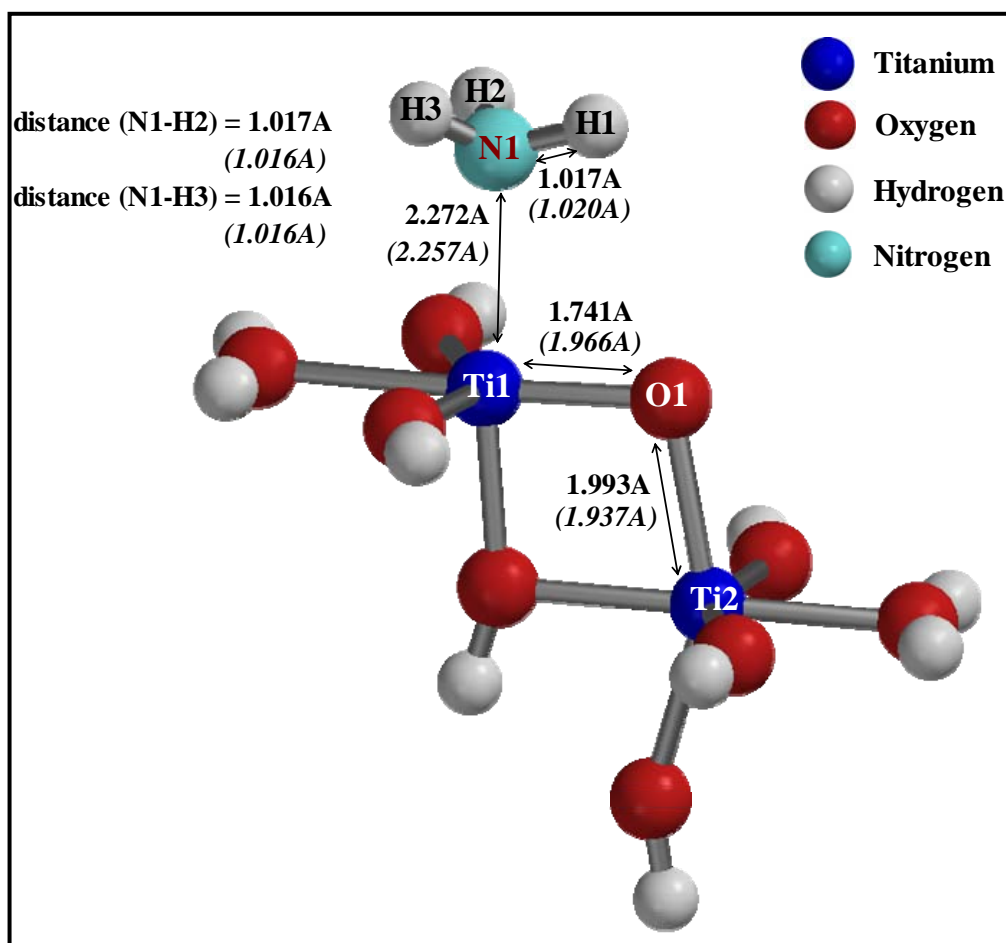
Figure 4.36. Equilibrium geometry of ammonia adsorption on fixed and relaxed (101) $Ti_2O_9H_{10}$ clusters (Bond lengths without parentheses belong to the partially relaxed (101) cluster, while the values given in parentheses are for the fixed cluster).

The optimized geometry of H-bonded ammonia molecule on pre-water dissociated relaxed and fixed (101) $Ti_2O_9H_{10}$ cluster surface is illustrated in Figure 4.38. Ammonia adsorption has relative energy differences of 13.22 and 14.38 kcal/mol on relaxed and fixed (101) $Ti_2O_9H_{10}$ clusters, respectively.
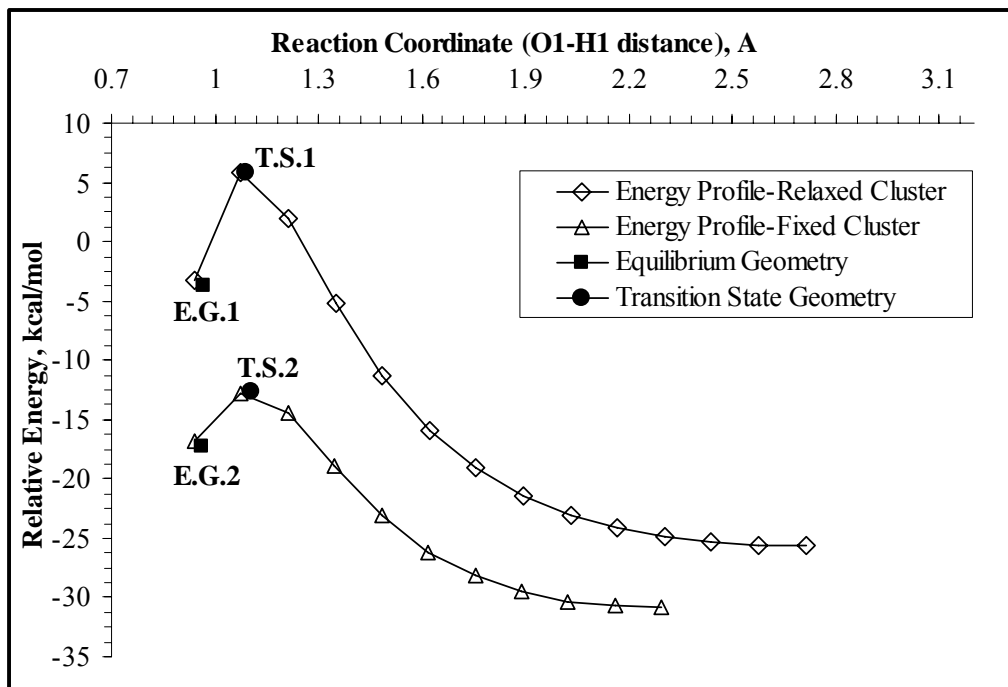
Figure 4.37. Energy profile for ammonia dissociation on relaxed and fixed (101) $Ti_2O_9H_{10}$ clusters (E.G.1 and E.G.2 represent equilibrium geometries; T.S.1 and T.S.2 stands for the transition state geometries calculated on relaxed and fixed (101) clusters, respectively).
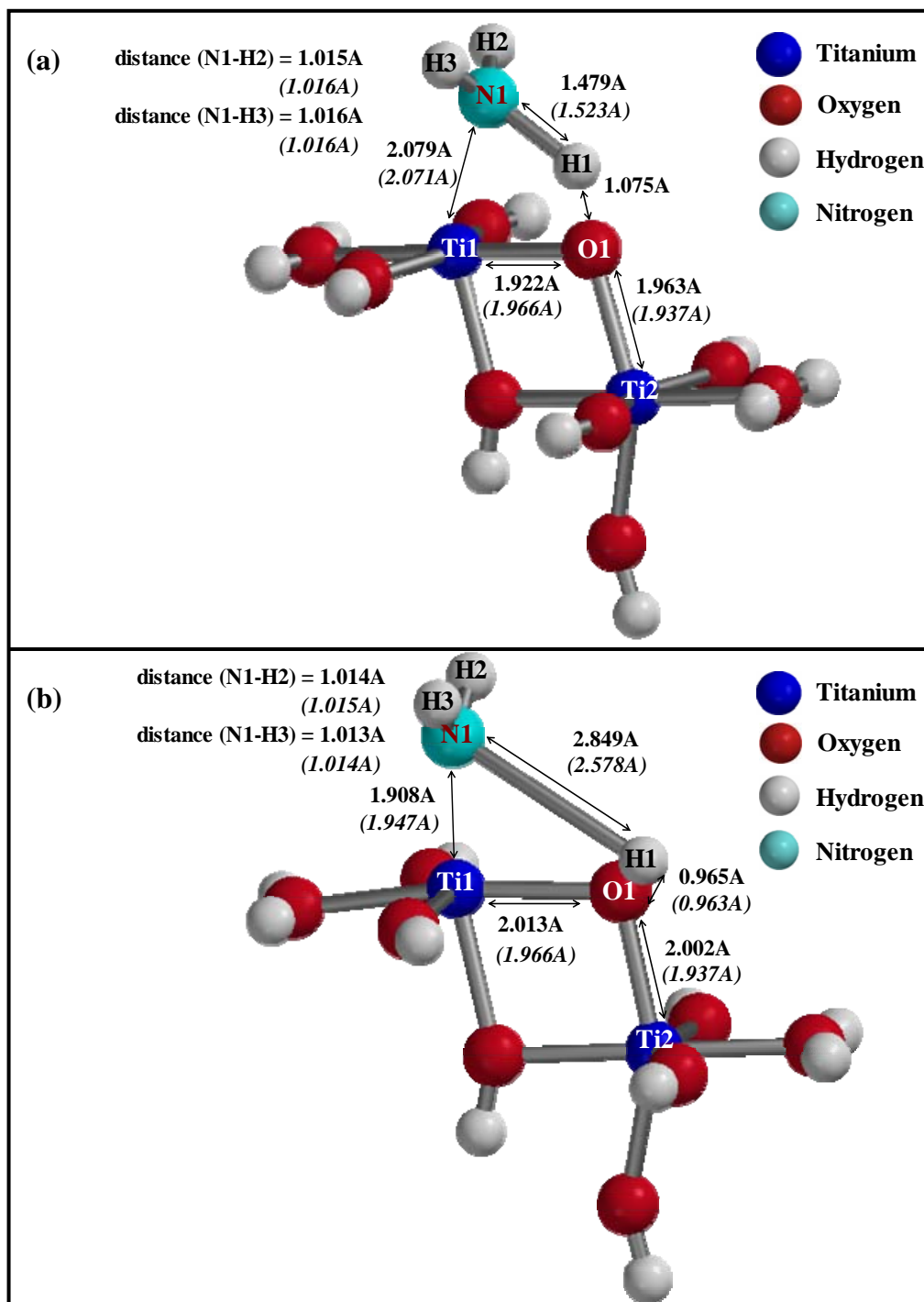
Figure 4.38. (a) Transition state and **(b)** Equilibrium geometries of dissociated ammonia on relaxed and fixed (101) $Ti_2O_9H_{10}$ clusters. (Bond lengths without parentheses belong to the partially relaxed (101) cluster, while the values given in parentheses are for the fixed cluster)

Obtaining the equilibrium geometries of dissociated ammonia, the adsorption of another NH_3 molecule by H-bonding on this system is studied by single point equilibrium geometry calculations. H-bonded ammonia on relaxed and fixed (101) $Ti_2O_9H_{10}$ clusters (shown in Figure 4.39) have exothermic relative energy differences of 13.22 and 14.38, respectively.
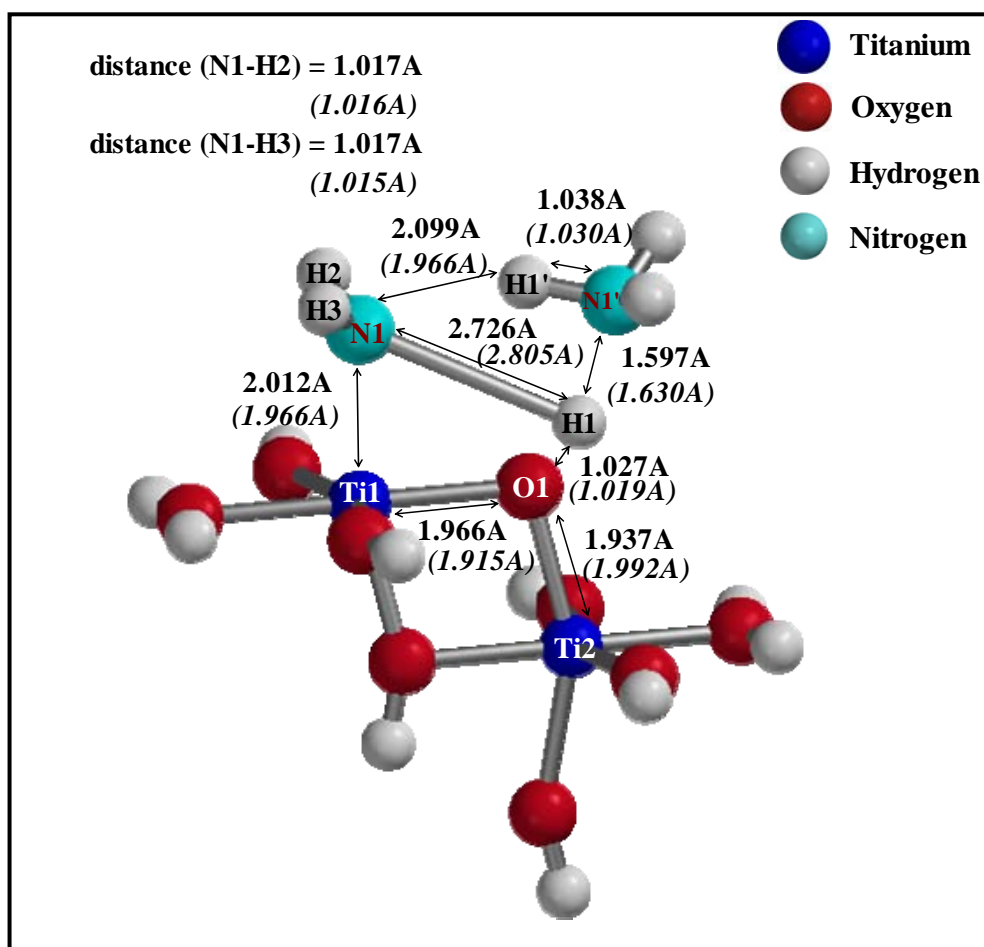
Figure 4.39. Equilibrium geometry of H-bonded ammonia on relaxed and fixed (101) $Ti_2O_9H_{10}$ clusters (Bond lengths without parentheses belong to the partially relaxed (101) cluster, while the values given in parentheses are for the fixed cluster).

4.2.1.2. NH₃ Adsorption on (001) Surface

For both relaxed (Ti1, O1 and Ti2 are relaxed) and fixed clusters, ammonia molecule is located at a chosen distance from the cluster and reaction coordinate is selected as the distance between the nitrogen atom of the ammonia molecule (N1) and the titanium atom (Ti1) of the cluster surface. According to the resultant energy profiles given in Figure 4.40, it is seen that NH_3 molecule is adsorbed on the cluster exhibiting a non-activated mode with adsorption energies of -26.57 and -23.72 kcal/mol on relaxed and fixed clusters, respectively. The equilibrium geometry of this reaction is also obtained which is illustrated in Figure 4.41. Ammonia molecule is adsorbed on the relaxed cluster having a N1-Ti1 distance of 2.272 A while on the fixed cluster this distance comes out to be 2.261 A.
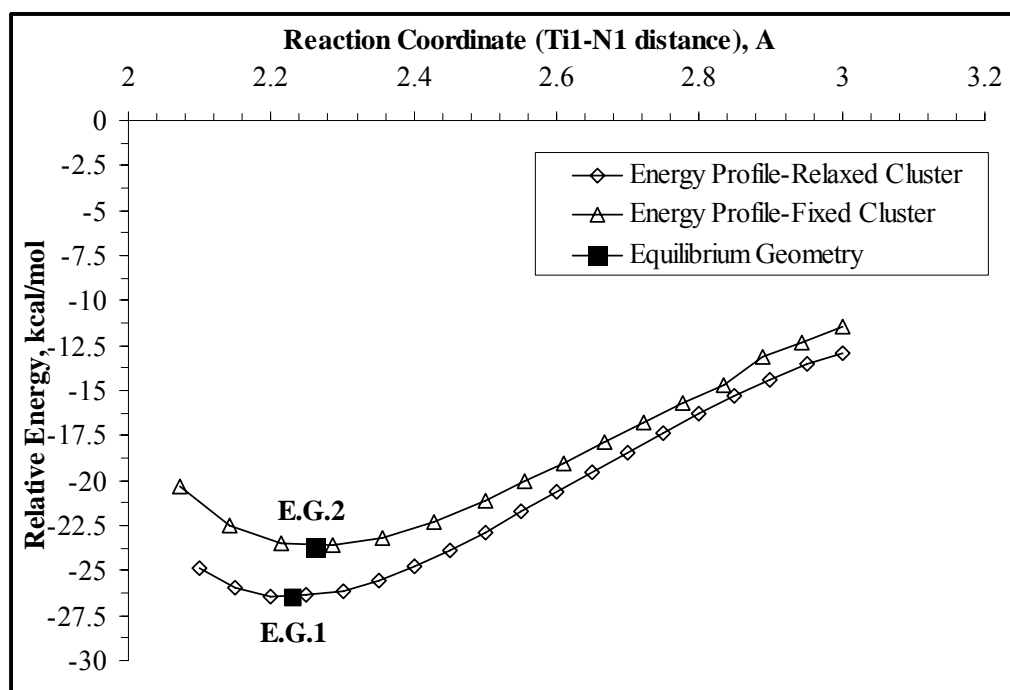
Figure 4.40. Energy profiles for ammonia adsorption on relaxed and fixed (001) $Ti_2O_9H_{10}$ clusters (E.G.1 and E.G.2 represent equilibrium geometries for relaxed and fixed (001) clusters, respectively).
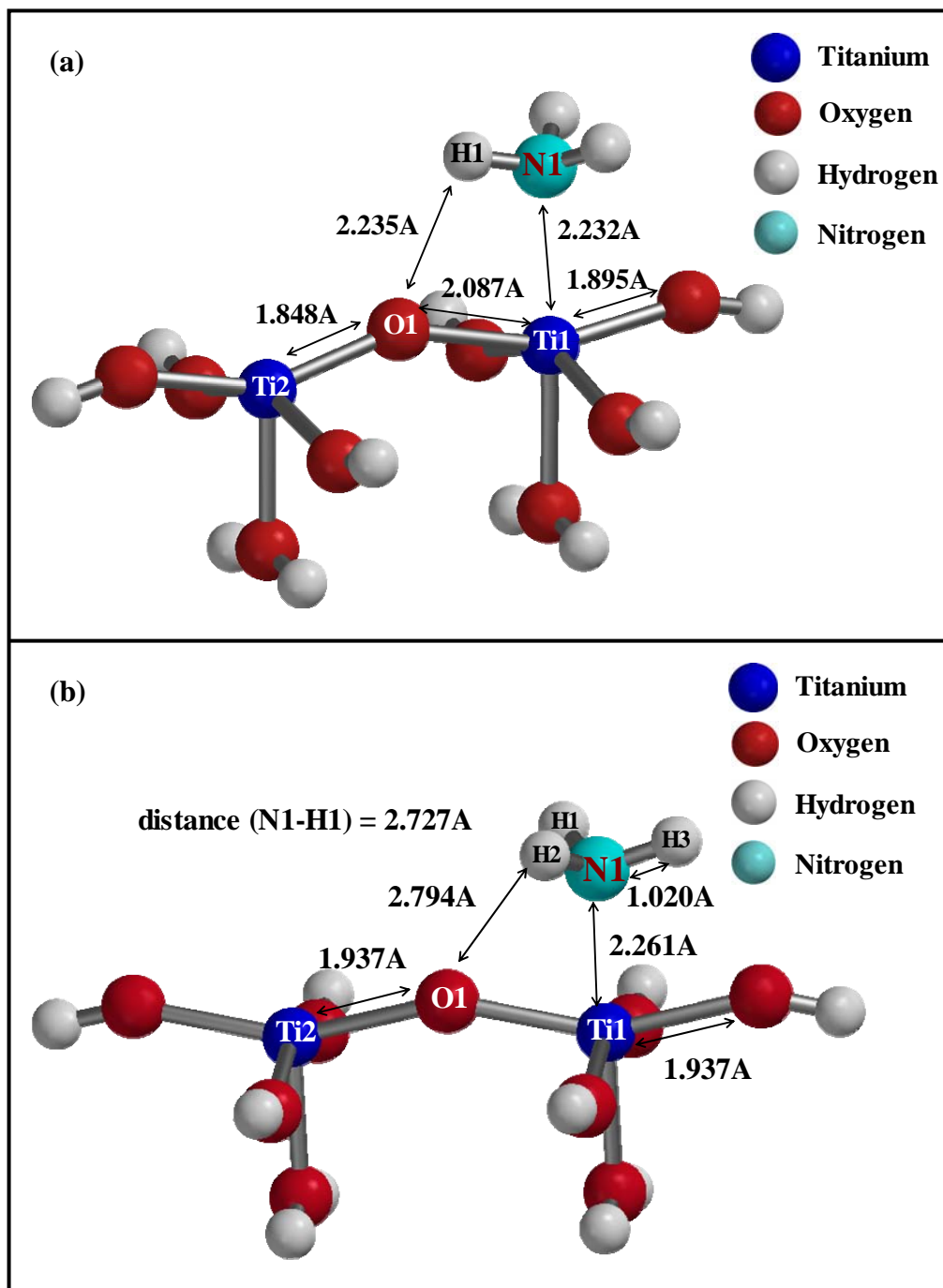
Figure 4.41. Equilibrium geometry for NH_3 adsorption on **(a)** relaxed (001) $Ti_2O_9H_{10}$ cluster, **(b)** fixed (001) $Ti_2O_9H_{10}$ cluster.

Ammonia dissociation is studied starting from molecularly adsorbed ammonia geometries given in Figure 4.41. Coordinate driving calculations are performed by choosing the distance between O1 and H1 atoms as reaction coordinates. Since the resulting energy profile obtained for fixed cluster shows a continuous increase with decreasing reaction coordinate (see Figure 4.42), it is concluded that ammonia dissociation on fixed (001) $Ti_2O_9H_{10}$ cluster turns out to be an unfavorable process.
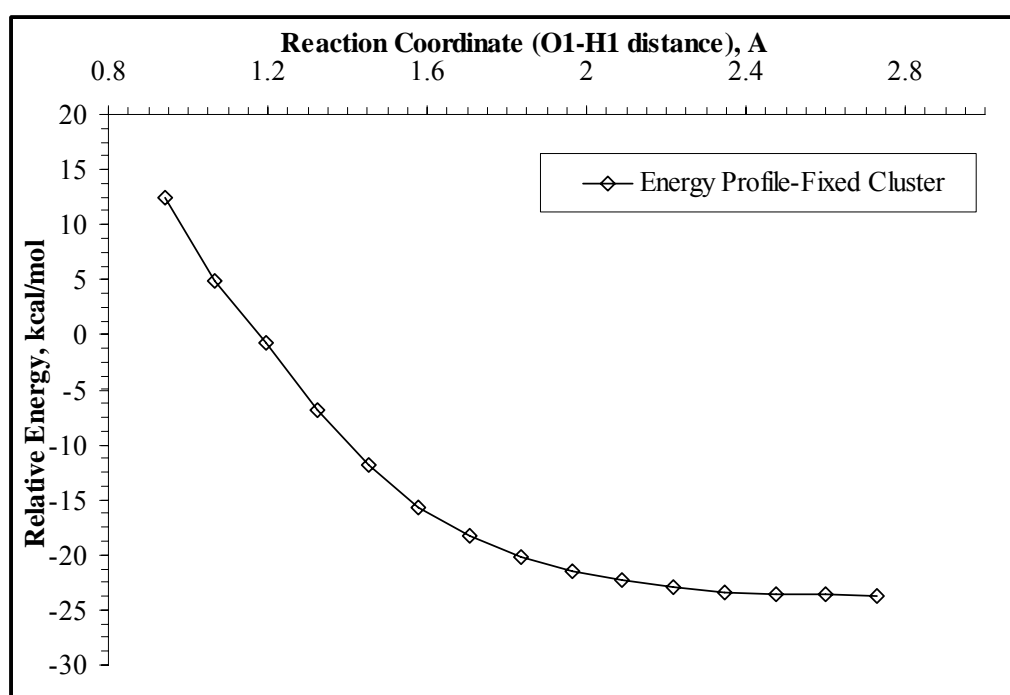
Figure 4.42. Energy profile for ammonia dissociation on fixed (001) $Ti_2O_9H_{10}$ cluster.

On contrary to the fixed cluster, ammonia dissociation occurs on relaxed $Ti_2O_9H_{10}$ cluster with an exothermic relative energy difference of 9.75 kcal/mol by a small activation barrier of 3.63 kcal/mol as given in Figure 4.43. Approximate transition state and equilibrium geometry of this reaction are given in Figure 4.44. At the approximate transition state N1-H1 bond is about to be broken as O1-H1 bond is about to be formed. At the equilibrium geometry ammonia molecule is dissociated into NH_2 and H atom destroying the bridge structure of the cluster. This configuration has Ti1-N1 and O1-H1 distances of 1.955A and 1.005A, respectively.
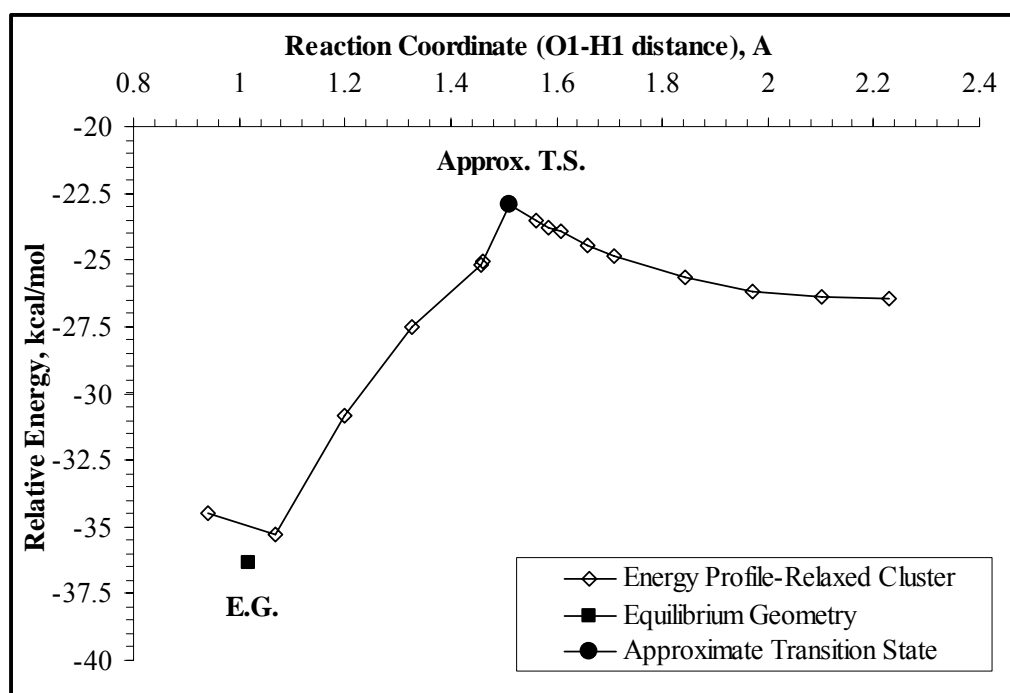
Figure 4.43. Energy profile for ammonia dissociation on relaxed (001) $Ti_2O_9H_{10}$ cluster.
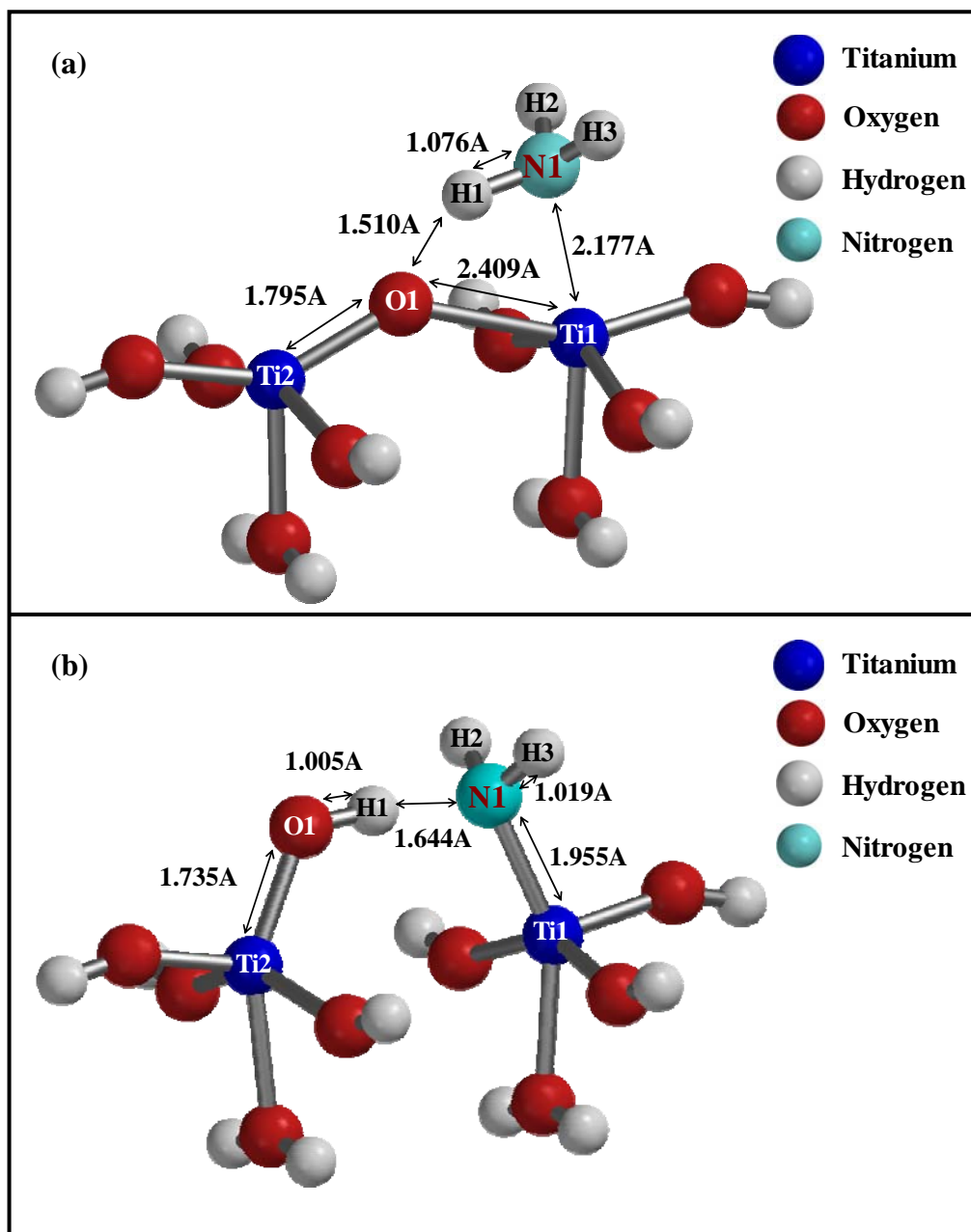
Figure 4.44. (a) Approximate transition state and **(b)** Equilibrium geometry of dissociated ammonia on relaxed (001) $Ti_2O_9H_{10}$ cluster.

Ammonia adsorption by H-bonding on the geometric configuration shown in Figure 4.44 (b) is studied by single point equilibrium geometry calculations. It is found that ammonia molecule is adsorbed by H-bonding (Figure 4.45) with an exothermic relative energy difference of 6.02 kcal/mol.
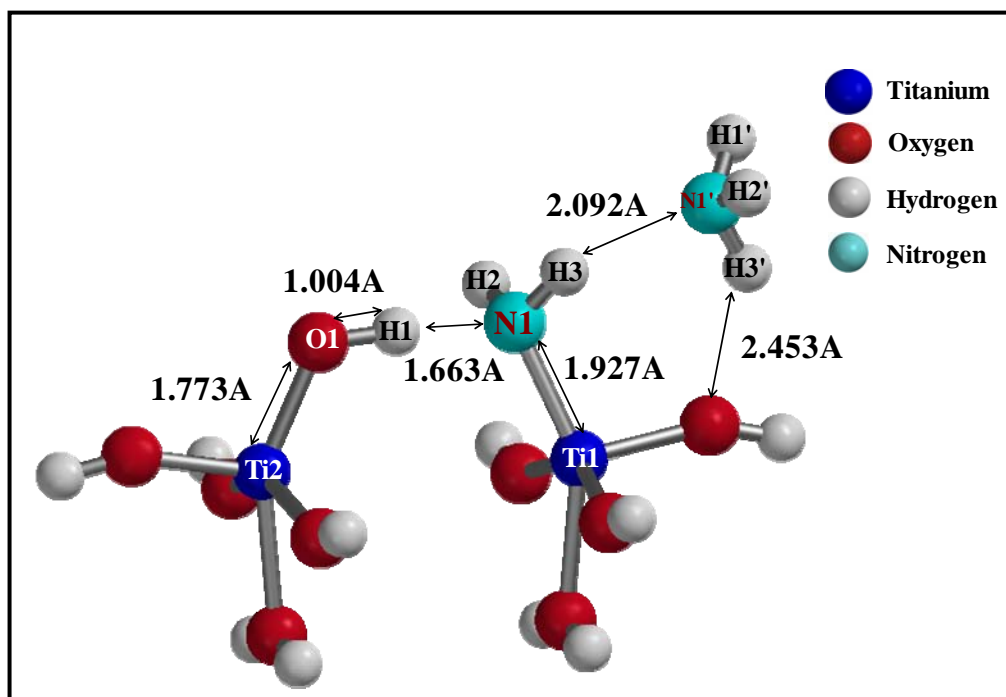
Figure 4.45. Equilibrium geometry of H-bonded ammonia on relaxed (001) $Ti_2O_9H_{10}$ cluster.

A comparison of the calculated NH_3 adsorption energies on (101) and (001) cluster surfaces with the literature values are given in Table 4.7. The calculated results are compared only with what is available in the experimental literature since there is no theoretical study on this topic. Molecular ammonia adsorption energies of -13.22 and -25.66 kcal/mol obtained on relaxed (101) $Ti_2O_9H_{10}$ cluster are comparable with -14 and -27 kcal/mol of ammonia desorption enthalpy reported by Srnak et al. (1992). This is reasonable in view of the fact that (101)

surface is a majority surface in anatase. The enthalpy values obtained on fixed (101) cluster (-14.38 and -30.78 kcal/mol) deviate slightly from the experimental values. On the other hand, only one enthalpy value for ammonia adsorption agrees with the experiment (-26.57 vs -27 kcal/mol) on relaxed (001) surface. This could also be expected since (001) surface is minority in anatase. Dissociation of ammonia is more favorable on relaxed (001) surface than (101) relaxed surface (-37 vs -3.64 kcal/mol); however, there seems to be no experimental data concerning this aspect.

Vibration frequencies for ammonia adsorption on these clusters are also calculated by single point energy calculations. A comparison of these findings with experimental data is given in Table 4.8. As it is evident from the table, vibration frequency data for molecular ammonia adsorption on Ti^{4+} sites resemble each other for all of the cluster models. The theoretical data also agrees with the experimental stretching and bending frequencies with the exception of symmetric bending frequency (1070-1132 cm^{-1} vs 1215 cm^{-1}). However, when vibration frequency calculations with regard to H-bonded NH$_3$ molecules are considered for (101) relaxed and fixed clusters , all of the values agree quite well with the experimental data including symmetric bending frequency value (1221 and 1258 vs 1215 cm^{-1}). The symmetric bending frequency of 1070 cm^{-1} for H-bonded ammonia adsorption on (001) relaxed surface deviates substantially from the experimental value of 1215 cm^{-1}. This is also consistent with enthalpy information. It should be also noted that all of the calculated deformation vibration frequencies except for H-bonded ammonia on relaxed (001) cluster agree well with the experimental estimate of 1480 cm^{-1}. The calculated vibration frequency for scissoring mode of NH$_2$ species on (001) relaxed cluster fits with the other experimental value of 1540 cm^{-1}.

Table 4.7. Comparison of the calculated NH_3 adsorption energy with the literature.

| Method | | Surface | Adsorption Energy (kcal/mol) | |
			Molecular	Dissociative
Theoretical Values				
This Work	DFT B3LYP 6-31G**	101 Anatase Relaxed $Ti_2O_9H_{10}$ Cluster	-13.22 [a], -25.66	-3.64
		101 Anatase Fixed $Ti_2O_9H_{10}$ Cluster	-14.38 [a], -30.78	-17.20
		001 Anatase Relaxed $Ti_2O_9H_{10}$ Cluster	-6.02 [a], -26.57	-36.32
		001 Anatase Fixed $Ti_2O_9H_{10}$ Cluster	-23.72	-
Experimental Values				
Srnak et al. (1992)	TPD	TiO_2 Anatase	-14, -27	-
Sprinceana et al. (1999)	DTA	TiO_2 Anatase	-31, -36	-

[a] Values for molecularly adsorbed H_2O molecule by H bonding on hydroxyl groups

Table 4.8. Comparison of the vibrational frequencies (cm-1) of NH_3 adsorbed on (101) and (001) $Ti_2O_9H_{10}$ clusters with the literature.

| NH₃ Adsorption on 101 Anatase Ti₂O₉H₁₀ Cluster[a] | | | | NH₃ Adsorption on 001 Anatase Ti₂O₉H₁₀ Cluster[a] | | | | Experimental Values | |
| Relaxed Cluster | | Fixed Cluster | | Relaxed Cluster | | Fixed Cluster | | | |
Molecular	Dissociative	Molecular	Dissociative	Molecular	Dissociative	Molecular	Dissociative	Molecular	Dissociative
1115		1132		1103		1070		1190, 1225[c], 1215[d] (sym. bend.)	
1618	1486	1642	1485	1605	1485	1609			1480[e], 1540[e] (NH₂ scis.)
3350		3338		3339		3358	-	1599[d], 1600[e] (asym. bend.)	
3478		3462		3477		3498			
1221[b]		1258[b]		1071[b]				3350[e] (sym. stret.)	
1624[b]	1486	1618[b]	1490	1644[b]	1528	-	-		
3380[b]		3359[b]		3327[b]				3400[e] (asym. stret.)	
3486[b]		3411[b]		3454[b]					

[a] Calculated values are scaled by 0.9613 (Ming et al., 1996)
[b] Values for molecularly adsorbed NH_3 molecule by H bonding on hydroxyl groups
[c] Amores et al. (1997)
[d] Terammura et al. (2003)
[e] Schneider et al. (1994)
[f] Lietti et al. (1998)

4.3. SCR Reaction on (001) TiO_2 Catalyst Surface

SCR reaction on titania was not studied before in the theoretical literature. In vanadia/titania catalysts commercially anatase phase is used. Moreover, due to its geometric complementary of with (010) vanadium oxide, (001) anatase surface is used in this study to model the support phase of vanadia/titania catalyst. SCR reaction on (010) V_2O_5 surface was previously studied by Onal et al. (2005). First of all ammonia adsorption reaction, then dissociation, is studied on $Ti_2O_9H_8$ cluster representing (001) surface of anatase as described previously. According to an Eley Rideal type mechanism NO interaction from gas phase is also considered.

Before performing mechanism calculations over the catalytic surface represented by the $Ti_2O_9H_8$ cluster, the reactants (NH_3 and NO) were initially optimized by means of the equilibrium geometry calculations. Then the computational procedure described previously is applied for investigating the SCR reaction mechanism. The computations showed that on $Ti_2O_9H_8$ cluster the formation of nitrosamide (NH_2NO) species takes place; however this cluster does not play a role in the decomposition of this product.

It is found that NH_2NO formation reaction on $Ti_2O_9H_{10}$ cluster consists of four reaction steps:

- Reaction Step I: Ammonia adsorption
- Reaction Step II: Ammonia dissociation
- Reaction Step III: NH_2NO formation
- Reaction Step IV: NH_2NO desorption

4.3.1. Reaction Step I: Ammonia Adsorption

According to Eley Rideal mechanism, the adsorption of ammonia is considered on relaxed and fixed $Ti_2O_9H_{10}$ cluster surfaces. Ammonia NH_3 molecule is adsorbed on the cluster exhibiting a non-activated mode with adsorption energies of -26.57 and -23.72 kcal/mol on relaxed and fixed clusters, respectively (as given in Figure 4.41). NO interaction with molecularly NH_3 adsorbed system is found to be an energetically unfavorable process. Therefore, before investigating NO interaction, ammonia dissociation on the cluster surface is considered.

4.3.2. Reaction Step II: Ammonia Dissociation

As previously mentioned, a coordinate driving calculation was employed starting from the equilibrium geometry of molecular ammonia adsorption given in Figure 4.41. Selecting the distance between O1 and H1 atoms as decreasing reaction coordinate, the energy profile given in Figure 4.43 was obtained for relaxed cluster. Ammonia dissociates on the cluster with an exothermic relative energy of 36.32 kcal/mol with a slight activation barrier of about 3.63 kcal/mol. Since ammonia dissociation on fixed (001) $Ti_2O_9H_{10}$ cluster turns out to be an unfavorable process, NO interaction is considered on relaxed cluster.

4.3.3. Reaction Step III: NH$_2$NO Formation

Considering the interaction of NO molecule with the equilibrium geometry of ammonia dissociation, firstly NO is located at a chosen distance from the configuration given in Figure 44 (b). Then a coordinate driving calculation is performed in which the distance between N1 atom and the nitrogen atom of the nitric oxide is selected as the reaction coordinate. The resulting energy profile is

123

given in Figure 4.46. As a result of this profile NH_2NO formation occurred with an endothermic relative energy difference of 6.52 kcal/mol with an activation barrier of 11.60 kcal/mol. An approximate transition state and the equilibrium geometry of this reaction step are shown in Figure 4.47.

NH_2NO formation and decomposition on a $V_2O_9H_8$ cluster in SCR reaction were previously given in Figure 4.7. As it is evident from the figure, the formation of nitrosamide species on $V_2O_9H_8$ cluster representing (010) vanadia surface is achieved by high activation barriers of 18.34 and 43.99 kcal/mol (Onal et al., 2005). However, the activation barriers required for nitrosamide formation on (001) anatase surface are lower values of 3.63 to 11.60 kcal/mol.

It should be noted that the nitrosamide formed in this step can not be decomposed on a $Ti_2O_9H_{10}$ cluster since this cluster does not have active oxygen sites as (010) $V_2O_9H_8$ cluster has. This finding is in line with the experimental information indicating that titania does not exhibit significant NO conversion (Schneider at al., 1994) Therefore nitrosamide should be removed from the titania surface to be decomposed on vanadia.
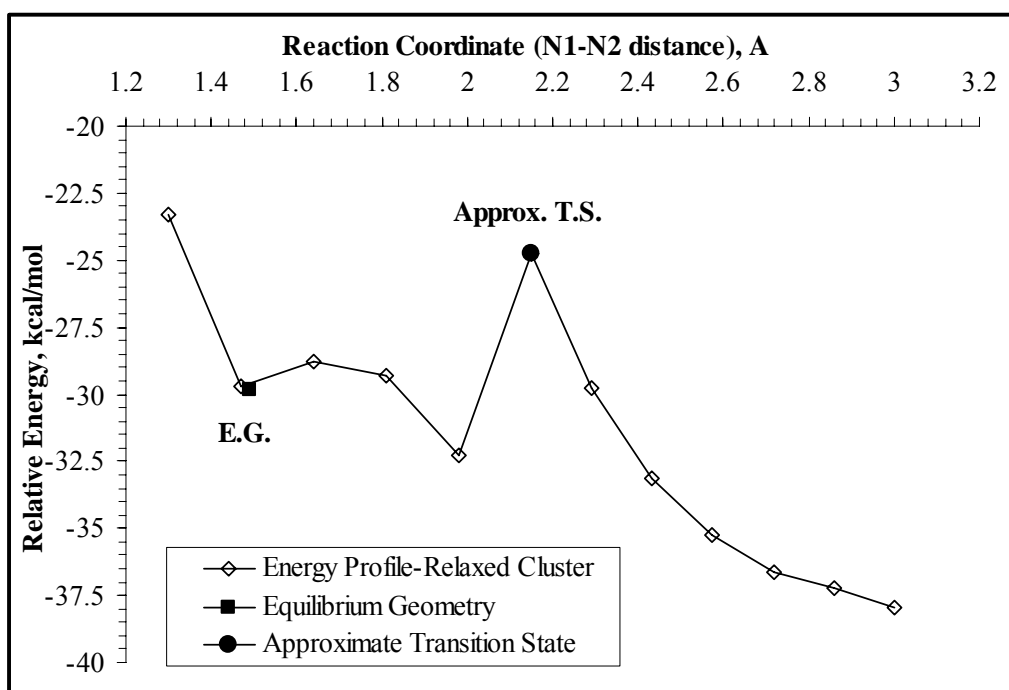
Figure 4.46. Energy profile for NO interaction with pre-ammonia dissociated system to form NH_2NO species on (001) $Ti_2O_9H_{10}$ cluster.
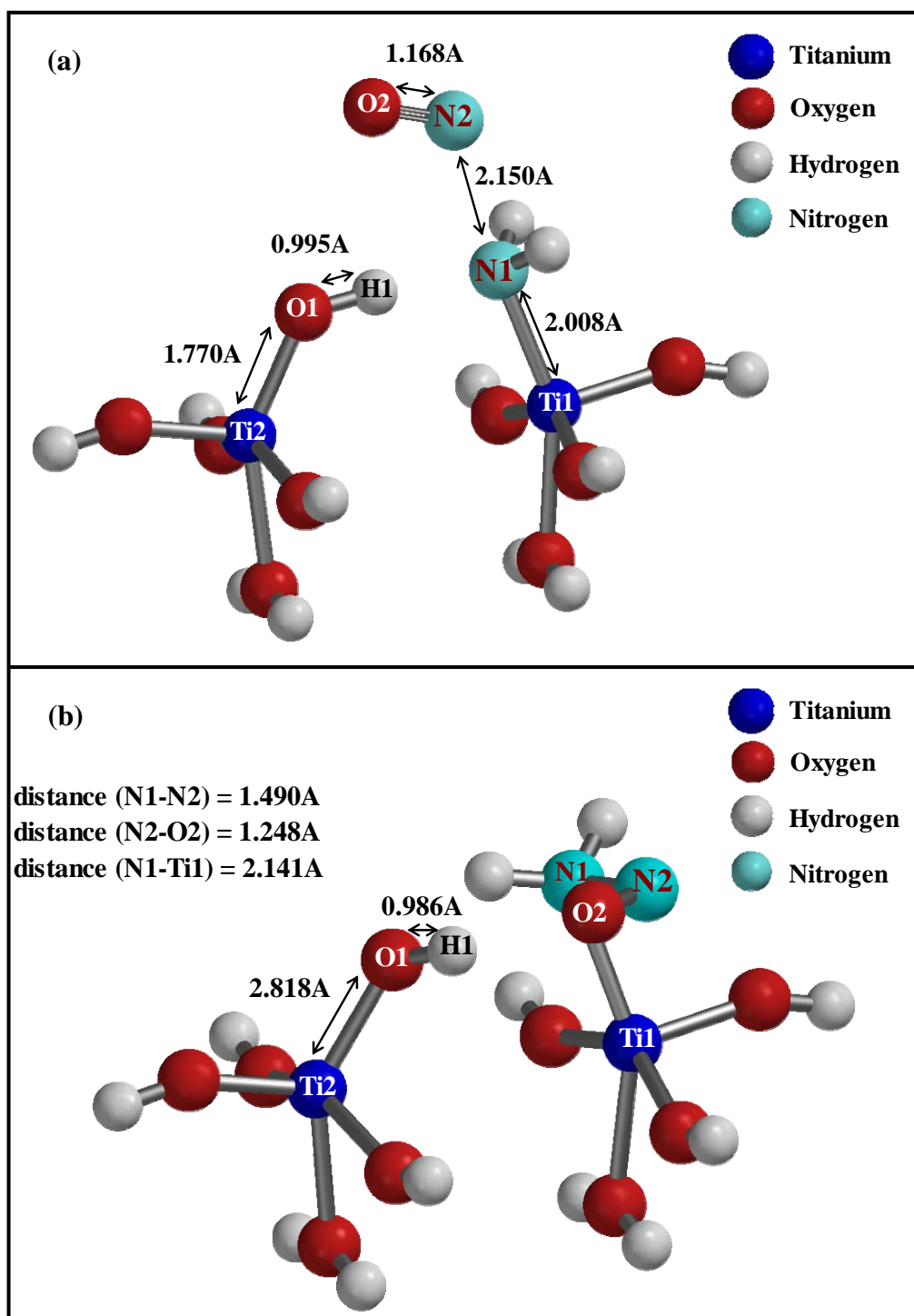
Figure 4.47. (a) Approximate transition state and **(b)** Equilibrium geometry for NH$_2$NO formation reaction on (001) Ti$_2$O$_9$H$_{10}$ cluster.

4.3.4. Reaction Step IV: NH₂NO Desorption

A coordinate driving driving calculation is employed by selecting Ti1-N1 distance in Figure 4.47 (b) as increasing reaction coordinate. This resulted in an energy profile illustrated in Figure 4.48.

It is evident from the profile that a desorption energy of 9.46 kcal/mol of is required to remove the nitrosamide species from $Ti_2O_9H_{10}$ cluster surface. The desorbed NH_2NO species from $Ti_2O_9H_{10}$ cluster is given in Figure 4.49.
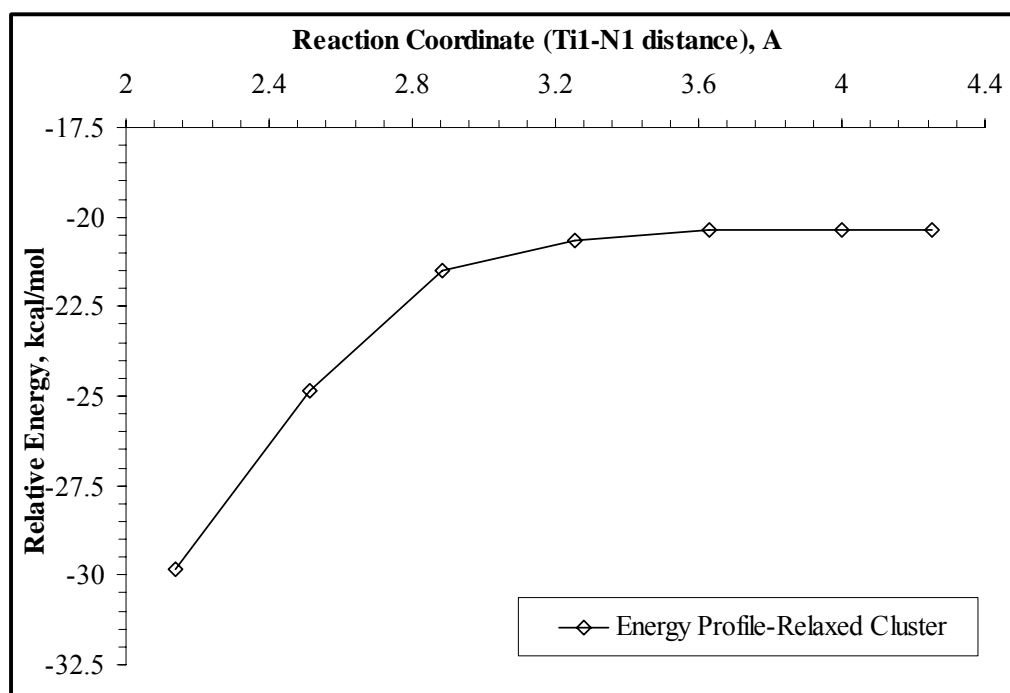
Figure 4.48. Energy profile for NH_2NO desorption from (001) $Ti_2O_9H_{10}$ cluster.
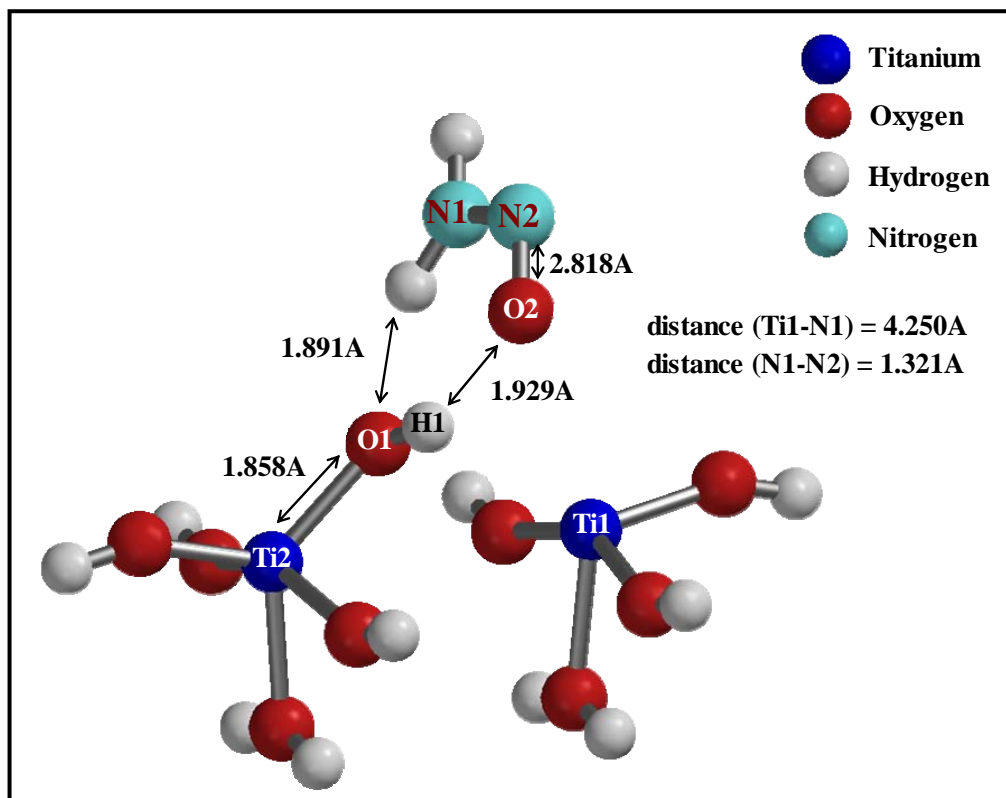
Figure 4.49. Desorbed NH_2NO from (001) $Ti_2O_9H_{10}$ cluster surface.

These reaction steps with regard to NH_2NO formation are summarized in a potential energy diagram shown in Figure 4.50 where the relative energy is calculated with respect to the energies of $Ti_2O_9H_{10}$ cluster, NH_3 (g) and NO (g). As it is seen in the figure, the formation of nitrosamide species on titania cluster requires low activation barriers of 3.63 to 11.60 kcal/mol. However, on vanadia surface the barriers required for NH_2NO formation are calculated as 18.34 and 43.99 kcal/mol (Onal et al., 2005). Therefore, by DFT computations employed, it is concluded that the main role of titania catalyst on SCR reaction could be in providing the formation of NH_2NO species since nitrosamide formation on titania is calculated to be energetically more favorable than on vanadia surface. The role of vanadia is still crucial in terms of dissociating this species into NH_3 and H_2O by the hydrogen transfer mechanism between the active sites of the cluster and the

adsorbed species. In other words, it is possible to conclude that both Lewis acid sites on titanium dioxide (in the formation of NH_2NO) and the Brønsted acid sites (in the decomposition of NH_2NO) are responsible for SCR reaction.
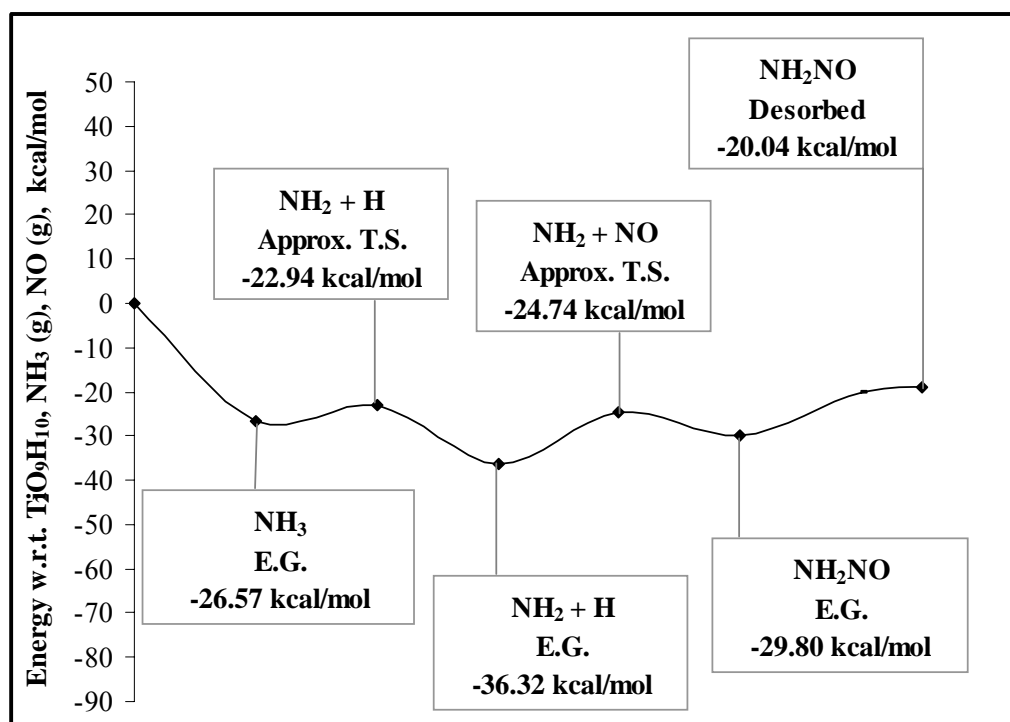
Figure 4.50. Potential energy profile for the NH_2NO formation reaction steps on (001) relaxed $Ti_2O_9H_{10}$ cluster (Approx. T. S. represents the approximate transition states, while E. G. stands for the equilibrium geometries).

4.4. NH_3 Adsorption on V_2O_5 /TiO_2 Catalyst Surface

$V_2TiO_{14}H_{14}$ cluster (Figure 3.8) is proposed for a vanadia/titania surface as described in Section 3.2. By this cluster model, it is aimed to make a direct comparison between the $V_2O_9H_8$ and $V_2TiO_{14}H_{14}$ clusters in terms of ammonia adsorption energetics. Equilibrium geometry of the Brønsted acidic ammonia adsorption on this cluster is obtained by a single point equilibrium geometry

calculation as given in Figure 4.51. NH_3 is adsorbed with an exothermic relative energy of 28.62 kcal/mol as the relative energy of ammonia adsorption is calculated as -28.65 on $V_2O_9H_8$ cluster. In a recent theoretical study published by Bredow et al. (2004), vanadia/titania cluster models are proposed and it is reported by use of semiempirical methods that ammonia adsorption energies on these clusters are -128 and -117 kJ/mol. Moreover, desorption activation energies for NH_3 adsorption are estimated from vacuum TPD studies as 14, 27 kcal/mol on V_2O_5/TiO_2 surface (Srnak et al., 1992). The Mulliken charge of the NH_4^+ ion on $V_2TiO_{14}H_{14}$ cluster is +0.764 as this value is +787 on $V_2O_9H_8$ cluster. The system is considered as neutral and with singlet spin multiplicity in this calculation.

Similar to the of Brønsted acidic NH_3 adsorption on $V_2O_9H_8$ cluster NH_4^+ ion has also a symmetric configuration on $V_2TiO_{14}H_{14}$ cluster as shown in Figure 4.51. The comparison of the geometric parameters for the equilibrium geometry structure of Brønsted acidic NH_3 adsorption on $V_2O_9H_8$ and $V_2TiO_{14}H_{14}$ Clusters is given in Table 4.9.

The results of this part indicate that titanium atom employed in a $V_2TiO_{14}H_{14}$ cluster model does not cause a significant effect in terms of NH_3 adsorption energy, geometry, and Mulliken charge.
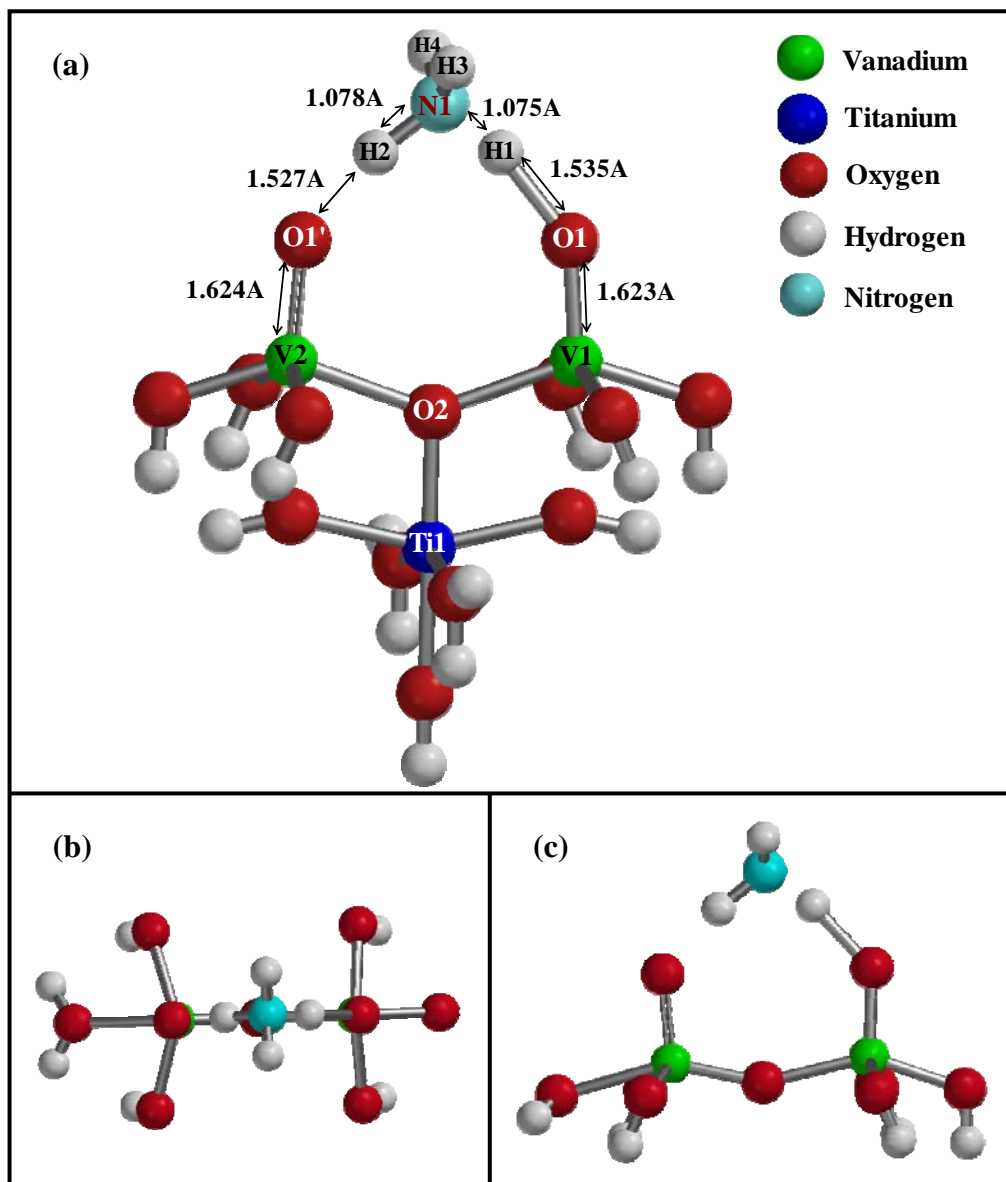
Figure 4.51. **(a)** Equilibrium geometry of Brønsted acidic NH_3 adsorption on $V_2TiO_{14}H_{14}$ cluster, **(b)** Top view, **(c)** Side view.

Table 4.9. Bond distance and angle values (A and °) for the equilibrium geometry structure of Brønsted acidic NH_3 adsorption on $V_2O_9H_8$ and $V_2TiO_{14}H_{14}$ clusters.

Geometry	Equilibrium Geometry	
	on $V_2O_9H_8$ Cluster	on $V_2Ti_1O_{14}H_{14}$ Cluster
distance (H1-O1)	1.549	1.535
distance (H2-O1')	1.545	1.527
distance (N1-H1)	1.072	1.075
distance (N1-H2)	1.071	1.078
distance (O1-V1)	1.612	1.623
distance (O1'-V2)	1.607	1.624
angle (O1-V1-O2)	107.00	105.29
angle (O1'-V2-O2)	105.23	105.44
angle (V1-O2-V2)	154.97	140.92

CHAPTER 5

CONCLUSIONS

Density functional theory calculations carried out at B3LYP/6-31G** level are employed to investigate the following aspects:

- Catalytic pathway for the selective catalytic reduction reaction of nitric oxide by ammonia reaction (SCR) on (010) $V_2O_9H_8$ cluster surface,
- Adsorption of H_2O and NH_3 on (101) and (001) anatase surfaces both of which are represented by relaxed and fixed $Ti_2O_9H_{10}$ clusters,
- The role of anatase support in SCR reaction,
- Ammonia adsorption on a $V_2TiO_{14}H_{14}$ cluster.

Ammonia activation mode over $V_2O_9H_8$ cluster surface was first investigated. as an initiation reaction for SCR of NO on pure vanadia. It is concluded that the SCR reaction is initiated more favorably by the ammonia activation on Brønsted acidic V-OH site, where NH_4^+ ion is formed. This reaction step is calculated to occur through a non-activated process with an exothermic relative energy of 28.65 kcal/mol. These findings are in agreement with previous experimental and theoretical studies. Vibration frequencies are also calculated for the optimized geometry of the Brønsted acidic adsorption reaction and it is found that all the vibration frequencies agree well with what has been observed experimentally in literature. For the second part of the SCR reaction that involves the interaction of NO with the ammonia adsorbed cluster, reaction steps leading to the formation of NH_3NHO adduct and NH_2NO species take place sequentially. NH_3NHO formation having an activation barrier of 43.99 kcal/mol turns out to be the rate

limiting step of the SCR reaction. In the third part, catalytic decomposition reactions of NH_2NO species into N_2 and H_2O are considered and the findings of this part are in accordance with the theoretical literature. The reaction steps on the cluster surface involve a push-pull type transfer of the H atoms between the species formed and the V=O and V-OH sites of the cluster surface. It is found that the activation barriers of the NH_2NO decomposition on the cluster surface are much lower than those for gas phase reactions. Hence, catalytic nitrosamide decomposition is found to be more favorable than gas phase decomposition of this species. The catalytic cycle of the SCR reaction can be completed by the oxidation of the V-OH site formed during the last step of this part.

The molecular adsorption and dissociation of H_2O and NH_3 on (101) and (001) TiO_2 anatase surfaces both represented by totally fixed and partially relaxed $Ti_2O_9H_{10}$ cluster models are simulated as a pre-stage of investigating the role of anatase support in SCR reaction. The results indicate that the favorable adsorption mode of these molecules depend on the surface relaxations. Molecular water adsorption is more favorable on relaxed (101) $Ti_2O_9H_{10}$ cluster than dissociative water adsorption; however, on the fixed cluster it is seen that opposite situation is valid. Non-activated dissociation of water takes place on relaxed (001) $Ti_2O_9H_{10}$ cluster while on fixed (001) cluster molecular adsorption is found to be more favored. The adsorption of water with previously H_2O dissociated surfaces is also considered. The adsorption energy and vibration frequency of water molecule adsorbed by H-bonding on relaxed (001) and (101) cluster, and on (101) fixed cluster compare very well with the experimental estimates. For ammonia adsorption, molecular adsorption is found to be more favorable on both relaxed and fixed (101) $Ti_2O_9H_{10}$ cluster models than dissociative adsorption. On (001) fixed $Ti_2O_9H_{10}$ cluster, ammonia dissociation turns out to be energetically an unfavorable process while on (001) relaxed surface dissociation occurs with a slight activation barrier having an exothermic relative energy difference. As in the case of water adsorption, the adsorption of ammonia with H-bonding with

134

previously NH_3 dissociated systems is also considered. The adsorption energy of ammonia molecule adsorbed by H-bonding on (101) relaxed and fixed clusters agree with the experimental data. Moreover, it is found that these geometries whose adsorption energy compares with TPD results show agreement with the experimental data for vibration frequencies as well.

The role of anatase support of vanadia/titania catalyst on selective catalytic reduction (SCR reaction) of NO by ammonia is investigated by use of a relaxed (001) TiO_2H_{10} cluster. Following ammonia dissociation on this cluster, the interaction of NO from the gas phase is considered. The results showed that (001) anatase support provides the formation of NH_2NO with activation barriers of 3.63 to 11.60 kcal/mol. Previously, the barriers required for NH_2NO formation are calculated as 18.34 and 43.99 kcal/mol on vanadia surface. Therefore, it is concluded that the main role of titania support on SCR reaction could be in providing the formation of NH_2NO species since nitrosamide formation on titania is calculated to be energetically more favorable than on vanadia surface. Dissociation of nitrosamide species into H_2O and N_2 can not be achieved on $Ti_2O_9H_{10}$ cluster since its surface sites can not provide a hydrogen push- pull mechanism to decompose this intermediate as it is the case for vanadia phase. Hence, it is possible to conclude that both Lewis acid sites on titanium dioxide (in the formation of NH_2NO) and the Brønsted acid sites (in the decomposition of NH_2NO) are responsible for SCR reaction.

$V_2TiO_{14}H_{14}$ cluster is proposed as model for a vanadia/titania catalyst and tested for NH_3 adsorption. Ammonia adsorption takes place on this cluster with an exothermic relative energy of -28.65 kcal /mol and of +0.764 Mulliken charge. Therefore, titanium atom employed in a $V_2TiO_{14}H_{14}$ cluster model does not cause a significant effect in terms of NH_3 adsorption energy, geometry, and Mulliken charge.

REFERENCES

Alemany, L.J., Berti, F., Busca, G., Ramis, G., Robba, D., Toledo, G.P., Trombetta, M., Appl. Catal. B., 248, 299 (1996).

Anstrom, M., Topsøe, N-Y., Dumesic, J.A., Catal. Lett., 78, 1-4, 281 (2002).

Anstrom, M., Topsøe, N-Y., Dumesic, J.A., J. Catal., 213, 115 (2003).

Becke, A. D., Phys. Rev. B., 38, 3098 (1988).

Becke, A. D., Roussel, M. R., Phys. Rev., A., 39, 3761 (1989).

Beltran, A.; Sambrano, J.R.; Calatayud, M.; Sensato, F.R.; Andres, J., Surface Science, 490, 116 (2001).

Blushev, D.A., Minsker, L.K., Rainone, F., Renken, A., J. Cat., 205, 115 (2002).

Bredow, T., Jug, K., Surf. Sci., 327, 398 (1995).

Bredow, T., Homann, T., Jug, K., Res. Chem. Intermed., 30, 65 (2004).

Bredzona, T., Puchkovska, G., Shymanovska, V., Baran, J., Ratajczak, H., J. Mol. Struc., 700, 175 (2004).

Busca, G., Lietti, L., Ramis, G., Berti, F., Appl. Catal. B: Env., 18, 1 (1998).

Campbell, L.M., Stone, D.K., Shareef, G.S., "Sourcebook: NO_x Control Technology Data", EPA Report NO. EPA600/S2-91/029., Washington, D.C., (Aug. 1991).

Cheremisinoff P.N. (Ed.), "Air Pollution Control and Design for Industry", Dekker, New York (1993).

Clark, T., "A Handbook of Computational Chemistry", John Wiley & Sons, New York (1985).

Dumesic, J.A., Topsøe, N-Y., Topsøe, H., Chen, Y., Slabiak, T., J. Catal., 163, 409 (1996).

Fahmi, A., Minot, C., Surf. Sci., 304, 343 (1994).

Farrauto, R. J., Heck, R. M., Speronnelo, B. K., C & EN, 34–44 (Sept. 7, 1992).

Flagan, R.C., Seinfeld, J. H., "Fundamentals of Air Pollution Engineering", Prentice Hall Inc., New Jersey (1988).

Forzatti, P., Appl. Catal. A., 222, 221 (2001).

Gasior, M.G., Haber, J., Machej, T., Czeppe, T., J. Mol. Catal. 43, 359 (1988).

Gilardoni, F., Weber, J., Baiker, A., Inter. J. Quan. Chem., 61, 683 (1997).

Gilardoni, F., Weber, J., Baiker, A., J. Phys. Chem. A, 101, 6069 (1997).

Gokhale, A.A., Kandoi, S., Greeley, J.P., Mavrikakis, M., Dumesic, J.A., Chem. Eng. Sci., 59, 4679 (2004).

Heck, R.M., Farrauto, R.J., "Catalytic Air Pollution Control, Commercial Technology", Van Nostrand Reinhold, New York, (1995).

Hehre, W., Burke, L. D., Shusterman, A. J., "A Spartan Tutorial", Wavefunction, Inc., Irvine CA (1993).

Hehre, W., Radom, L., Schleyer, P. Pople, J., "Ab initio Molecular Orbital Theory", John Wiley & Sons, New York (1986).

Hehre, W., Yu, J., Klunzinger, P. E., "A Guide to Density Fuctional Calculations in SPARTAN", Wavefunction, Inc., Irvine CA (1997).

Hengerer, R., Bolliger, B., Erbudak, M., Gratzel., M., Surf. Sci., 460, 162 (2000).

Henry J.G., Heinke G.W., "Environmental Science and Engineering", Prentice Hall, Englewood Cliffs, NJ (1989).

Hermann, K., Witko, M., Druzinic, R., Faraday Discuss., 114, 53 (1999).

Hermann, K., Witko, M., Druzinic, R., Chakrabarti, A., Tepper, B., Elsner, M.,Gorschlüter, A., Kuhlenbeck, H., Freund, H.J., J. Elect. Spec. And Relat. Phen., 98-99, 245 (1999).

Homann, T., Bredow, T., Jug, K., Surf. Sci., 555, 135 (2004).

Inomata, M., Miyamoto, A., Murakami, Y., J. Catal., 62, 140 (1980).

Inomata, M., Miyamoto, A., Murakami, Y., J. Phys. Chem., 85, 2372 (1981).

Izumi, Y., Kiyotaki, F., Yoshitake, H., Aika, K., Sugihara, T., Tatsumi, T., Tanizawa, Y., Shido, T., Iwasawa, Y., Chem. Commun., 2402 (2002).

Janssen, F.J.J.G., van den Kerkhof, F.M.G., Bosch, H., Ross, J.R.H., J. Phys. Chem., 91, 5921 (1987).

Janssen, F.J.J.G., van den Kerkhof, F.M.G., J. Phys. Chem., 91, 6633 (1987).

Jensen, F., "Introduction to Computational Chemistry", John Wiley & Sons, New York (1998).

Jug, K., Homann, T., Bredow, T., J. Phy. Chem. A, 108, 2966, (2004).

Kachurovskaya, N.A., Mikheeva, E.P., Zhidomirov, G.M., J. Mol. Catal. A: Chem., 178,191 (2002).

Kohn, W., Sham, L. J., Phys. Rev., 140 A1133 (1965).

Kryukova, G.N., Klenov, D.O., Zenkovets, G.A., React. Kinet. Catal. Lett., 60, 179 (1997).

Lee, C., Yang, W., Parr, R. G. Phys. Rev., B., 37, 785, (1988).

Lietti, L., Nova, I., Tronconi, E., Forzatti, P., Catal.Today, 45, 85 (1998).

Lietti, L., Ramis, G., Berti, F., Toledo, G., Robba, D., Busca, G., Forzatti, P., Catal. Today, 42, 101 (1998).

Lin, C-H., Bai, H., Appl.Catal. B, 42, 279 (2003).

Michalak, A., Witko, M., Hermann, K., Surface Science, 375, 385 (1997).

Mikheeva, E.P., Kachurovskaya, N.A., Zhidomirov, G.M., Kin. and Catal., 43, 223, (2002).

Ming, W. W., Chem. Phy. Lett., 256, 4-5, 391 (1996).

Morterra, C., J. Chem. Soc., Faraday Trans. 1, 84, 1617, (1988).

Munuera, G., Moreno, F., Gonzales, F. "A Model for Anatase TiO_2 Surfaces: Interpretation of Some Interface Processes. Reactivity of Solids, in: Proceedings of the 7th International Symposium Reaction Solids", Chapman & Hall, London, p.681 (1972).

Ozkan, U.S., Cai, Y., Kumthekar, M.W., J. Catal., 149, 375 (1994).

Ozkan, U.S., Cai, Y., Kumthekar, M.W., J. Catal., 149, 390 (1994).

Perdew, J. P., Wang, Y., Phys. Rew. B., 33, 8800, (1986).

Perdew, J. P., Wang, Y., Phys. Rew. B., 45, 13244, (1992).

Pople J. A., Beveridge, D.L., "Approximate Molecular Orbital Theory", McGraw-Hill, New-York (1970).

Pople, J. A., Gill, P. M. W., Handy, N. C., Int. J. Quantum Chem., 56, 303 (1995).

Primet, M., Pichat, P., Mathieu, M-V., J. Phys. Chem., 75, 1216 (1971).

Ramis, G., Yi, L., Busca, G., Turco, M., Kotur, E., Willey, R.J., J. Catal., 157, 523 (1995).

Ramis, G., Yi, L., Busca, G., Catal. Today, 28, 373 (1996).

Redfern, P. C.; Zapol, P.; Curtiss, L. A.; Rajh, T.; and Thurnauer, M. C., J. Phys. Chem. B, 107, 11419 (2003).

van Santen, R.A., Neurock, M., Catal. Rev.-Sci. Eng., 37, (1995) 557.

Schneider, H., Tschudin, S., Schneider, M., Wokaun, A., Baiker, A., J. Catal., 147, 5 (1994).

Selloni, A., Vittadini, A., Grätzel, M., Surf. Sci., 402, 219 (1998).

Shareef, G.S., Stone, D.K., Ferry, K.R., Johnson, K.L., Locke, K.S. "Selective Catalytic Reduction NO_x Control for Small Natural Gas-fired Prime Movers," paper 92-136.06, presented at 85th Annual AWMA Meeting & Exhibition, Kansas City, Mo., June 21–26 (1992).

Slater, J.C., Phys. Rev., 36, 57 (1930).

Slater, J.C., Phys. Rev., 81, 385, (1951).

Spartan'02 Windows, "Tutorial and User's Guide", Wavefunction, Inc., Irvine CA (2001).

Speronello, B.K., Chen, J.M., Heck, R.M., "Family of Versatile Catalyst Technologies for NO_x and CO Removal in Co-generation," paper 92-109.06,

presented at 85th Annual AWMA Meeting & Exhibition, Kansas City, Mo., June 21–26 (1992).

Sprinceana, D., Caldararu, M., Ionescu, N. I., Auroux, A. J. Ther. Anal. and Calor., 56, 109, (1999).

Srnak, T.Z., Dumesic, J.A., Clausen, B.S., Törnqvist, E., Topsøe, N-Y., J. Catal., 135, 246 (1992).

Takagi, M., Kawai, T., Soma, M., Onishi, T., Tamaru, K., J. Phys. Chem., 80, 4, 430 (1976).

Teramura, K., Tanaka, T., Funabiki, T., Langmuir, 19, 1209 (2003).

Teramura, K., Tanaka, T., Yamazoe, S., Arakaki, K., Funabiki, T., Appl. Catal. B: Env., 53, 29 (2004).

Topsøe, N-Y., J. Catal., 128, 499 (1991).

Topsøe, N-Y., Topsøe, H., Dumesic, J.A., J. Catal., 151, 226 (1995).

Topsøe, N-Y., Topsøe, H., Dumesic, J.A., J. Catal,, 151, 241 (1995).

Topsøe, N-Y., Anstrom, M., Dumesic, J.A., Catal. Lett., 76, 1-2, 11 (2001).

Uzun, A., MSc. Dissertation, METU, Ankara (2003).

Went, G.T., Oyama, S.T., Bell, A.T., J. Phys. Chem., 94, 4240 (1990).

Went, G.T., Leu, L-J., Bell, A.T., J. Catal., 134, 479 (1992).

Wyckoff, R.W.G., "Crystal Structures", 2nd Edition, Volume 2, John Wiley & Sons, New York (1963).

Xuefeng, Z., Wheeless, C.J.M., Ruifeng, L., Vibr. Spect., 12, 1, 53 (1996).

Zhanpeisov, N. U., Higashimoto, S., Anpo, M., Inter. J. Quan. Chem., 84, 677 (2001).

APPENDICES

A. Theory

A.1 Background of the Computational Quantum Chemistry

Classical mechanics is concerned with the trajectories of particles which theoretically can be calculated from knowledge of the initial conditions and the structure of the Hamilton H, or the sum of a kinetic - energy contribution T and potential-energy function V.

$$H = T + V \tag{A.1}$$

However, the existence of the atom can not be explained classically, but rather by the wave properties of the electron bounded to the nucleus. For this reason Schrödinger suggested to replace the classical kinetic and potential energy functions of (A.1) with linear operators $\hat{T}$ and $\hat{V}$ set up a wave equation of the form

$$\hat{H} \Psi = E\Psi \tag{A.2}$$

where the solutions Ψ, the so called wave functions, would describe the behavior of all the particles and the quantum-mechanical Hamilton above is

$$\hat{H} = \hat{T} + \hat{V} \tag{A.3}$$

For one electron system such as the hydrogen atom, with the electron centered on the atomic nucleus, kinetic and potential energy operators are

$$\hat{T} = -\frac{h}{8\pi^2 m}\nabla^2 \tag{A.4}$$

$$\hat{V} = -\frac{Ze^2}{r} \tag{A.5}$$

where m is the mass of the electron, r is the distance of the electron from the nucleus, Z is the atomic number, and e is the unit of the electronic charge, and in equation (A.3) the Laplacian ∇^2 is in cartesian coordinates.

Born-Oppenheimer approximation states that because the nuclei are so much more massive than the electrons, the electrons adjust essentially instantaneously to any motion of the nuclei, consequently we may consider the nuclei to be fixed at some internuclear separation in order to solve the Schrödinger equation (A.2) for the electronic wave function in other words separation of wave function into

$$\Psi \approx \Psi_N \Psi_{elec} \tag{A.6}$$

where the first term in the product of equation (A.6) accounts for the motion of the nuclei and the second term involves the electron motion. Furthermore, introducing center-of mass and relative coordinates, the nuclear wave function reduces to

$$\Psi_N \approx \Psi_{trans}(C.M.)\Psi_{rot}\Psi_{vib} \tag{A.7}$$

where the center-of mass translation, and rotational and vibrational contributions to the nuclear wave function are now explicitly shown. Thus, the problem of determining the structure of a complex molecule reduces to solving each

Schrödinger equation for the electronic motion, the translational motion of the center of mass, and the rotational and vibrational of the nuclei separately. The electronic energy is estimated therefore by the Schrödinger equation for a molecule with n electrons calculation procedure is similar for the other types of motion

$$\hat{H}_{elec}(1,2,\ldots,n)\Psi_{elec}(1,2,\ldots,n) = E_{elec}\Psi_{elec}(1,2,\ldots,n) \tag{A.8}$$

and for a given intermolecular distance the total energy of the system is

$$E_T^0 \approx E_{elec} + \sum_{A<B} e^2 Z_A Z_B r_{AB}^{-1} \tag{A.9}$$

where the second term is the electrostatic inter-nuclear repulsion energy and A, B designate different nucleus.

Molecular orbital theory is concerned with electronic wave functions only, and henceforth the electronic subscripts will be dropped from the electronic Hamiltonian and wave function. The molecular energy given by equation (A.9) is the energy at absolute zero with no contributions from the translational, rotational or vibrational motions. The later forms of energy must be considered to determine thermochemistry under conditions of practical interest as

$$E_T \approx E_{trans} + E_{vib} + E_{rot} + E_{elec} \tag{A.10}$$

Once the total energy E_T^0 of equation (A.9) is known for a given molecular geometry, a potential energy hypersurface (PES) can be generated as function of geometry, and the minima on the (PES) corresponds to the most stable configuration, or in mathematical terms for molecules or radicals,

$$\partial E_T^0 \Big/ \delta g_i = 0$$

$$\partial^2 E_T^0 \Big/ \delta \ (g_i)^2 \ > 0$$

where g_i is any geometrical variable.

The heat of formation for the molecule can then be obtained from the total energy of equation (A.10) via

$$\Delta H_f = E_T - \sum_{k=1}^{n} E_k^A + \sum_{i=1}^{N} \Delta H_{fi}^A \qquad\qquad (A.11)$$

where E_k^A and ΔH_{fi}^A are the electron energies and the heats of formation of individual atoms, respectively. Clearly, this approach requires the accurate knowledge of the atomic heats of formation, which may or may not be available.

The electronic Hamilton (non-relativistic) of a molecule is given by the following expression in atomic units ($h/2\pi = e = m = 1$)

$$\hat{H} = -\sum_{p} \frac{1}{2} \nabla_p^2 - \sum_{A} \sum_{P} Z_A r_{Ap}^{-1} + \sum_{p<q} r_{pq}^{-1} \qquad\qquad (A.12)$$

where A designate the nuclei, p, q electrons, and r is the interparticle distance.

The solutions to the electronic Schrödinger equation (A.8) are infinite but for stationary, bound states only the continuous, single-value eigenfunctions that vanish at infinity need to be considered, and the electronic energies are the eigenvalues E_i or

$$\hat{H} \Psi_i = E_i \Psi_i \qquad\qquad (A.13)$$

The eigenfunctions are normalizable and mutually orthogonal (i.e., orthonormal) or mathematically they satisfy the condition

$$\int \Psi_i \Psi_j d\tau = \left\langle \Psi_i \mid \Psi_j \right\rangle = \delta_{ij} \qquad\qquad \text{all i ,j} \qquad\qquad (A.14)$$

In equation A.14, the interaction is over the volume element for the electron, and it is given with the matrix or Dirac notation for the integral, where δ_{ij} is the Kronecker delta. The electronic energy of the system E_i is the expectation value of the Hamiltonian or the solution for E_i is

$$\int \Psi_i \, \hat{H} \, \Psi_j d\tau = \left\langle \Psi_i \mid \hat{H} \mid \Psi_j \right\rangle = E_i \qquad\qquad (A.15)$$

The complete treatment of a quantum-mechanical problem involving electronic structure requires the complete solution of the Schrödinger equation (A.8). This is only possible for one-electron systems, and for many-electron systems, where the electron repulsion term in the Hamilton renders an analytical solution impossible, the variation principle is applied. This method in its full form is completely equivalent to the differential equations, and it has many advantages in the ways it can be adapted to approximate solution wave functions (Pople, 1970). The variation principle states that if ψ is a solution to equation (A.8) then for any small change δψ

$$\delta E = \delta \left\langle \Psi \mid \hat{H} \mid \Psi \right\rangle = 0 \qquad\qquad (A.16)$$

If this criterion is applied to an electronic wave function ψ, in the appropriate number of dimensions, all the eigenfunctions ψ_i for the Hamilton will be obtained. If only an approximation to the wave function ψ is used, and then the eigenfunctions ψ_i and eigenvalues E_i are only approximations to the correct

values, with the accuracy of the estimates improving as better approximations for the total wave function ψ is used.

The orbital approximation suggests that the total electron wave function ψ can be written as the Hartree product of one-electron wave functions, $\psi_i\eta(\zeta)$, called spin orbitals (Gasiorowicz, 1974) consisting of the product of spatial and spin functions, where $\eta(\zeta)$ is the spin function that can take values α or β, or

$$\Psi(1,2,\ldots,n) = O(s)A\big[\psi_1(1)\alpha(1)\psi_2(2)\beta(2)\psi_3(3)\alpha(3)\ldots\psi_n(n)\beta(n)\big]$$

(A.17)

In equation (A.17) A is the antisymmetrizer, ensuring that the wave function changes sign on interchange of any two electrons in accordance with the Pauli exclusion principle, and O(S) is a spin projector operator that ensures that the wave function remains an eigenfunction of the spin-squared operator S^2

$$S^2\Psi = S(S+1)\Psi$$

(A.18)

O(S) can become quite complex but for a closed shell molecule, with all electrons paired in the spin orbitals O(S)=1. Thus, for a closed-shell system with 2n electrons, and two electrons paired in each spatial orbital, the many-electron wave function becomes

$$\Psi(1,2,\ldots,n) = A\big[\psi_1(1)\alpha(1)\psi_1(2)\beta(2)\psi_2(3)\alpha(3)..\psi_n(2n-1)\alpha(2n-1)\psi_n(n)\beta(n)\big]$$

(A.19)

Equation (A.19) is known as *Slater determinant* which is the proper form for the many electron wave function for closed shells as a single determinant of spin orbitals. The discussion now proceeds to the details of the actual determination of the electron spatial orbitals ψ_i for a closed-shell system. This involves the

application of the variational principle or equation (A.16) for the solution of (A.19). The best molecular orbitals, therefore, are obtained by varying all the contributing one-electron functions $\psi_1,\ \psi_2,\ \psi_3,...\ \psi_n$, in the Slater determinant equation (A.19) until the electronic energy achieves its minimum value. This will give the best approximation to the many-electron wave function, ψ and the electron orbital or molecular orbitals ψ_i so obtained are referred to as *self consistent* or *Hartree-Fock* molecular orbitals.

Mathematically, the problem involves the minimization of the total electron energy with the orthonormality constraint for the electron orbitals as

$$\text{Minimize } G = E - 2\sum_i \sum_j \varepsilon_{ij} S_{ij} \tag{A.20}$$

where, Orthonormality $S_{ij} = \int \psi_i * \psi_j d\tau = \delta_{ij}$ (A.21)

and $\quad E = \left\langle \Psi(1,2,\ldots,n) \left| \hat{H} \right| \Psi(1,2,\ldots,n) \right\rangle$ (A.22)

where $\psi(1,2,3,....,n)$ is given by equation (A.19).

The minimization consists of setting $\delta G = 0$ and leads to the following differential equations (see Pople, 1970 for derivations).

$$\left[\hat{H}^{core} + \sum_j 2\,\hat{J}_j - \hat{K}_j \right] \psi_i = \varepsilon_i \psi_i \qquad i = 1,2,\ldots,n \tag{A.23}$$

or, $\hat{F}\,\psi_i = \varepsilon_i \psi_i$ $\qquad\qquad i = 1,2,\ldots,n$ (A.24)

In equation (A.24) F is the one-electron Hartree-Fock Hamiltonian operator consisting of the terms defined in equation (A.23) within the square brackets.

Equation (A.24) is known as the *Hartree-Fock* equation and states that the best molecular orbitals are eigenfunctions of the Hartree-Fock equation Hamiltonian operator. The first operator of the Hartree-Fock Hamiltonian in equation (A.23) is the one-electron Hamiltonian for an electron moving in the field of the bare nuclei, which is defined as

$$\hat{H}(p)^{core} = -\tfrac{1}{2}\nabla_p^2 - \sum Z_A r_{pA}^{-1} \tag{A.25}$$

The second operator accounts for the average effective potential of all other electrons affecting the electron in the molecular orbital ψ_i, can be defined by

$$\hat{J}_j(1) = \int \psi_j^*(2)\frac{1}{r_{12}}\psi_j(2)d\tau_2 \tag{A.26}$$

The final operator in the square bracket of equation (A.23) is the exchange potential and it arises from the effect of the antisymmetry of the total wave function on the correlation between electrons of parallel spin and it can be defined by

$$K_j(1)\psi_i(1) = \left[\int \psi_j^*(2)\frac{1}{r_{12}}\psi_i(2)d\tau_2\right]\psi_j(1) \tag{A.27}$$

To account for the correlation of electrons of different spin, the term missing in equation (A.23), Configuration Interaction (CI) method can be applied. This method incorporates virtual orbitals or nonbonding orbitals into the total wave function. This is beyond the scope of this discussion. For more information see Pople (1970)

The eigenvalues of equation (A.23) or (A.24) are the energies of electrons occupying the orbitals ψ_i are thus known as orbital energies, defined as

$$\varepsilon_i = H_{ij}^{core} + \sum_i \left(2J_{ij} - K_{ij} \right) \tag{A.28}$$

where the one-electron core energy for an electron moving in the field of bare nuclei is

$$H_{ij}^{core} = \int \psi_i^*(1) \hat{H}^{core} \psi_i d\tau_j \tag{A.29}$$

the coulomb interaction energy is given by

$$J_{ij} = \iint \psi_i^*(1)\psi_j^*(2) \frac{1}{r_{12}} \psi_i(1)\psi_j(2) d\tau_1 d\tau_2 \tag{A.30}$$

and the exchange energy is

$$K_{ij} = \iint \psi_i^*(1)\psi_j^*(2) \frac{1}{r_{12}} \psi_j(1)\psi_i(2) d\tau_1 d\tau_2 \tag{A.31}$$

The general procedure for solving the Hartree-Fock equations is iterative. A first solution for the molecular orbitals ψ_i is assumed for generating the Hartree-Fock operator F. The set of molecular orbitals generated by this estimate of the Hartree-Fock operator is then used to repeat the calculations and so on until the orbital no longer changes, within a certain tolerance, on further interaction. These orbitals are said to be *self consistent with the potential field they generate*. In addition to the n occupied orbitals, there will be unoccupied orbitals called virtual orbitals of higher energy.

The method outlined above for solving the Hartree-Fock equation is impractical or molecular systems of any size and other approaches must be found (Pople, 1970). The most rewarding approach consists of approximating the molecular orbitals by a *linear combination of atomic orbitals* or LCAO in the form

$$\psi_i = \sum_\mu c_{\mu i}\phi_\mu \tag{A.32}$$

where the ϕ_μ are the atomic orbitals constituting the molecular orbital or basis set.

In carrying out numerical calculations of molecular orbitals, it is necessary to have convenient analytical forms for the atomic orbitals of equation (A.32) for each type of atom in the molecule. The solutions of the Schrödinger equation for one-electron systems (H-atom) can be written in the form by separation of variables

$$\Phi(r, \theta, \phi) = R_{n,l}(r) Y_{lm}(\theta, \phi) \tag{A.33}$$

where r, θ, and ϕ are the spherical coordinates centered on the atom. The angular part of the above equation or $Y_{lm}(\theta,\phi)$ are the spherical harmonics defined as

$$Y_{lm}(\theta,\varphi) = \Theta_{lm}(\theta)\phi_m(\varphi) \tag{A.34}$$

where l is the azimutal quantum number, and m is the magnetic quantum number. For the radical part of the atomic function, the so called *Slater Type Orbitals* (STO) are used with the form

$$R_{n,l}(r) = (2\varsigma)^{n+1/2}\left[(2n)!\right]^{-1/2} r^{n-1} \exp(-\varsigma r) \tag{A.35}$$

where n is the principle quantum number, and l is the orbital exponent, a function of the atomic number.

The variational principle is then applied as previously outlined except the total electron wave function consists of the product of molecular orbitals such as given in equation (A.32) above and the orthonormality of the electron wave function leads to

$$\sum_{\mu\nu} c_{\mu i}^{*} c_{\nu j} S_{\mu\nu} = \delta_{ij} \tag{A.36}$$

where $S_{\mu\nu}$ is the overlap integral for the atomic orbitals, defined as

$$S_{\mu\nu} = \int \phi_{\mu}(1)\phi_{\nu}(1)d\tau_1 \tag{A.37}$$

This leads to the so called *Roothan equations* given by

$$\sum_{\nu}\left(F_{\mu\nu} - \varepsilon_i S_{\mu\nu}\right)C_{\nu i} = 0 \qquad\qquad i = 1,2,\ldots,n \tag{A.38}$$

where the elements of the matrix representation of the Hartree-Fock hamiltonian are

$$F_{\mu\nu} = H_{\mu\nu} + \sum_{\lambda\sigma} P_{\lambda\sigma}\left[\left(\mu\nu|\lambda\sigma\right) - \tfrac{1}{2}\left(\mu\lambda|\nu\sigma\right)\right] \tag{A.39}$$

and

$$H_{\mu\nu} = \int \phi(1)\,\hat{H}^{core}\,\phi_{\nu}(1)d\tau_1 \tag{A.40}$$

$$P_{\mu\nu} = 2\sum_{i}^{occ} c_{\mu i}^{*} c_{\nu i} \tag{A.41}$$

$$\left(\mu\nu|\lambda\sigma\right) = \iint \phi_{\mu}^{*}(1)\phi_{\nu}^{*}(1)\frac{1}{r_{12}}\phi_{\lambda}(2)\phi_{\sigma}(2)d\tau_1 d\tau_2 \tag{A.42}$$

The matrix of elements $P_{\mu\nu}$ is the electron density matrix, $H_{\mu\nu}$ are the elements of the core Hamiltonian with respect to atomic orbitals, and equation (A.42) is the general two-electron interaction integral over atomic orbitals. Equations (A.38) are algebraic equations in contrast with the differential equations (A.23) or (A.24) previously derived.

The Roothan equation (A.38) can be written in matrix from as

$$FC = SCE \qquad\qquad\qquad\qquad\qquad\qquad (A.43)$$

where E is the diagonal matrix of the ε_i. The matrix elements of the Hartree-Fock Hamiltonian operator are dependent on the orbitals through the elements $P_{\mu v}$, and the Roothan equations are solved by first assuming an initial set of linear expansion coefficients $c_{\mu i}$, generating the corresponding density matrix $P_{\mu v}$ and computing a first guess to $F_{\mu v}$. The diagonalization procedure is effected by standard matrix eigenvalue techniques, and new expansion coefficients are calculated. The whole process is repeated until the coefficients no longer change within a given tolerance on repeated iteration (Pople, 1970).

A.2. Basis Sets

Ab initio methods try to derive information by solving the Schrödinger equation without fitting parameters to experimental data. Actually, *ab initio* methods also make use of experimental data, but in a somewhat more subtle fashion. Many different approximate methods exist for solving the Schrödinger equation, and the one to use for a specific problem is usually chosen by comparing the performance against known experimental data. Experimental data thus guides the selection of the computational model, rather than directly entering the computational procedure.

One of the approximations inherent in essentially all *ab initio* methods is the introduction of a basis set. Expanding an unknown function, such as a molecular orbital, in a set of known functions is not an approximation, if the basis is complete. However, a complete basis means that an infinite number of functions must be used, which is impossible in actual calculations. An unknown molecular orbital (MO) can be thought of as a function in the infinite coordinate system spanned by the complete basis set. When a finite basis is used, only the

components of the MO along those coordinate axes corresponding to the selected basis can be represented. The smaller the basis, the poorer the representation. The type of basis functions used also influence the accuracy. The better a single basis function is able to reproduce the unknown function, the fewer are basis functions necessary for achieving a given level of accuracy. Knowing that the computational effort of *ab initio* methods scales formally as at least M^4, it is of course of prime importance to make the basis set as small as possible without compromising the accuracy.

A.2.1. Slater and Gaussian Type Basis Sets

There are two types of basis functions (also called *Atomic Orbitals,* AO, although in general they are not solutions to an atomic Schrödinger equation) commonly used in electronic structure calculations: *Slater Type Orbitals* (STO) and *Gaussian Type Orbitals* (GTO). Although STO provides more accurate results, GTO is more favored due to the ease of the calculation process. Slater type orbitals have the functional form

$$X_{\xi,n,l,m}(r,\theta,\varphi) = NY_{l,m}(\theta,\varphi)r^{n-1}e^{-\zeta r} \tag{A.44}$$

N is a normalization constant and $Y_{l,m}$ are the usual spherical harmonic functions. The exponential dependence on the distance between the nucleus and the electron mirrors the exact orbitals for the hydrogen atom. However, STOs do not have any radial nodes.

Nodes in the radial part are introduced by making linear combinations of STOs. The exponential dependence ensures a fairly rapid convergence with increasing number of functions. However, the calculation of three- and four-centre two-electron integrals cannot be performed analytically. STOs are primarily used for

atomic and diatomic systems where high accuracy is required and in semi-empirical methods where all three- and four-centre integrals are neglected.

Gaussian type orbitals can be written in terms of polar or cartesian coordinates:

$$X_{\xi,n,l,m}(r,\theta,\varphi) = NY_{l,m}(\theta,\varphi)r^{(2n-2-l)}e^{-\zeta r^2 r}$$
$$X_{\xi,l_x,l_y,l_z}(x,y,z) = Nx^{l_x}y^{l_y}z^{l_z}e^{-\zeta r^2}$$

(A.45)

where the sum of l_x, l_y and l_z determines the type of orbital (for example $l_x + l_y + l_z = 1$ is a p-orbital). Although a GTO appears similar in the two sets of coordinates, there is a subtle difference. A d-type GTO written in terms of the spherical functions has five components $(Y_{2.2}, Y_{2.1}, Y_{2.0}, Y_{2.-1}, Y_{2.-2})$, but there appear to be six components in the Cartesian coordinates $(x^2, y^2, z^2, xy, xz. yz)$. The latter six functions, however, may be transformed to the five spherical d-functions and one additional s-function $(x^2 + y^2 + z^2)$. Similarly, there are 1O cartesian "f-functions" which may be transformed into seven spherical f-functions and one set of spherical p-functions. Modem programs for evaluating two-electron integrals are geared to Cartesian coordinates, and they generate pure spherical d-functions by transforming the six Cartesian components to the five spherical functions. When only one d-function is present per atom the saving by removing the extra s-function is small, but if many d-functions and or higher angular moment functions (f-, g-, h- etc. functions) are present, the saving can be substantial. Furthermore, the use of only the spherical components reduces the problems of linear dependence for large basis sets.

The r^2 dependence in the exponential makes the GTO inferior to the STOs in two aspects. At the nucleus the GTO has zero slope, in contrast to the STO which has a "cusp" (discontinuous derivative), and GTOs have problems representing the proper behavior near the nucleus. The other problem is that the GTO falls off too rapidly far from the nucleus compared with an STO, and the "tail" of the wave

function is consequently represented poorly. Both STOs and GTOs can be chosen to form a complete basis, but the above considerations indicate that more GTOs are necessary for achieving a certain accuracy compared with STOs. A rough guideline says that three times as many GTOs as STOs are required for reaching a given level of accuracy. The increase in number of basis functions, however, is more than compensated for by the ease by which the required integrals can be calculated. In terms of computational efficiency, GTOs are therefore preferred, and used almost universally as basis functions in electronic structure calculations. Furthermore, essentially all applications take the GTOs to be centered at the nuclei. For certain types of calculation the centre of a basis function may be taken not to coincide with a nucleus, for example being placed at the centre of a bond.

There are many different basis sets available in the literature or built into programs, and the average user usually only needs to select a suitable quality basis for the calculation. Below is a short description of some basis sets which often used in routine calculations (generally called Pople Style Basis Sets).

a) STO-nG basis sets: Slater Type Orbital consisting of n PGTOs. This is a minimum type basis where the exponents of the PGTO are determined by fitting to the STO, rather than optimizing them by a variational procedure. Although basis sets with n = 2-6 have been derived, It has been found that using more than three PGTOs to represent the STOs gives little Improvement, and the STO-3G basis is a widely used minimum basis. This type of basis set has been determined for many elements of the periodic table. The designation of the carbon/hydrogen STO-3G basis is (6s3p/3s) → [2s1p/1s].

b) k-nlmG basis sets These basis sets have been designed by Pople and co-workers. And are of the split valence type, with the *k* in front of the dash indicating how many PGTOs are used for representing the core orbitals. The *n/m* after the dash indicates both how many functions the valence orbitals are split

into, and how many PGTOs are used for their representation. Two value s (e.g. *nI)* indicate a split valence, while three values (e.g. *nlm)* indicate a triple split valence. The values before the G (for Gaussian) indicate the s- and p-functions in the basis; the polarization functions are placed after the G. This type of basis sets has the further restriction that the same exponent is used for both the sand p-functions in the valence. This increases the computational efficiency, but of course decreases the flexibility of the basis set. The exponents in the PGTO have been optimized by variational procedures.

c) 3-21G This is a split va1ence basis, where the core orbitals are a contraction of three PGTOs, the inner part of the valence orbitals is a contraction of two PGTOs and the outer part of the valence is represented by one PGTO. The designation of the carbon/hydrogen 3-21G basis is (6s3p/3s) ➔ [3s2p/2s]. Note that the 3-21G basis contains the same number of primitive GTOs as the STO-3G, however, it is much more flexible as there are twice as many valence functions which can combine freely to make MOs.

d) 6-31G This is also a split valence basis, where the core orbitals are a contraction of six PGTOs, the inner part of the valence orbitals is a contraction of three PGTOs and the outer part of the valence represented by one PGTO. The designation of the carbon/hydrogen 6-31G basis is (10s4p/4s) ➔ [3s2p/2s]. In terms of contracted basis functions it contains the same number as 3-2IG, but the representation of each functions is better since more PGTOs are used.

e) 6-311G This is a triple split valence basis, where the core orbitals are a contraction of six PGTOs and the valence split into three functions, represented by three, one and one PGTOs, respectively.

To each of these basis sets can be added diffuse and/or polarization functions. Diffuse functions are normally s- and p-functions and consequently go before the

G. They are denoted by + or ++, with the first + indicating one set of diffuse s- and p-functions on heavy atoms, and the second + indicating that a diffuse s- function is also added to hydrogens. The arguments for adding only diffuse functions on non-hydrogen atoms is the same as that for adding only polarization functions on non-hydrogens. Polarization functions are indicated after the G, with a separate designation for heavy atoms and hydrogens. The 6- 31+G(d) is a split valence basis with one set of diffuse sp-functions on heavy atoms only and a single d-type polarization function on heavy atoms. A 6-311++G(2df,2pd) is similarly a triple split valence with additional diffuse sp-functions, and two d- and one f-functions on heavy atoms and diffuse s- and two p- and one d-functions on hydrogens. The largest standard Pople style basis set is 6-311++G(3df, 3pd). These types of basis sets have been derived for hydrogen and the first row elements, and some of the basis sets have also been derived for second and higher row elements.

If only one set of polarization functions is used, an alternative notation in terms of * is also widely used. The 6-31G* basis is identical to 6-31G(d), and 6-31G** is identical to 6-31G(d,p). A special note should be made for the 3-21G* basis. The 3-21G basis is basically too small to support polarization functions (it becomes unbalanced). However, the 3-21G basis by itself performs poorly for hypervalent molecules, such as sulfoxides and sulfones. This can be substantially improved by adding a set of d-functions. The 3-21G* basis has only d-functions on second row elements (it is sometimes denoted 3-21G(*) to indicate this), and should not be considered a polarized basis. Rather, the addition of a set of d-functions should be considered an ad hoc repair of a known flaw.

B. Sample Input and Output Files

The text versions of the input and output files of SPARTAN'04 for the Brønsted acidic ammonia activation are presented in this part.

Table B1. Input file of the equilibrium geometry calculation for the Brønsted acidic ammonia activation given in Figure 4.2 (The geometry with the minimum energy point in the energy profile shown in Figure 4.1).

```
C OPT B3LYP 6-31G** PARTIAL CONVERGE NOSYMTRY
C SCF_CONVERGENCE=4 SCFCYCLE=10000 GEOMETRYCYCLE=1000
C GRADIENTTOLERANCE=1.E-3 DISTANCETOLERANCE=1.E-2
 PRINTLEV=4
M001
0 1
 8  -1.113501624  -0.065878152   2.784877086
 8  -1.101211778  -0.141017184  -0.778270995
 8   3.028452522   0.395092877   2.789442369
23   2.508226935   0.826071843   0.998799972
23  -1.049953506   0.482405828   0.989771255
 8   2.457257676   2.436476720   0.963114649
 8   4.619250983   0.511010030   1.010097393
 8  -2.686982131  -0.302123660   1.002044310
 8   3.040742265   0.319953955  -0.773705663
 8   0.905519314   0.284677153   1.003684987
 1   3.509418045  -0.511293937  -0.669054169
 1   3.497662360  -0.439721379   2.722293074
 1  -1.393656764  -0.979023204   2.688642914
 1  -2.610717535  -1.258864891   1.022333424
 1  -1.382168360  -1.049363902  -0.645789077
 8  -1.311357685   2.066802980   0.957067807
 1  -0.397356863   3.313306818   0.977193623
 1   5.080795988   0.150815550   1.770899432
 1   5.057359788   0.187831002   0.219401754
 1   0.330443377   4.613948737   1.830935073
 7   0.386562268   4.042950752   0.989701208
 1   0.328647126   4.638678850   0.165687563
```

```
  1   1.296567599   3.477263212   0.980832010
ENDCART


ATOMLABELS
"O8"
"O18"
"O37"
"V15"
"V16"
"O41"
"O20"
"O46"
"O47"
"O49"
"H7"
"H21"
"H25"
"H44"
"H48"
"O1"
"H2"
"H5"
"H10"
"H0"
"N1"
"H1"
"H3"
ENDATOMLABELS
FROZEN
  1   2   3   7   8   9   11   12   13   14   15   18
 19
ENDFROZEN
HESSIAN
  0   0   0   0   0   9   0   0   0   0   13   13
 13  13  13   8  13  13  13  13   5  13  13
  3   4   1
  7   4   1
  9   4   1
  4  10   1
 10   5   1
```

```
 1   5   1
 5   2   1
 5   8   1
 4   6   2
 9  11   1
 3  12   1
 1  13   1
 8  14   1
 2  15   1
16  17   1
 5  16   1
19   7   1
18   7   1
20  21   1
21  22   1
21  23   1
ENDHESS
BEGINCONSTRAINTS
DIST  17  21  1.071000
ENDCONSTRAINTS
BEGINPROPIN

ENDPROPIN
```

Table B2. Normal output file of the equilibrium geometry calculation for the Brønsted acidic ammonia activation given in Figure 4.2.

```
Spartan '04 Mechanics Program:  (PC/x86)                    Release  121

 Run Type            :         Frequency
 Method              :             MMFF94s (with extensions)
 Stoichiometry       :      H11 N O9 V2
 Number of Atoms     :              23
 Point Group         :              C1
 Degrees of Freedom  :              63


Cycle    E           Gmax    maxDist   MaxTors
   0  369.53359     735.12


  Turning off symmetry/constraints for frequency calculation
 Run Type            :         Frequency
 Method              :             MMFF94s (with extensions)
 Stoichiometry       :      H11 N O9 V2
 Number of Atoms     :              23
 Point Group         :              C1
 Degrees of Freedom  :              63

Adjusted 23 (out of 69) low frequency modes

  Reason for exit: Successful completion
  QmMm CPU Time : 000:00:00.2
  QmMm Wall Time: 000:00:00.5
Spartan '04 Quantum Mechanics Program:  (PC/x86)           Release  121

Job type: Geometry optimization.
Method: RB3LYP
Basis set: 6-31G**
Number of shells: 87
Number of basis functions: 263

SCF model:
 A restricted hybrid HF-DFT SCF calculation will be
 performed using Pulay DIIS extrapolation

         ... 1   -2626.9221847       5.00E-002
         ... 2   -2624.3342330       1.66E-002
         ... 3   -2579.7272372       7.41E-002
         ... 4   -2620.6279381       3.07E-002
         ... 5   -2608.0756367       4.60E-002
         ... 6   -2624.8693903       1.66E-002
         ... 7   -2606.5819888       3.77E-002
         ... 8   -2617.4383343       3.22E-002
         ... 9   -2625.5405205       1.07E-002
         ...10   -2624.4645173       1.96E-002
         ...11   -2626.2843864       5.18E-003
         ...12   -2626.2218756       6.37E-003
         ...13   -2626.4073165       3.29E-003
         ...14   -2626.4744642       6.01E-004
         ...15   -2626.4761155       3.92E-004
         ...16   -2626.4770957       1.75E-004
```

```
Optimization:
        Step      Energy        Max Grad.     Max Dist.
          1   -2626.4772564    0.074218      0.510258
        ... 1   -2626.4418033    4.96E-003
        ... 2   -2626.4859227    1.33E-003
        ... 3   -2626.3726531    4.26E-003
        ... 4   -2626.4878933    1.45E-003
        ... 5   -2626.4993885    4.25E-004
        ... 6   -2626.4999086    2.56E-004
        ... 7   -2626.4899236    1.29E-003
        ... 8   -2626.5002126    1.37E-004
          2   -2626.5003242    0.076710      0.405193
        ... 1   -2626.4407556    6.06E-003
        ... 2   -2626.4912383    1.00E-003
        ... 3   -2626.4674683    2.15E-003
        ... 4   -2626.4922827    1.24E-003
        ... 5   -2626.5000419    4.43E-004
        ... 6   -2626.5011306    1.33E-004
        ... 7   -2626.4998488    4.64E-004
        ... 8   -2626.5011439    1.44E-004
          3   -2626.5012565    0.069594      0.189158
        ... 1   -2626.5265485    3.34E-003
        ... 2   -2626.5162832    8.26E-004
        ... 3   -2626.4570325    3.31E-003
        ... 4   -2625.7851072    9.85E-003
        ... 5   -2626.4912460    2.20E-003
        ... 6   -2626.5155265    9.76E-004
        ... 7   -2626.5138452    1.05E-003
        ... 8   -2626.5206915    3.21E-004
        ... 9   -2626.5212108    1.32E-004
          4   -2626.5213250    0.040310      0.351387
        ... 1   -2626.5131847    4.01E-003
        ... 2   -2626.5226594    5.34E-004
        ... 3   -2626.4932693    2.33E-003
        ... 4   -2626.0532975    8.03E-003
        ... 5   -2626.5132786    1.34E-003
        ... 6   -2626.5210718    7.81E-004
        ... 7   -2626.5210466    7.51E-004
        ... 8   -2626.5244957    1.99E-004
          5   -2626.5246870    0.043005      0.226661
        ... 1   -2626.5519493    2.69E-003
        ... 2   -2626.5289293    3.66E-004
        ... 3   -2626.5230329    1.03E-003
        ... 4   -2626.4343071    3.75E-003
        ... 5   -2626.5256149    7.95E-004
        ... 6   -2626.5297443    1.59E-004
          6   -2626.5298581    0.016039      0.247365
        ... 1   -2626.4941646    3.13E-003
        ... 2   -2626.5222429    8.23E-004
        ... 3   -2626.4792115    2.67E-003
        ... 4   -2623.3524965    2.50E-002
        ... 5   -2626.4743047    2.91E-003
        ... 6   -2626.5144440    1.47E-003
        ... 7   -2626.5249648    6.30E-004
        ... 8   -2626.5274504    2.07E-004
        ... 9   -2626.5276899    1.14E-004
          7   -2626.5277649    0.030377      0.323049
        ... 1   -2626.5054793    3.03E-003
        ... 2   -2626.5274953    5.72E-004
        ... 3   -2626.5122241    1.60E-003
        ... 4   -2625.8748070    1.08E-002
        ... 5   -2626.5226572    1.04E-003
```

```
... 6    -2626.5283772     5.94E-004
... 7    -2626.5297647     3.73E-004
  8      -2626.5305706     0.025780        0.309811
... 1    -2626.5079312     4.62E-003
... 2    -2626.5140727     7.95E-004
... 3    -2626.4913621     2.00E-003
... 4    -2625.6479053     1.27E-002
... 5    -2626.4947309     1.90E-003
... 6    -2626.5157695     8.22E-004
... 7    -2626.5195221     2.32E-004
  9      -2626.5198282     0.050040        0.132668
... 1    -2626.5297265     2.89E-003
... 2    -2626.5341358     3.60E-004
... 3    -2626.5274913     1.13E-003
... 4    -2626.3851147     4.81E-003
... 5    -2626.5327601     5.85E-004
... 6    -2626.5347775     2.25E-004
... 7    -2626.5349930     1.26E-004
 10      -2626.5350637     0.012658        0.224495
... 1    -2626.5298279     2.01E-003
... 2    -2626.5316812     4.43E-004
... 3    -2626.5238458     1.16E-003
... 4    -2626.4130971     4.18E-003
... 5    -2626.5262999     1.08E-003
... 6    -2626.5331809     1.29E-004
... 7    -2626.5331877     1.29E-004
 11      -2626.5332527     0.018102        0.157984
... 1    -2626.5307354     1.46E-003
... 2    -2626.5340250     2.34E-004
... 3    -2626.5317457     6.19E-004
... 4    -2626.4843753     2.80E-003
... 5    -2626.5327557     5.00E-004
 12      -2626.5343469     0.019635        0.269740
... 1    -2626.5044193     2.18E-003
... 2    -2626.5279980     4.76E-004
... 3    -2626.5153055     1.50E-003
... 4    -2626.0274037     9.74E-003
... 5    -2626.5259760     7.38E-004
... 6    -2626.5279079     5.15E-004
... 7    -2626.5291847     2.27E-004
 13      -2626.5294707     0.032894        0.163014
... 1    -2626.5425421     1.58E-003
... 2    -2626.5373320     2.83E-004
... 3    -2626.5354144     6.12E-004
... 4    -2626.5075922     2.17E-003
... 5    -2626.5356689     5.55E-004
... 6    -2626.5376777     1.08E-004
 14      -2626.5377543     0.011111        0.226399
... 1    -2626.5417844     1.70E-003
... 2    -2626.5356362     3.13E-004
... 3    -2626.5313341     8.37E-004
... 4    -2626.4192314     4.38E-003
... 5    -2626.5336880     6.29E-004
... 6    -2626.5360312     2.15E-004
 15      -2626.5363015     0.023207        0.361413
... 1    -2626.5314984     2.55E-003
... 2    -2626.5341291     5.28E-004
... 3    -2626.5180440     1.67E-003
... 4    -2625.9310902     1.07E-002
... 5    -2626.5252470     1.25E-003
... 6    -2626.5345634     5.62E-004
... 7    -2626.5360668     2.50E-004
```

```
16    -2626.5364242        0.019793        0.230851
... 1    -2626.4585242        3.14E-003
... 2    -2626.5233819        7.60E-004
... 3    -2626.4857644        2.58E-003
... 4    -2624.8564418        1.82E-002
... 5    -2626.4760826        2.75E-003
... 6    -2626.5133373        1.58E-003
... 7    -2626.5268620        4.83E-004
... 8    -2626.5281313        1.67E-004
17    -2626.5282978        0.040249        0.137427
... 1    -2626.5616961        2.35E-003
... 2    -2626.5374548        3.68E-004
... 3    -2626.5297463        1.18E-003
... 4    -2626.3370314        5.76E-003
... 5    -2626.5340492        8.21E-004
... 6    -2626.5378668        3.26E-004
... 7    -2626.5384352        1.29E-004
18    -2626.5385063        0.010084        0.166431
... 1    -2626.5372003        1.98E-003
... 2    -2626.5366019        3.66E-004
... 3    -2626.5300550        1.07E-003
... 4    -2626.3412400        5.86E-003
... 5    -2626.5337729        7.51E-004
... 6    -2626.5370881        2.80E-004
... 7    -2626.5374517        1.57E-004
19    -2626.5375776        0.018269        0.258316
... 1    -2626.5280808        2.50E-003
... 2    -2626.5357701        4.13E-004
... 3    -2626.5297512        1.02E-003
... 4    -2626.4331858        3.92E-003
... 5    -2626.5321851        8.99E-004
... 6    -2626.5371996        1.63E-004
20    -2626.5373103        0.015390        0.213487
... 1    -2626.4811788        2.63E-003
... 2    -2626.5258138        8.56E-004
... 3    -2626.4910374        2.56E-003
... 4    -2626.0412434        8.03E-003
... 5    -2626.5077488        1.96E-003
... 6    -2626.5270242        9.12E-004
... 7    -2626.5287238        7.42E-004
... 8    -2626.5306670        4.54E-004
21    -2626.5320057        0.031874        0.113803
... 1    -2626.5507074        1.46E-003
... 2    -2626.5382731        3.18E-004
... 3    -2626.5373979        4.75E-004
... 4    -2626.5256197        1.43E-003
... 5    -2626.5366825        6.05E-004
... 6    -2626.5387837        1.32E-004
22    -2626.5389033        0.011154        0.174179
... 1    -2626.5489815        1.94E-003
... 2    -2626.5349291        4.38E-004
... 3    -2626.5250177        1.31E-003
... 4    -2626.1595688        8.38E-003
... 5    -2626.5324239        7.51E-004
... 6    -2626.5347696        4.78E-004
... 7    -2626.5358962        2.30E-004
23    -2626.5361906        0.030064        0.120740
... 1    -2626.5193248        1.15E-003
... 2    -2626.5384592        3.87E-004
... 3    -2626.5303625        1.20E-003
... 4    -2626.3909323        4.64E-003
... 5    -2626.5361449        6.95E-004
```

```
... 6   -2626.5391421      2.18E-004
... 7   -2626.5392460      1.74E-004
... 8   -2626.5393295      1.29E-004
 24     -2626.5394298      0.006747       0.177125
... 1   -2626.5407300      1.41E-003
... 2   -2626.5384019      2.49E-004
... 3   -2626.5337954      8.87E-004
... 4   -2626.4536036      3.59E-003
... 5   -2626.5363746      5.81E-004
... 6   -2626.5385681      1.39E-004
... 7   -2626.5385974      1.22E-004
 25     -2626.5386740      0.011304       0.072838
... 1   -2626.5343206      7.92E-004
... 2   -2626.5396834      1.11E-004
... 3   -2626.5392224      3.01E-004
... 4   -2626.5396903      1.34E-004
 26     -2626.5397846      0.006486       0.290279
... 1   -2626.5087486      9.13E-004
... 2   -2626.5384834      2.18E-004
... 3   -2626.5366866      5.60E-004
... 4   -2626.5387499      1.83E-004
... 5   -2626.5388577      1.28E-004
 27     -2626.5389522      0.026357       0.208400
... 1   -2626.5427005      6.59E-004
... 2   -2626.5398461      1.19E-004
... 3   -2626.5386500      4.60E-004
 28     -2626.5399205      0.004312       0.085575
... 1   -2626.5374635      7.47E-004
... 2   -2626.5396143      2.08E-004
... 3   -2626.5349967      8.94E-004
... 4   -2626.5397270      1.78E-004
 29     -2626.5399210      0.005841       0.072874
... 1   -2626.5396658      4.41E-004
 30     -2626.5401270      0.003177       0.064552
... 1   -2626.5351206      5.55E-004
... 2   -2626.5376299      6.33E-004
... 3   -2626.4927054      2.69E-003
... 4   -2626.5390854      4.12E-004
 31     -2626.5401348      0.003731       0.059141
... 1   -2626.5412217      2.54E-004
... 2   -2626.5395254      3.55E-004
... 3   -2626.5196514      1.82E-003
 32     -2626.5402470      0.002820       0.082856
... 1   -2626.5417320      3.99E-004
... 2   -2626.5399884      2.31E-004
... 3   -2626.5315332      1.21E-003
 33     -2626.5403029      0.003336       0.088894
... 1   -2626.5394582      3.77E-004
... 2   -2626.5402207      1.76E-004
... 3   -2626.5355115      9.00E-004
 34     -2626.5403913      0.002988       0.016225
... 1   -2626.5394974      2.69E-004
 35     -2626.5403876      0.003468       0.021795
... 1   -2626.5400238      5.07E-004
... 2   -2626.5064504      2.29E-003
... 3   -2624.8803414      1.81E-002
... 4   -2626.5289970      1.38E-003
... 5   -2626.5363983      8.16E-004
... 6   -2626.5401893      2.13E-004
 36     -2626.5404613      0.002406       0.036490
... 1   -2626.5417665      2.74E-004
... 2   -2626.5404568      1.07E-004
```

```
                   ... 3   -2626.5390342        4.93E-004
                    37   -2626.5405095        0.001853        0.020012
                   ... 1   -2626.5403009        1.71E-004
                    38   -2626.5404969        0.001724        0.014175
                   ... 1   -2626.5395647        3.93E-004
                   ... 2   -2626.5243713        1.57E-003
                   ... 3   -2625.9044904        1.09E-002
                   ... 4   -2626.5355823        8.63E-004
                   ... 5   -2626.5378714        6.66E-004
                   ... 6   -2626.5401603        2.48E-004
                    39   -2626.5405320        0.001247        0.012671
                   ... 1   -2626.5408652        8.45E-005
                    40   -2626.5405105        0.001729        0.103599
                   ... 1   -2626.5380588        9.49E-004
                   ... 2   -2626.5038458        2.40E-003
                   ... 3   -2624.7639489        1.90E-002
                   ... 4   -2626.5098899        2.19E-003
                   ... 5   -2626.5290974        1.37E-003
                   ... 6   -2626.5397138        2.70E-004
                    41   -2626.5401501        0.007120        0.078316
                   ... 1   -2626.5407588        7.87E-004
                   ... 2   -2626.5403081        1.85E-004
                   ... 3   -2626.5362193        8.37E-004
                   ... 4   -2626.5404801        1.13E-004
                    42   -2626.5405579        0.001853        0.012877
                   ... 1   -2626.5402606        1.59E-004
                    43   -2626.5405725        0.001114        0.011953
                   ... 1   -2626.5413241        1.36E-004
                   ... 2   -2626.5386739        5.53E-004
                   ... 3   -2626.4937058        2.80E-003
                   ... 4   -2626.5398165        3.35E-004
                    44   -2626.5405731        0.000965        0.004984
    Reason for exit: Sucessful completion
    Quantum Mechanics Program CPU Time : 017:21:53.0
    Quantum Mechanics Program Wall Time: 011:33:44.2

Spartan '04 Semi-Empirical Program:  (PC/x86)                 Release  121
    Semi-empirical Property Calculation


   M001


Parameters for element 23 not available for AM1  -- ABORTING...



These semiempirical levels can handle this calculation:
PM3(tm)


  Reason for exit: Ignoring solvation calculation
  Semi-Empirical Program CPU Time : 000:00:00.1
  Semi-Empirical Program Wall Time: 000:00:00.2

Spartan '04 Properties Program:  (PC/x86)                     Release  121


  Reason for exit: Successful completion
  Properties Program CPU Time : 000:00:05.8
  Properties Program Wall Time: 000:00:08.8
```

Table B3. Verbose output file of the equilibrium geometry calculation for the Brønsted acidic ammonia activation given in Figure 4.2.

```
              Spartan '04
          build 121 (Nov 14 2003)

 Wavefunction Developers:
    B.J. Deppmeier, A.J. Driessen, T.S. Hehre, W.J. Hehre,
    J.A. Johnson, P.E. Klunzinger, J.M. Leonard, I.N. Pham
    W.J. Pietro, Jianguo Yu

 Q-Chem Developers:
   J. Kong, C.A. White, A.I. Krylov, C.D. Sherrill,
   R.D. Adamson, T.R. Furlani, M.S. Lee, A.M. Lee,
   S.R. Gwaltney, T.R. Adams, C. Ochsenfeld, A.T.B. Gilbert,
   G.S. Kedziora,  V.A. Rassolov, D. R. Maurice, N. Nair,


   Y. Shao, N.A. Besley, P.E. Maslen, J.P. Dombroski,
   H. Dachsel, W.M. Zhang, P.P. Korambath, J. Baker,
   E.F. C. Byrd, T. Van Voorhis, M. Oumi, S. Hirata,
   C.P. Hsu, N. Ishikawa, J. Florian, A. Warshel,
   B.G. Johnson, P.M.W. Gill, M. Head-Gordon, J.A. Pople

 Wavefunction Inc.           Sales:   sales@wavefun.com
 Irvine CA                   Support: support@wavefun.com
                             Web:     www.wavefun.com


Copyright © 1995 – 2003
-------------------------------------------------------

          Spartan 'O4 Quantum Mechanics Module    121

 Windows PC (Intel x86)

 -------------------------------------------------------------
User input:
 -------------------------------------------------------------
$comment
M001
$end
$molecule
 0 1
    8       3.284574288     -0.811285118      2.27027406
    8       3.279051244      2.751885703     2.345295831
    8      -0.880954359     -0.81502177      2.141087762
   23      -0.346150347      0.973626959     1.754260941
   23       3.089171718      0.981287654     1.791645144
    8      -0.174726613      1.008662791     0.195590791
    8      -2.475564588      0.964656713     2.151975444
    8       4.87225297       0.971248126     2.379854805
    8      -0.88647731       2.748149002     2.216109416
    8       1.351808244      0.966589522      2.34175557
    1      -1.287391323      2.64378871      3.082112071
    1      -1.282080858     -0.747580203     3.010646641
    1       3.636679517     -0.714909699     3.158146363
    1       4.87252603       0.951190079      3.33963658
```

```
     1      3.631525495      2.619543577      3.228376246
     8      2.961641293      1.018504301       0.07138295
     1      2.052100354      1.025375242      -0.28940135
     1     -2.907071924      0.204038358      2.548013914
     1     -2.886342064      1.755523871      2.508873667
     1      1.289489332      0.246434981     -2.240655795
     7      1.368876536      1.052930691     -1.624484085
     1      1.264467218      1.869396457     -2.223556354
     1      0.538067801      1.033925995     -1.036435701
$end
$rem
JOBTYPE     OPT
TIDY_SYM    TRUE
EXCHANGE      B3LYP
CORRELATION   none  (built-in)
INCDFT        TRUE
VARTHRESH     2
BASIS         6-31G**
VARTHRESH     0
SMALL_PROD_XCMAT    10
SYMMETRY      FALSE
SCF_CONVERGENCE    4
MAX_SCF_CYCLES      10000
GEOM_OPT_MAX_CYCLES        1000
GEOM_OPT_TOL_GRADIENT       1000
GEOM_OPT_TOL_DISPLACEMENT  10000
GEOM_OPT_PRINT      4
TERSE_OUTPUT 4
USE_SP_DERIV 2
GEOM_OPT_HESSIAN       READ
EXTERNAL_HESSIAN       TRUE
GUI            GUI_SPARTAN
$end
$opt
FIXED
1   XYZ
2   XYZ
3   XYZ
7   XYZ
8   XYZ
9   XYZ
11   XYZ
12   XYZ
13   XYZ
14   XY
15   XYZ
18   XYZ
19   XYZ
ENDFIXED
$end
-------------------------------------------------------------
Processing $rem in C:\PROGRA~1\WAVEFU~1\SPARTA~1\auxdir\preferences.
   (Site specific preferences.)
  ... THRESH            9
  ... SCF_CONVERGENCE   7
  ... SMALL_PROD_XCMAT  9
  ... BASIS_LIN_DEP_THRESH      5
  ... GUI              GUI_SPARTAN
  ... TERSE_OUTPUT      TRUE
Querying system for available memory
  ... MEM_TOTAL 496 MB
Processing $rem in the input.
```

```
    ... JOBTYPE     OPT
    ... TIDY_SYM    TRUE
    ... EXCHANGE     B3LYP
    ... CORRELATION  none  (built-in)
    ... INCDFT       TRUE
    ... VARTHRESH    2
    ... BASIS        6-31G**
    ... VARTHRESH    0
    ... SMALL_PROD_XCMAT    10
    ... SYMMETRY     FALSE
    ... SCF_CONVERGENCE     4
    ... MAX_SCF_CYCLES      10000
    ... GEOM_OPT_MAX_CYCLES 1000
    ... GEOM_OPT_TOL_GRADIENT     1000
    ... GEOM_OPT_TOL_DISPLACEMENT  10000
    ... GEOM_OPT_PRINT      4
    ... TERSE_OUTPUT  4
    ... USE_SP_DERIV  2
    ... GEOM_OPT_HESSIAN      READ
    ... EXTERNAL_HESSIAN      TRUE
    ... GUI              GUI_SPARTAN

Total Memory Limit in MB = 496
Mega-Array Size in MB = 31

#######################################################
#  Entering fldman.exe on Wed Feb 23 17:25:47 2005  #
#######################################################

 Requested basis set is 6-31G(d,p)
 There are 87 shells and 263 basis functions

#######################################################
#  Entering gesman.exe on Wed Feb 23 17:25:50 2005  #
#######################################################

 Smallest overlap matrix eigenvalue = 3.62E-003
 Multipole matrices computed through 2nd order

#######################################################
#  Entering scfman.exe on Wed Feb 23 17:25:52 2005  #
#######################################################

 Exchange:     0.2000 Hartree-Fock + 0.0800 Slater + 0.7200 Becke
 Correlation: 0.8100 LYP + 0.1900 VWN1RPA
 Using SG-1 standard quadrature grid
 A restricted hybrid HF-DFT SCF calculation will be
 performed using Pulay DIIS extrapolation
 Exchange:     0.2000 Hartree-Fock + 0.0800 Slater + 0.7200 Becke
 Correlation: 0.8100 LYP + 0.1900 VWN1RPA
 Using SG-1 standard quadrature grid
 SCF converges when DIIS error is below 1.0E-004
 ------------------------------------
  Cycle       Energy         DIIS Error
 ------------------------------------
    1   -2626.9221846778     5.00E-002
    2   -2624.3342330341     1.66E-002
    3   -2579.7272371601     7.41E-002
    4   -2620.6279381246     3.07E-002
    5   -2608.0756366977     4.60E-002
Switching Grids 0 -> 1
    6   -2624.8693903057     1.66E-002
```

```
 7   -2606.5819888061      3.77E-002
 8   -2617.4383343044      3.22E-002
 9   -2625.5405205320      1.07E-002
10   -2624.4645172586      1.96E-002
11   -2626.2843863561      5.18E-003
12   -2626.2218756301      6.37E-003
13   -2626.4073165055      3.29E-003
14   -2626.4744641830      6.01E-004
15   -2626.4761155342      3.92E-004
16   -2626.4770956603      1.75E-004
17   -2626.4772563920      8.28E-005 Convergence criterion met
 ------------------------------------
 SCF time:  CPU 1121.53 s  wall 1745640.00 s

#####################################################
#  Entering anlman.exe on Wed Feb 23 17:55:03 2005  #
#####################################################

  +++F6+++
 Analysis of SCF Wavefunction

        Mulliken Net Atomic Charges

    Atom                Charge (a.u.)
  ---------------------------------------
    1 O                  -0.573687
    2 O                  -0.573337
    3 O                  -0.632710
    4 V                   1.406043
    5 V                   1.350922
    6 O                  -0.529923
    7 O                  -0.559746
    8 O                  -0.617729
    9 O                  -0.636092
   10 O                  -0.705196
   11 H                   0.289265
   12 H                   0.289605
   13 H                   0.299112
   14 H                   0.282831
   15 H                   0.299169
   16 O                  -0.558629
   17 H                   0.388745
   18 H                   0.336149
   19 H                   0.336090
   20 H                   0.263004
   21 N                  -0.768539
   22 H                   0.262787
   23 H                   0.351867
  ---------------------------------------
  Sum of atomic charges =   0.000000


  ------------------------------------------------------------------
                 Cartesian Multipole Moments
  ------------------------------------------------------------------
    Charge (ESU x 10^10)
             0.0000
    Dipole Moment (Debye)
        X       8.5062    Y      -4.1147    Z      -0.0011
       Tot       9.4491
    Quadrupole Moments (Debye-Ang)
       XX     -79.7079    XY      -4.4889   YY     -62.8814
       XZ      -0.1621    YZ      -0.0294   ZZ    -105.0766
```

```
      Traceless Quadrupole Moments (Debye-Ang)
         QXX        8.5423   QYY        59.0216   QZZ       -67.5639
         QXY      -13.4667   QXZ        -0.4864   QYZ        -0.0882
      Octapole Moments (Debye-Ang^2)
         XXX       230.2305  XXY       -78.0889   XYY        16.8560
         YYY        39.2944  XXZ        -0.6303   XYZ        -0.6069
         YYZ         0.214   XZZ        31.2236   YZZ        12.7484
         ZZZ        -0.3710
      Traceless Octapole Moments (Debye-Ang^2)
         XXX       948.6664  YYY       823.8307   ZZZ         1.5141
         XXY     -1093.1953  XXZ        -7.0955   XYY      -582.0905
         XYZ        -9.1032  XZZ      -366.5758   YYZ         5.5814
         YZZ       269.3646
      Hexadecapole Moments (Debye-Ang^3)
         XXXX    -2292.4661  XXXY     -160.7686   XXYY     -402.1056
         XYYY       11.6818  YYYY     -585.9198   XXXZ        -3.7264
         XXYZ       -1.2844  XYYZ       -0.0754   YYYZ        -0.0909
         XXZZ     -527.9939  XYZZ      -26.7670   YYZZ      -187.6412
         XZZZ       -1.7642  YZZZ        0.1838   ZZZZ      -645.6184
      Traceless Hexadecapole Moments (Debye-Ang^3)
         XXXX    -2513.4095  XXXY    -8967.2787   XXXZ      -140.7993
         XXYY     6473.9356  XXYZ     -114.2297   XXZZ     -3960.5262
         XYYY     9140.0078  XYYZ       75.5724   XYZZ      -172.7292
         XZZZ       65.2270  YYYY    -7546.9521   YYYZ        52.3410
         YYZZ     1073.0165  YZZZ       61.8887   ZZZZ      2887.5097
      ----------------------------------------------------------------

    ---F6---


  ######################################################
  #  Entering drvman.exe on Wed Feb 23 17:55:03 2005  #
  ######################################################

  Calculating analytic gradient of the SCF energy

  Spartan '04 Fast HF Program:  (PC/x86)                     Release  121
    Calculation started: Wed Feb 23 17:55:06 2005

    JOBNAME.TEMP

    Run type: Molecular gradient (no SCF)
    Model: RHF/ABASIS
    Number of shells:  87
      34 S shells
      11 P shells
      28 SP shells
      14 6D shells
    Number of basis functions: 263
    Number of electrons:       136
    Number of heavy atoms:      12
    Number of hydrogens:        11
    Use of molecular symmetry disabled
    Molecular charge:   0
    Spin multiplicity: 1
    Memory model: direct    21.6 Mb

    Point Group = C1  Order =  1 Nsymop =  1
    This system has   0 degrees of freedom


                  Cartesian gradient (a.u.)
       Atom          X            Y            Z
       ----    ------------ ------------ ------------
```

```
O    1    -0.0963596    -0.2346181    -0.0929089
O    2    -0.0966632    -0.2345611     0.0927315
O    3     0.1089487    -0.2244389    -0.0750937
V    4    -0.0512754     0.1288915     0.0002494
V    5     0.0128594     0.0211717    -0.0001894
O    6    -0.0024414    -0.1644986     0.0002417
O    7     0.2161896    -0.1989279    -0.0124484
O    8     0.0638626    -0.2447821     0.0001072
O    9     0.1091765    -0.2244244     0.0748826
O   10     0.0013479     0.0602121     0.0000662
H   11    -0.1151275     0.2427783    -0.0096615
H   12    -0.1152984     0.2430206     0.0093556
H   13     0.0949565     0.2557240     0.0160904
H   14     0.0118403     0.2709453     0.0000122
H   15     0.0950058     0.2557844    -0.0157397
O   16     0.2279406     0.0087841     0.0002669
H   17    -0.2104379    -0.1092898    -0.0000252
H   18    -0.1357287     0.1106110    -0.2297658
H   19    -0.1286711     0.0889204     0.2418949
H   20    -0.0129968    -0.1386362    -0.1907460
N   21     0.1923779     0.1300654     0.0043220
H   22    -0.0188610    -0.1429102     0.1875221
H   23    -0.1506448     0.1001785    -0.0011640

 E(HF)  =   -2626.4772564 a.u.
 Reason for exit: Successful completion
 Fast HF Program CPU Time : 000:02:44.1
 Fast HF Program Wall Time: 000:04:05.9
Gradient of SCF Energy
            1          2          3          4          5          6
  1  -0.0238587  -0.0237692   0.0175388   0.0126934   0.0143233  -
0.0355928
  2  -0.0101240  -0.0100296  -0.0100934   0.0215772  -0.0269593
0.0217673
  3   0.0166523  -0.0166080   0.0215945   0.0002420  -0.0000256  -
0.0002408
            7          8          9         10         11         12
  1  -0.0131239   0.0030016   0.0170130  -0.0260067   0.0017876
0.0014492
  2   0.0037916  -0.0013951  -0.0103963   0.0021049   0.0121033
0.0118444
  3   0.0003044   0.0000231  -0.0217959  -0.0001424   0.0081823  -
0.0083751
           13         14         15         16         17         18
  1   0.0082548   0.0108656   0.0082124   0.0552149  -0.0121709  -
0.0045542
  2   0.0073470   0.0092163   0.0073649   0.0742184  -0.0371366  -
0.0039305
  3  -0.0125087   0.0000103   0.0125529  -0.0001980   0.0005362  -
0.0095269
           19         20         21         22         23
  1  -0.0043390   0.0065131  -0.0166790   0.0066676  -0.0034410
  2  -0.0044241   0.0011180  -0.0421001   0.0012714  -0.0171358
  3   0.0096145  -0.0024307  -0.0004909   0.0027401  -0.0001096
 Max gradient component =      7.422E-002
 RMS gradient           =      1.778E-002
 Gradient time:  CPU 209.38 s   wall 309703.00 s
  +++F6+++
  ---F6---

####################################################
#  Entering optman.exe on Wed Feb 23 18:00:16 2005  #
```

```
##########################################################


##########################################################
#  Entering fldman.exe on Wed Feb 23 18:00:19 2005  #
##########################################################

 Requested basis set is 6-31G(d,p)
 There are 87 shells and 263 basis functions
 Applying Cartesian multipole field
     Component          Value
     ---------          -----
      (2,0,0)        1.00000E-010
      (0,2,0)        2.00000E-010
      (0,0,2)       -3.00000E-010

##########################################################
#  Entering gesman.exe on Wed Feb 23 18:00:20 2005  #
##########################################################

 Smallest overlap matrix eigenvalue = 3.57E-003
 Multipole matrices computed through 2nd order
##########################################################
#  Entering scfman.exe on Wed Feb 23 18:00:24 2005  #
##########################################################

 A restricted hybrid HF-DFT SCF calculation will be
 performed using Pulay DIIS extrapolation
 Exchange:     0.2000 Hartree-Fock + 0.0800 Slater + 0.7200 Becke
 Correlation:  0.8100 LYP + 0.1900 VWN1RPA
 Using SG-1 standard quadrature grid
 SCF converges when DIIS error is below 1.0E-004
 ---------------------------------------
  Cycle        Energy         DIIS Error
 ---------------------------------------
    1   -2626.4418033101    4.96E-003
    2   -2626.4859226981    1.33E-003
    3   -2626.3726531218    4.26E-003
    4   -2626.4878933476    1.45E-003
    5   -2626.4993884540    4.25E-004
Switching Grids 0 -> 1
    6   -2626.4999085977    2.56E-004
    7   -2626.4899236463    1.29E-003
    8   -2626.5002125719    1.37E-004
    9   -2626.5003241730    3.92E-005 Convergence criterion met
 ---------------------------------------
 SCF time:  CPU 531.48 s  wall 773468.00 s

##########################################################
#  Entering anlman.exe on Wed Feb 23 18:13:22 2005  #
##########################################################

  +++F6+++
 Analysis of SCF Wavefunction

        Mulliken Net Atomic Charges
     Atom              Charge (a.u.)
 ---------------------------------------
      1 O                 -0.569882
      2 O                 -0.569863
      3 O                 -0.630453
      4 V                  1.393226
```

```
      5 V                         1.362900
      6 O                        -0.531920
      7 O                        -0.553074
      8 O                        -0.611714
      9 O                        -0.634035
     10 O                        -0.709672
     11 H                         0.283646
     12 H                         0.283770
     13 H                         0.300215
     14 H                         0.281093
     15 H                         0.300337
     16 O                        -0.588284
     17 H                         0.412831
     18 H                         0.326686
     19 H                         0.327257
     20 H                         0.278584
     21 N                        -0.779888
     22 H                         0.278310
     23 H                         0.349929
 ----------------------------------
 Sum of atomic charges =    0.000000


 ------------------------------------------------------------------
                   Cartesian Multipole Moments
 ------------------------------------------------------------------
   Charge (ESU x 10^10)
             0.0000
   Dipole Moment (Debye)
       X        6.8069      Y       -3.7488      Z       -0.0269
     Tot        7.7709
   Quadrupole Moments (Debye-Ang)
       XX      -84.5451      XY       -5.5610      YY      -59.3681
       XZ       -0.1832      YZ       -0.0504      ZZ     -105.0740
   Traceless Quadrupole Moments (Debye-Ang)
      QXX       -4.6480     QYY       70.8829     QZZ      -66.2348
      QXY      -16.6831     QXZ       -0.5495     QYZ       -0.1511
   Octapole Moments (Debye-Ang^2)
      XXX      218.5298     XXY      -76.2700     XYY       11.5862
      YYY       56.4925     XXZ       -0.7275     XYZ       -0.5553
      YYZ        0.124      XZZ       29.5814     YZZ       16.2869
      ZZZ       -0.4034
   Traceless Octapole Moments (Debye-Ang^2)
      XXX      940.6706     YYY      878.8027     ZZZ        3.0027
      XXY    -1133.5782     XXZ       -7.8941     XYY     -605.2995
      XYZ       -8.3300     XZZ     -335.3711     YYZ        4.8914
      YZZ      254.7755
   Hexadecapole Moments (Debye-Ang^3)
    XXXX    -2350.2493    XXXY     -154.1236    XXYY     -407.1783
    XYYY       -1.0176    YYYY     -561.8258    XXXZ       -3.9747
    XXYZ       -1.2705    XYYZ       -0.0497    YYYZ       -0.3578
    XXZZ     -531.2763    XYZZ      -26.1409    YYZZ     -187.8454
    XZZZ       -1.7778    YZZZ        0.0711    ZZZZ     -646.2629
   Traceless Hexadecapole Moments (Debye-Ang^3)
    XXXX    -3091.2715    XXXY    -8025.2807    XXXZ     -156.2441
    XXYY     6496.7670    XXYZ     -108.9817    XXZZ    -3405.4955
    XYYY     8050.8411    XYYZ       81.8153    XYZZ      -25.5604
    XZZZ       74.4288    YYYY    -7173.6988    YYYZ       35.7041
    YYZZ      676.9318    YZZZ       73.2776    ZZZZ     2728.5637
 ------------------------------------------------------------------


   ---F6---
```

```
#######################################################
#  Entering drvman.exe on Wed Feb 23 18:13:23 2005  #
#######################################################

 Calculating analytic gradient of the SCF energy

Spartan '04 Fast HF Program:  (PC/x86)
                Release  121
  Calculation started: Wed Feb 23 18:13:26 2005

  JOBNAME.TEMP

  Run type: Molecular gradient (no SCF)
  Model: RHF/ABASIS
  Number of shells:  87
    34 S shells
    11 P shells
    28 SP shells
    14 6D shells
  Number of basis functions: 263
  Number of electrons:      136
  Number of heavy atoms:     12
  Number of hydrogens:       11
  Use of molecular symmetry disabled
  Molecular charge:   0
  Spin multiplicity:  1
  Memory model: direct    21.6 Mb

  Point Group = C1  Order =  1 Nsymop =  1
  This system has    0 degrees of freedom

                Cartesian gradient (a.u.)
    Atom         X            Y            Z
    ----     ------------ ------------ ------------


    O   1   -0.0964071   -0.2340386   -0.0941981
    O   2   -0.0967431   -0.2340242    0.0940447
    O   3    0.1092081   -0.2212083   -0.0746233
    V   4   -0.0581972    0.0805274    0.0002329
    V   5    0.0112677    0.0253411   -0.0000493
    O   6   -0.0198917   -0.1459477    0.0000209
    O   7    0.2185645   -0.1947668   -0.0124707
    O   8    0.0647351   -0.2432731    0.0001111
    O   9    0.1094129   -0.2212088    0.0746317
    O  10    0.0265839    0.0685819    0.0000908
    H  11   -0.1158031    0.2411397   -0.0091059
    H  12   -0.1159658    0.2413120    0.0088241
    H  13    0.0952127    0.2560382    0.0154281
    H  14    0.0125711    0.2706723    0.0000088
    H  15    0.0952697    0.2561184   -0.0150782
    O  16    0.1666190   -0.0016561   -0.0007131
    H  17   -0.1453228   -0.1127166    0.0007494
    H  18   -0.1335405    0.1094533   -0.2275714
    H  19   -0.1265805    0.0879875    0.2397184
    H  20    0.0014014   -0.1355760   -0.1977367
    N  21    0.1712820    0.1339745    0.0039522
    H  22   -0.0041671   -0.1393142    0.1950131
    H  23   -0.1695094    0.1125841   -0.0012795

  E(HF)  =   -2626.5003242 a.u.
  Reason for exit: Successful completion
  Fast HF Program CPU Time : 000:03:24.3
```

```
   Fast HF Program Wall Time: 000:06:01.3
 Gradient of SCF Energy
               1          2          3          4          5          6
    1  -0.0240256 -0.0239818  0.0240249 -0.0767105  0.0458840
0.0131189
    2  -0.0078655 -0.0078088 -0.0015268 -0.0505425 -0.0339626
0.0380719
    3   0.0166485 -0.0165362  0.0219410 -0.0005257 -0.0002082
0.0001150
               7          8          9         10         11         12
    1  -0.0099992  0.0005919  0.0235317  0.0024489  0.0010441
0.0007204
    2   0.0068565  0.0022350 -0.0018421  0.0110032  0.0129609
0.0127324
    3   0.0000718  0.0000287 -0.0217409  0.0000703  0.0092282  -
0.0093855
              13         14         15         16         17         18
    1   0.0083333  0.0115095  0.0082894 -0.0010956  0.0095658  -
0.0052509
    2   0.0076918  0.0099762  0.0077045  0.0357872 -0.0286946  -
0.0032414
    3  -0.0135194  0.0000108  0.0135661  0.0000174  0.0001867  -
0.0081261
              19         20         21         22         23
    1  -0.0049140  0.0038194 -0.0032362  0.0040620 -0.0077304
    2  -0.0038568 -0.0002201  0.0015160  0.0001365 -0.0071110
    3   0.0082904  0.0007654  0.0000169 -0.0008015 -0.0001135
 Max gradient component =      7.671E-002
 RMS gradient            =      1.763E-002
 Gradient time:  CPU 261.77 s  wall 485515.00 s
  +++F6+++

  ---F6---

#####################################################
#  Entering optman.exe on Wed Feb 23 18:21:32 2005  #
#####################################################


#####################################################
#  Entering fldman.exe on Wed Feb 23 18:21:34 2005  #
#####################################################

 Requested basis set is 6-31G(d,p)
 There are 87 shells and 263 basis functions
 Applying Cartesian multipole field
    Component         Value
    ---------         -----
     (2,0,0)       1.00000E-010
```

<div align="center">
.
.
.
.
.
.
.
.
.
.
.
.
</div>

```
                                    .
                                    .
                                    .
                                    .
                                    .
                                    .


     #######################################################
     #  Entering drvman.exe on Thu Feb 24 04:40:58 2005   #
     #######################################################

      Calculating analytic gradient of the SCF energy

     Spartan '04 Fast HF Program: (PC/x86)                    Release  121
       Calculation started: Thu Feb 24 04:41:01 2005

       JOBNAME.TEMP

       Run type: Molecular gradient (no SCF)
       Model: RHF/ABASIS
       Number of shells:  87
         34 S shells
         11 P shells
         28 SP shells
     14 6D shells
       Number of basis functions: 263

       Number of electrons:        136
       Number of heavy atoms:       12
       Number of hydrogens:         11
       Use of molecular symmetry disabled
       Molecular charge:   0
       Spin multiplicity:  1
       Memory model: direct     21.6 Mb

       Point Group = C1  Order =  1 Nsymop =  1
       This system has   0 degrees of freedom

                        Cartesian gradient (a.u.)
          Atom         X            Y            Z
          ----    ------------ ------------ ------------

          O   1   -0.0994867   -0.2300567   -0.0898897
          O   2   -0.0997953   -0.2299809    0.0900997
          O   3    0.1090917   -0.2208701   -0.0737122
          V   4   -0.0579658    0.0901134    0.0008339
          V   5   -0.0204838    0.0774673   -0.0004560
          O   6   -0.0184181   -0.1504563    0.0001567
          O   7    0.2117373   -0.1959997   -0.0124566
          O   8    0.0758185   -0.2388488    0.0000737
          O   9    0.1094511   -0.2213269    0.0736101
          O  10    0.0548197    0.0436632   -0.0000549
          H  11   -0.1140803    0.2410683   -0.0106604
          H  12   -0.1139600    0.2408241    0.0103689
          H  13    0.0931326    0.2523525    0.0173777
          H  14    0.0132124    0.2728954    0.0000388
          H  15    0.0932485    0.2526486   -0.0169833
          O  16    0.0255373   -0.1503736    0.0006313
          H  17    0.1294406    0.1033543    0.0040617
          H  18   -0.1348368    0.1103219   -0.2286574
```

180

```
    H  19   -0.1278859    0.0888141    0.2408212
    H  20    0.0061461   -0.1311161   -0.2060695
    N  21   -0.0030623    0.0481906    0.0018543
    H  22    0.0057406   -0.1464163    0.1956591
    H  23   -0.1374015    0.0937316    0.0033529

  E(HF)  =   -2626.5405725 a.u.
  Reason for exit: Successful completion
  Fast HF Program CPU Time : 000:02:40.8
  Fast HF Program Wall Time: 000:04:15.5
 Gradient of SCF Energy
            1          2          3          4          5          6
    1  -0.0251159  -0.0250014   0.0134169  -0.0005748  -0.0001834
0.0001795
    2  -0.0112402  -0.0111000  -0.0101808   0.0000903  -0.0006703   -
0.0009561
    3   0.0142087  -0.0137498   0.0172670  -0.0005968  -0.0005318
0.0000154
            7          8          9         10         11         12
    1  -0.0206042   0.0288953   0.0128978  -0.0000921   0.0028102
0.0026528
    2   0.0068016   0.0028330  -0.0107447   0.0002618   0.0109555
0.0104752
    3   0.0001950   0.0000895  -0.0170865  -0.0000264   0.0062730   -
0.0064310
           13         14         15         16         17         18
    1   0.0052664   0.0069967   0.0052450   0.0002798  -0.0003834   -
0.0034437
    2   0.0062631   0.0077226   0.0064283   0.0011143  -0.0000602   -
0.0039150
    3  -0.0107017  -0.0000037   0.0107438  -0.0000151   0.0000657   -
0.0092580
           19         20         21         22         23
    1  -0.0033595  -0.0000089   0.0005389  -0.0000965  -0.0003157
    2  -0.0042900   0.0002971  -0.0008661   0.0003737   0.0004069
    3   0.0095211   0.0004582  -0.0002803  -0.0003755   0.0002190
 Max gradient component =       2.890E-002
 RMS gradient            =       8.850E-003
 Gradient time:  CPU 211.31 s   wall 326188.00 s
   +++F6+++

   ---F6---

########################################################
#  Entering optman.exe on Thu Feb 24 04:46:28 2005   #
########################################################


########################################################
#  Entering fldman.exe on Thu Feb 24 04:46:30 2005   #
########################################################

 Requested basis set is 6-31G(d,p)
 There are 87 shells and 263 basis functions
 Applying Cartesian multipole field
    Component         Value
    ---------         -----
     (2,0,0)      1.00000E-010
     (0,2,0)      2.00000E-010
     (0,0,2)     -3.00000E-010

########################################################
```

```
#  Entering gesman.exe on Thu Feb 24 04:46:31 2005  #
#####################################################

 Smallest overlap matrix eigenvalue = 3.66E-003
 Multipole matrices computed through 2nd order

#####################################################
#  Entering scfman.exe on Thu Feb 24 04:46:34 2005  #
#####################################################

 A restricted hybrid HF-DFT SCF calculation will be
 performed using Pulay DIIS extrapolation
 Exchange:     0.2000 Hartree-Fock + 0.0800 Slater + 0.7200 Becke
 Correlation:  0.8100 LYP + 0.1900 VWN1RPA
 Using SG-1 standard quadrature grid
 SCF converges when DIIS error is below 1.0E-004
 --------------------------------------
  Cycle       Energy        DIIS Error
 --------------------------------------
    1   -2626.5413240557    1.36E-004
 Switching Grids 0 -> 1
    2   -2626.5386739168    5.53E-004
    3   -2626.4937057530    2.80E-003
    4   -2626.5398165098    3.35E-004
    5   -2626.5405730847    4.98E-005 Convergence criterion met
 --------------------------------------
  SCF time:  CPU 313.97 s  wall 488688.00 s

#####################################################
#  Entering anlman.exe on Thu Feb 24 04:54:49 2005  #
#####################################################

   +++F6+++
 Analysis of SCF Wavefunction

         Mulliken Net Atomic Charges

     Atom              Charge (a.u.)
   --------------------------------------
      1 O                 -0.606402
      2 O                 -0.605244
      3 O                 -0.656979
      4 V                  1.407184
      5 V                  1.364226
      6 O                 -0.624477
      7 O                 -0.561038
      8 O                 -0.631838
      9 O                 -0.658876
     10 O                 -0.686715
     11 H                  0.281485
     12 H                  0.281781
     13 H                  0.290666
     14 H                  0.283035
     15 H                  0.290927
     16 O                 -0.613102
     17 H                  0.417516
     18 H                  0.329474
     19 H                  0.329503
     20 H                  0.325125
     21 N                 -0.696722
     22 H                  0.324591
     23 H                  0.415880
```

```
                 ----------------------------------------
                 Sum of atomic charges =      0.000000

          ------------------------------------------------------------------
                            Cartesian Multipole Moments
          ------------------------------------------------------------------
             Charge (ESU x 10^10)
                        0.0000
             Dipole Moment (Debye)
                  X       6.6318      Y       0.9372      Z       0.1597
                  Tot     6.6996
             Quadrupole Moments (Debye-Ang)
                  XX    -86.0156      XY    -10.5908      YY    -45.4390
                  XZ     -0.3365      YZ      0.6340      ZZ   -107.1415
             Traceless Quadrupole Moments (Debye-Ang)
                  QXX   -19.4507      QYY   102.2790      QZZ   -82.8283
                  QXY   -31.7725      QXZ    -1.0096      QYZ     1.9019
             Octapole Moments (Debye-Ang^2)
                  XXX   224.2079      XXY   -74.4649      XYY    -3.3381
                  YYY    99.9965      XXZ    -0.0065      XYZ    -0.6591
                  YYZ     2.384       XZZ    27.8012      YZZ    20.6798
                  ZZZ     3.1431
             Traceless Octapole Moments (Debye-Ang^2)
                  XXX  1125.0795      YYY  1084.0445      ZZZ    -2.5431
                  XXY -1255.6073      XXZ   -16.6608      XYY  -796.0846
                  XYZ    -9.8871      XZZ  -328.9949      YYZ    19.2039
                  YZZ   171.5628
             Hexadecapole Moments (Debye-Ang^3)
                  XXXX -2456.9631     XXXY  -176.9306     XXYY  -407.6160
                  XYYY   -40.9526     YYYY  -384.3007     XXXZ    -6.7375
                  XXYZ    -1.5165     XYYZ    -0.3492     YYYZ     0.2119
                  XXZZ  -560.6897     XYZZ   -29.9002     YYZZ  -182.2641
                  XZZZ    -2.8638     YZZZ    -3.3443     ZZZZ  -661.2197
             Traceless Hexadecapole Moments (Debye-Ang^3)
                  XXXX -1939.5372     XXXY -7427.4633     XXXZ  -259.6668
                  XXYY  5781.1905     XXYZ   -94.6663     XXZZ -3841.6533
                  XYYY  6850.2297     XYYZ   112.5929     XYZZ   577.2336
                  XZZZ   147.0739     YYYY -4907.9074     YYYZ   215.9604
                  YYZZ  -873.2831     YZZZ  -121.2942     ZZZZ  4714.9364
          ------------------------------------------------------------------
             ---F6---
          ####################################################
          #  Entering drvman.exe on Thu Feb 24 04:54:49 2005  #
          ####################################################

           Calculating analytic gradient of the SCF energy

          Spartan '04 Fast HF Program: (PC/x86)                    Release  121
            Calculation started: Thu Feb 24 04:54:52 2005

            JOBNAME.TEMP
            Run type: Molecular gradient (no SCF)
            Model: RHF/ABASIS
            Number of shells:  87
              34 S shells
              11 P shells
              28 SP shells
              14 6D shells
            Number of basis functions: 263
            Number of electrons:       136
            Number of heavy atoms:      12
            Number of hydrogens:        11
```

```
 Use of molecular symmetry disabled
 Molecular charge:    0
 Spin multiplicity:  1
 Memory model: direct    21.6 Mb
 Point Group = C1  Order =  1 Nsymop =  1
 This system has   0 degrees of freedom

                  Cartesian gradient (a.u.)
    Atom        X            Y            Z
    ----    -----------  -----------  -----------

    O   1   -0.0995144   -0.2303849   -0.0897339
    O   2   -0.0998196   -0.2302131    0.0898101
    O   3    0.1090281   -0.2212202   -0.0737819
    V   4   -0.0574583    0.0907144    0.0007116
    V   5   -0.0209637    0.0779911   -0.0004158
    O   6   -0.0186356   -0.1504357    0.0002567
    O   7    0.2116938   -0.1961002   -0.0123647
    O   8    0.0754985   -0.2389818    0.0000855
    O   9    0.1092131   -0.2212123    0.0736981
    O  10    0.0551075    0.0435316    0.0000321
    H  11   -0.1138681    0.2407831   -0.0106752
    H  12   -0.1140227    0.2410467    0.0103762
    H  13    0.0932425    0.2526978    0.0173389
    H  14    0.0132588    0.2729598    0.0000309
    H  15    0.0933122    0.2528622   -0.0169451
    O  16    0.0253516   -0.1508357    0.0006416
    H  17    0.1303577    0.1038730    0.0039861
    H  18   -0.1348486    0.1103665   -0.2287055
    H  19   -0.1278505    0.0888150    0.2407461
    H  20    0.0056123   -0.1314659   -0.2066346
    N  21   -0.0036688    0.0482460    0.0019774
    H  22    0.0056871   -0.1466890    0.1959886
    H  23   -0.1367129    0.0936515    0.0035771

  E(HF) =    -2626.5405731 a.u.
  Reason for exit: Successful completion
  Fast HF Program CPU Time : 000:02:41.3
  Fast HF Program Wall Time: 000:03:29.5
 Gradient of SCF Energy
             1           2           3           4           5           6
    1  -0.0251129  -0.0250155   0.0132643  -0.0009649  -0.0002335  -
0.0000412
    2  -0.0113045  -0.0111057  -0.0104975   0.0001563  -0.0001418  -
0.0002559
    3   0.0141519  -0.0139382   0.0170428  -0.0000707  -0.0002174
0.0000281
             7           8           9          10          11          12
    1  -0.0206424   0.0285644   0.0127537   0.0008396   0.0029457
0.0026178
    2   0.0066836   0.0027626  -0.0109626   0.0000287   0.0108859
0.0106385
    3   0.0002661   0.0000609  -0.0172401   0.0000229   0.0062182  -
0.0064216
            13          14          15          16          17          18
    1   0.0053413   0.0070618   0.0052813   0.0001762   0.0001030  -
0.0034740
    2   0.0064858   0.0078150   0.0065517   0.0003617   0.0001496  -
0.0038690
    3  -0.0107685  -0.0000037   0.0108094  -0.0000783  -0.0000414  -
0.0093101
            19          20          21          22          23
```

```
  1  -0.0032614   0.0000711   0.0000653   0.0000050  -0.0003447
  2  -0.0043055   0.0001423  -0.0006940   0.0001710   0.0003042
  3   0.0094441   0.0000836   0.0001000  -0.0001465   0.0000084
Max gradient component =      2.856E-002
RMS gradient          =      8.847E-003
Gradient time:  CPU 209.91 s  wall 271797.00 s
 +++F6+++
 ---F6---
#######################################################
#  Entering optman.exe on Thu Feb 24 04:59:25 2005  #
#######################################################

#######################################################
#  Entering anlman.exe on Thu Feb 24 04:59:28 2005  #
#######################################################

 +++F6+++
Analysis of SCF Wavefunction

        Mulliken Net Atomic Charges

      Atom              Charge (a.u.)
    ---------------------------------------
      1 O                -0.606402
      2 O                -0.605244
      3 O                -0.656979
      4 V                 1.407184
      5 V                 1.364226
      6 O                -0.624477
      7 O                -0.561038
      8 O                -0.631838
      9 O                -0.658876
     10 O                -0.686715
     11 H                 0.281485
     12 H                 0.281781
     13 H                 0.290666
     14 H                 0.283035
     15 H                 0.290927
     16 O                -0.613102
     17 H                 0.417516
     18 H                 0.329474
     19 H                 0.329503
     20 H                 0.325125
     21 N                -0.696722
     22 H                 0.324591
     23 H                 0.415880
    ---------------------------------------
 Sum of atomic charges =    0.000000
 ------------------------------------------------------------------
                 Cartesian Multipole Moments
 ------------------------------------------------------------------
   Charge (ESU x 10^10)
            0.0000
   Dipole Moment (Debye)
       X      6.6318     Y        0.9372     Z        0.1597
     Tot      6.6996
   Quadrupole Moments (Debye-Ang)
      XX     -86.0156    XY     -10.5908     YY     -45.4390
      XZ      -0.3365    YZ       0.6340     ZZ    -107.1415
   Traceless Quadrupole Moments (Debye-Ang)
      QXX     -19.4507    QYY    102.2790     QZZ    -82.8283
      QXY     -31.7725    QXZ     -1.0096     QYZ      1.9019
```

```
Octapole Moments (Debye-Ang^2)
   XXX     224.2079   XXY     -74.4649   XYY      -3.3381
   YYY      99.9965   XXZ      -0.0065   XYZ      -0.6591
   YYZ       2.384    XZZ      27.8012   YZZ      20.6798
   ZZZ       3.1431
Traceless Octapole Moments (Debye-Ang^2)
   XXX    1125.0795   YYY    1084.0445   ZZZ      -2.5431
   XXY   -1255.6073   XXZ     -16.6608   XYY    -796.0846
   XYZ      -9.8871   XZZ    -328.9949   YYZ      19.2039
   YZZ     171.5628
Hexadecapole Moments (Debye-Ang^3)
   XXXX  -2456.9631   XXXY   -176.9306   XXYY    -407.6160
   XYYY    -40.9526   YYYY   -384.3007   XXXZ      -6.7375
   XXYZ     -1.5165   XYYZ     -0.3492   YYYZ       0.2119
   XXZZ   -560.6897   XYZZ    -29.9002   YYZZ    -182.2641
   XZZZ     -2.8638   YZZZ     -3.3443   ZZZZ    -661.2197
Traceless Hexadecapole Moments (Debye-Ang^3)
   XXXX  -1939.5372   XXXY  -7427.4633   XXXZ    -259.6668
   XXYY   5781.1905   XXYZ    -94.6663   XXZZ   -3841.6533
   XYYY   6850.2297   XYYZ    112.5929   XYZZ     577.2336
   XZZZ    147.0739   YYYY  -4907.9074   YYYZ     215.9604
   YYZZ    -873.2831   YZZZ   -121.2942   ZZZZ    4714.9364
---------------------------------------------------------------
 ---F6---
Total job wall time:  4.2e+007 s
```